FOREWORD

This report reviews the results of an investigation of hypersonic flow separation and control characteristics conducted by the Research Department of Grumman Aircraft Engineering Corporation, Bethpage, New York. The program was supported primarily under Contract AF33(616)-8130, Air Force Task 821902, Project 8219. The Air Force Project Engineers were Messrs. Donald E. Hoak and Wilfred J. Klotzback of the Flight Control Division of the Air Force Flight Dynamics Laboratory. The laboratory, located at Wright-Patterson Air Force Base, Ohio, is part of the Research and Technology Division of the Air Force Systems Command.

The authors wish to thank Messrs. Hoak and Klotzback for their encouragement and guidance and thank Dr. Richard Oman, of the Grumman Research Department, for his many helpful discussions and consultations throughout the course of the investigation described herein.

ABSTRACT

Hypersonic flow separation and its effects on control characteristics were investigated analytically and experimentally. Included are conclusions drawn from extensive test data for hypersonic flows over "basic" geometries and over "typical" flight configurations with aerodynamic controls.

The basic flow geometries discussed include: separation on flat plates ahead of ramps (flaps); flows over sharp expansion corners; "breakaway" separation; and fin plate interactions. Force data and limited pressure and heating rate distributions are presented for the flight configurations for various trailing edge flap settings. As a supplement to this work, available sources of pertinent hypersonic controls data are tabulated in the Appendix.

This technical report has been reviewed and is approved.

C R Bryan
for W. A. SLOAN, Jr.
Colonel, USAF
Chief, Flight Control Division
AF Flight Dynamics Laboratory

TABLE OF CONTENTS

LIST OF ILLUSTRATIONS

LIST OF ILLUSTRATIONS (Cont)

LIST OF ILLUSTRATIONS (Cont)

LIST OF SYMBOLS

The principal symbols used in this report are listed below. All other auxiliary symbols are clarified by the context in which they are used.

C_A	axial force coefficient (see "Experimental Facilities..." section for reference areas and lengths for all force and moment coefficients)
C_ℓ	rolling moment coefficient
C_m	pitching moment coefficient
C_n	yawing moment coefficient
C_N	normal force coefficient
C_p	pressure coefficient, $C_p \equiv (p - p_\infty / q_\infty)$
C_y	side force coefficient
L	reference length (planform virtual length of model)
M_∞	free stream Mach number
p	pressure (psia)
p_∞	free stream static pressure (psia)
$\dot{q}$	aerodynamic heating rate (BTU/ft^2 sec)
q_∞	free stream dynamic pressure (psia)
Re_x	Reynolds number based on x, $Re_x \equiv \rho_\infty U_\infty x/\mu_\infty$
Re_∞/ft	Reynolds number per foot, $Re_\infty/ft \equiv \rho_\infty U_\infty/\mu_\infty$
S	reference area (planform virtual area)
t	time (sec)
T_{aw}	adiabatic wall temperature (^oR)
T_w	wall temperature (^oR)
T_∞	free stream static temperature (^oR)

LIST OF SYMBOLS (Cont.)

U_∞	free stream velocity (ft/sec)
x	streamwise surface distance
X	nondimensional streamwise distance
y	spanwise distance outboard from centerline
Y	nondimensional spanwise distance
z	distance normal to local surface
Z	nondimensional vertical distance
α	angle of attack (degrees)
β	sideslip angle (degrees)
δ	flap or ramp deflection angle (degrees)
μ_∞	free stream viscosity (slugs/ft sec)
ν	expansion corner angle (degrees)
ρ_∞	free stream density (slugs/ft^3)

Subscripts (used with δ)

L,R	refer to left and right flaps, respectively, of delta wing body combination
lower	refers to both lower surface flaps on pyramidal configuration
upper	refers to both upper (dihedral) surface flaps on pyramidal configuration
lower left	refers to left flap only on lower surface of pyramidal configuration
upper left	refers only to flap on left dihedral surface of pyramidal configuration

Increments (used with force data)

$$\Delta C_A \equiv C_{A_{\delta \neq 0}} - C_{A_{\delta = 0}}$$

$$\Delta C_m \equiv C_{m_{\delta \neq 0}} - C_{m_{\delta = 0}}$$

$$\Delta C_N \equiv C_{N_{\delta \neq 0}} - C_{N_{\delta = 0}}$$

Contrails

INTRODUCTION

Sudden and large changes in aerodynamic control characteristics frequently result when the airflow separates from a surface. The problem of flow separation, important for low speed flows, is even more severe for hypersonic flows because of the latter's high energy levels. Separated flows and their effects on control characteristics must be understood with reference to the future design of controllable hypersonic vehicles. This need led to the research investigation of hypersonic flow separation and control characteristics described herein. A comprehensive literature search, conducted at the outset of the investigation (Ref. 1), indicated a severe lack of hypersonic flow control data. To help fill the void, the subject investigation was principally experimental in nature, but includes some two dimensional flow analyses. To provide maximum usefulness of the test results as early as possible, they were presented without analyses in a series of widely available data reports (Refs. 2 through 23). Thus, the over-all program provides a broad base of experimental data required for the future development of analytical methods for estimating separation effects and aerodynamic control characteristics in hypersonic flows (see Fig. 1, page 2).

Pressure rises, due to trailing edge flaps for example, are propagated through the boundary layer and can cause separation far upstream of the flap. Depending on the severity of the separation, reattachment may not occur until the trailing edge of the flap (see sketch). In this event the load due to the pressure ahead of the flap may well exceed that due to the flap surface pressures (which are reduced by the blanketing separated flow), thereby reducing and possibly reversing the desired moment. In addition to causing possibly drastic shifts in loads, the high energy levels of hypersonic flows can cause extremely high heating rates and pressures at reattachment. Indeed, as shown herein, at reattachment the local pressures and aerodynamic heating rates can be more than twice as large as those at the stagnation points of blunt nosed entry configurations.

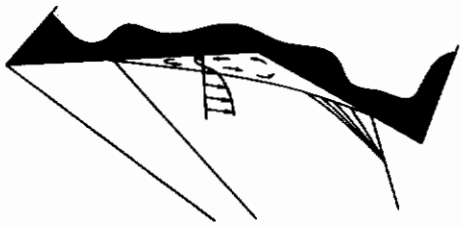

In hypersonic flows, pressure loads produced by compression surfaces are orders of magnitude larger than those produced by expansion surfaces. Consequently, effective aerodynamic controls usually involve compressions of the local stream flow (or pressure relief for

- - - - - - -

Manuscript released by authors in December 1964 for publication as an R&TD Technical Report.

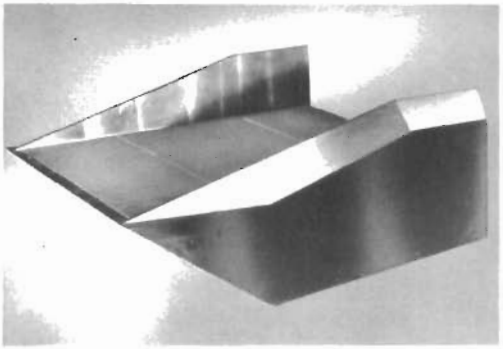

Separated Flows Ahead of Ramps
Fore and aft flaps, end plates
3 separate models:

1) Pressure and heat transfer, AEDC Tunnels A & B, M = 5 & 8, Refs. 5, 8, and 9.
2) Controlled wall temperature, pressure, AEDC Tunnel B, M = 8, Refs. 6 and 8.
3) Pressure and heat transfer, Grumman Shock Tunnel, M ≈ 13 & 19, Ref. 7.

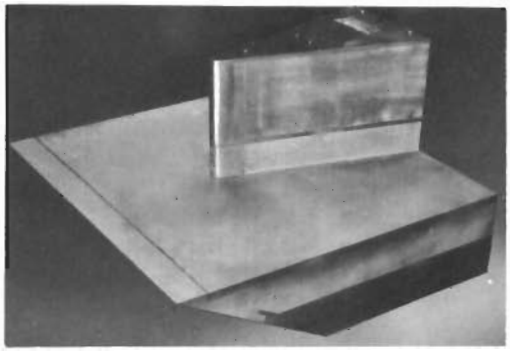

Fin-Plate Interaction
Small and large fins with sharp and blunt leading edges
2 separate models:

1) Pressure and heat transfer, AEDC Tunnels A & B, M = 5 & 8, Refs. 8 through 11.
2) Pressure and heat transfer, Grumman Shock Tunnel, M ≈ 13 & 19, Ref. 7.

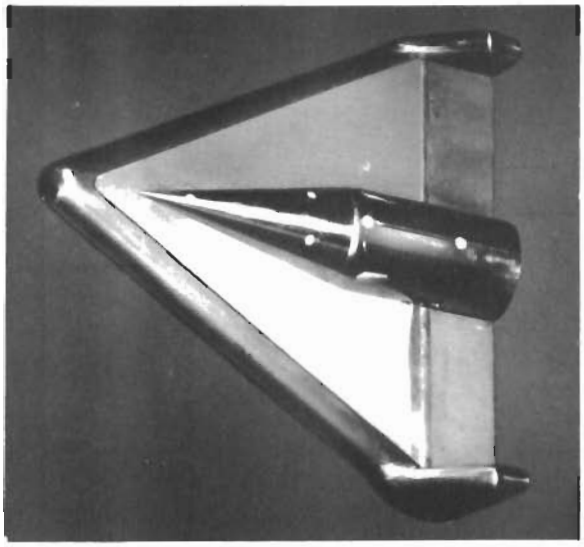

Clipped Delta, Blunt Leading Edge
Center body, T.E. flaps, drooped nose, spoiler, tip fins
3 separate models:

1) Pressure and heat transfer, AEDC Tunnels A & B, M = 5 & 8, Refs. 9 and 12 through 15.
2) Pressure, AEDC Hotshot 2, M ≈ 19, Refs. 16 and 17.
3) Six component force, AEDC Tunnels A & B, M = 5 & 8, Refs. 15 and 18.

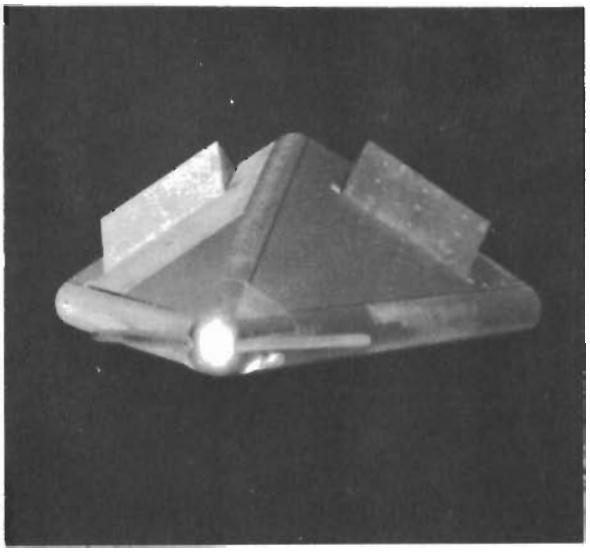

Pyramidal, Blunt Leading Edge, Dihedral
T.E. flaps, canard, ventral fin
3 separate models:

1) Pressure and heat transfer, AEDC Tunnels A & B, M = 5 & 8, Refs. 9 and 19 through 21.
2) Pressure and heat transfer, Grumman Shock Tunnel, M ≈ 21, Ref. 22.
3) Six component force, flap loads, AEDC Tunnels A & B, M = 5 & 8, Refs. 21 and 23.

Figure 1. Photographs of Models and Remarks for Over-All Program

preloaded control surfaces). Therefore, shock-induced separation ahead of compression surfaces is the most pertinent type for hypersonic controls and has received most attention (Ref. 1); it is the subject of the following two sections. Following these sections are summaries of the results of our investigations of flows over sharp expansion corners, and shock-wave boundary-layer interactions due to hypersonic flows past fins mounted on flat plates. The results include conclusions drawn from a substantial amount of hypersonic test data generated for the experimental portion of the investigation. The experimental techniques used in obtaining the data are described briefly and presented along with descriptions of the models.

In addition to pressure and heating rate distributions, force and moment data and flap loadings were obtained on two "typical" hypersonic flight configurations with assorted aerodynamic control surfaces (see Fig. 1). The data are used in describing the effects of separation on control characteristics and effectiveness. Literature sources of supplementary information on a wide variety of hypersonic aerodynamic controls are listed in the Appendix.

BOUNDARY LAYER METHODS FOR SEPARATED FLOWS

Boundary layer separation is generally well known to be a result of flow against a pressure gradient. Low-momentum layers, near a wall, that cannot overcome an adverse pressure gradient will slow down. If the normal component of the velocity gradient at the wall reaches zero, the boundary layer will separate from the wall. The point, where the shearing stress is zero, is defined as the separation point (in three-dimensional flow this is not a necessary condition for separation).

Despite this simple description, separation phenomena are rather complex. The adverse pressure gradient may be an effect of body geometry on the inviscid stream, or may be caused by a shock wave impinging on a boundary layer, or both. Thickening of a boundary layer from various causes including an adverse pressure gradient affects the pressure distribution. When significant, this phenomenon is known as a viscous interaction. Three-dimensional effects also complicate the problem. One might intuitively expect cross-flow of low energy layers near a wall to change the thickness of the boundary layer, affect the location and definition of the separation point, and distort the usual conception of a separation bubble.

Mathematically, the separation point in two-dimensional flow is a singularity in the boundary layer equations. To deal with the fluid mechanics rigorously in the neighborhood of this point requires the inclusion of more terms of the Navier-Stokes equations that are usually accounted for in boundary layer analysis.

Because of the complexity of a rigorous approach to the separation problem, attempts have been made, some more sophisticated than others, to use approximate or semi-empirical methods. In our previous survey (Ref. 1), we discussed the Crocco-Lees mixing theory and the attempts made to apply or modify it. This method, because of its complexity, and because it produces results that are no more accurate than simpler methods, seems to have been by-passed in the more recent investigations. A brief review of our work is presented below, followed by a summary of a few of the more promising of the recent investigations.

Modified Dorodnitsyn Strip Method

We attempted to use a Dorodnitsyn Strip Method (Ref. 24) modified as suggested by Donaldson (Ref. 25), to predict the location of a separation point together with velocity and temperature profiles within a separation bubble for two-dimensional or axially-symmetric laminar compressible flow.

The method appeared to have all the advantages of finite difference methods including the prospect of eventually allowing one to use second order terms of the Navier-Stokes equations. Also, it was hoped that increased accuracy could be attained eventually by using narrower strips.

The boundary layer was divided into N strips parallel to the wall. Across each strip, the momentum and energy equations were integrated. The integrand in each term was considered to be a linear function of the normal physical coordinate, z, which enabled us to use the trapezoidal rule to evaluate each integral.

The resulting set of simultaneous ordinary differential equations was solved with an Adam's Four Point numerical method on an IBM 7094 computer. We obtained reasonably accurate profiles for the compressible case with heat transfer and were able to predict the approximate location of the separation point, using a known adverse pressure distribution. We were not, however, able to pass through the separation point into the reverse flow region, apparently because of numerical instability of the solution.

The applicable numerical-stability criterion seems to follow the expression $\rho u(\Delta z)^2 / (\mu \Delta x)$, where ρ and u are the density and velocity, respectively; μ is the absolute viscosity; Δz, the strip width, and Δx the increment of the streamwise coordinate. The numerical value of this criterion at any strip must be greater than a certain positive number (see discussion in Ref. 26). Hence a negative velocity in the reverse flow region causes numerical instability. The criterion also limits the attainment of high accuracy without exhorbitant computer time; if Δz is divided in half then Δx must be divided by eight ($u \sim \Delta z$ near wall).

Summary of Selected Methods

We reviewed a large number of publications that have appeared since our previous survey (Ref. 1). However, rather than write an exhaustive supplement, we believed it would be more useful to limit our discussion here to a few that appeared to be both novel and promising either in method or results. The following four investigations seemed to fulfill this criterion.

Lees and Reeves (Ref. 27) developed an integral technique to predict pressure distributions generated by a viscous interaction in laminar flow. Integral techniques generally make use of polynomial expansions to express the velocity and enthalpy profiles in the various terms of the integral equations of the boundary layer. In the Pohlhausen method the coefficients of the polynomial are all expressed in terms of one parameter that relates the shape of the velocity profile in the boundary layer to the local pressure gradient. Lees and Reeves use a different parameter, following Tani (Ref. 28). This parameter is essentially the nondimensional slope of the velocity profile at the wall. However, rather than use a quartic polynomial expansion as Tani did, the authors use simple algebraic functions of

this parameter to represent flow terms of the integral equations. The functions were found by curve fitting the similar solutions of Cohen and Reshotko (Ref. 29), including the reverse-profile solutions for separated flow. Using these functions, the integral equations were solved simultaneously with a Prandtl-Meyer expression relating the inclination of the local external streamline with the local external Mach number. The results correlated rather well with experimental pressure distributions.

Erdos and Pallone (Ref. 30) exploit to good advantage the concept of a free interaction for both laminar and turbulent flows. A free interaction is defined as an interaction where the pressure distribution is not directly influenced by down-stream geometry. Chapman et al. (Ref. 31) found in their experiments, free-interactions up to the pressure-plateau region in laminar flow, and free-interactions up to the separation point in turbulent flow as shown in the following sketch.

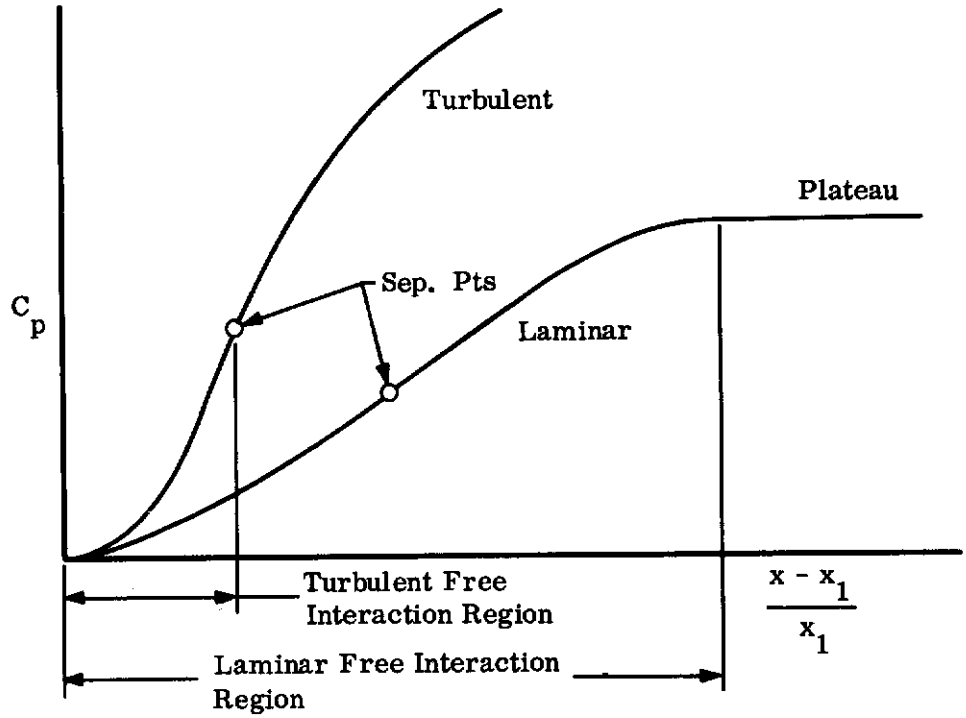

Erdos and Pallone follow the approach used in Ref. 31 and couple an inviscid linear relation with the boundary layer equations at a wall to derive an expression for the pressure distribution as follows:

$$C_p = \sqrt{\frac{\xi}{(Re_{x_1})^n}} \times f_3\left(\frac{x - x_1}{li}\right) \times g\left(M_1, \frac{T_{w_1}}{T_{\delta_1}}\right)$$

where C_p is the pressure coefficient based on conditions just upstream of the interaction;

Re_{x_1} is the Reynolds number based on x_1;

x is the streamwise surface distance; subscript 1 locates quantities in the local undisturbed flow just upstream of the interaction;

n = 1/2 for laminar flow and 1/5 for turbulent flow,

ξ is a factor to correct for the discrepancy between the inviscid linear relation and the nonlinear inviscid flow and has a value close to unity;

$f_3\left[(x-x_1)/li\right]$ is a universal function, determined empirically from a single set of pressure measurements (Ref. 31) for a free interaction (curves of f_3 are presented in Refs. 30 or 32 for both laminar and turbulent flow);

li is the length of the interaction region; and

$g(M_1, T_{w_1}/T_{\delta_1})$ is a function of the Mach number and ratio of wall temperature to temperature at the edge of the boundary layer, (this function is obtained from the solutions of Van Driest (Ref. 33), and plots of g are presented in Ref. 32).

This expression for the pressure distribution was used in conjunction with the boundary layer method of Ref. 34 to calculate reverse-flow profiles. Agreement with experimental data was good. Erdos and Pallone also derive an expression for the length of the interaction region that agrees reasonably well with experimental data.

They use the "dividing streamline" concept first suggested in Ref. 31 to develop an empirical method for calculating the length of the separating streamline and the locations of the separation and reattachment points for a compression corner.

Erdos and Pallone also show how the free-interaction concept can be used for estimating base pressure and the wake angle in the near wake of a slender body, by assuming that a free interaction occurs at the trailing shock. Further, they show how a shock interaction stronger than a free interaction must cause separation, throwing some light on the problem of incipient separation.

Pallone (Ref. 34) developed a modified Dorodnitsyn integral strip method combined with a Pohlhausen approach. The boundary layer was divided into a number of strips parallel to the flow and a set of governing equations for each strip was integrated from the wall to the boundary of each strip. Polynomial profiles were used to represent the flow terms in each strip. The set of ordinary differential equations that resulted was then solved numerically with an imposed

streamwise pressure gradient. This method was used successfully in the investigation discussed above (Ref. 30) to calculate reverse flow profiles in a separated region.

Libby et al. (Ref. 35) study effects of three-dimensional boundary layer flow in the neighborhood of a centerline of symmetry of a flat plate surface of a hypersonic inlet in laminar flow. Both a similar solution (with certain restrictions required for three-dimensional flow) and an integral method are used with known adverse pressure gradients. The solutions by both methods indicate that thinning of the boundary layer and delaying of separation can be quite significant as a result of the spilling of layers of low energy fluid near the wall away from the centerline of symmetry. The solutions also indicate, for the stream and body conditions considered, that very small angles of attack produce significantly large crossflows. The results indicate the general applicability of the method and, in particular, the applicability of the method to hypersonic control surfaces.

SEPARATION AHEAD OF RAMPS

Separation ahead of a ramp is probably the most important single type of separation pertinent to investigations of aerodynamic control characteristics. Depending on the flow conditions and the height of the ramp, the flow may or may not reattach on the ramp surface. Further, the separation can be either of the "free interaction" type mentioned in the preceding section, or can be influenced by downstream conditions. Flow separation ahead of ramps has been the subject of many experimental investigations in the supersonic range, however hypersonic flow data are sparse.

Models of simple geometry are essential for basic studies of flow separation phenomena. Accordingly, we tested flat plate models with various ramp shaped flaps. Pressure and heat transfer data were obtained for flows ahead of full and partial span trailing edge ramps (flaps) for wide ranges of ramp angles, plate angles of attack, and free stream conditions (Refs. 5 through 9). Three wind tunnel models were required to investigate aspect ratio, end plate, and wall temperature effects on separation for various Reynolds numbers and nominal free stream Mach numbers of 5, 8, 13 and 19. (See **sketch and pages 41 - 60** herein for descriptions of test facilities, ranges of test variables, and models.)

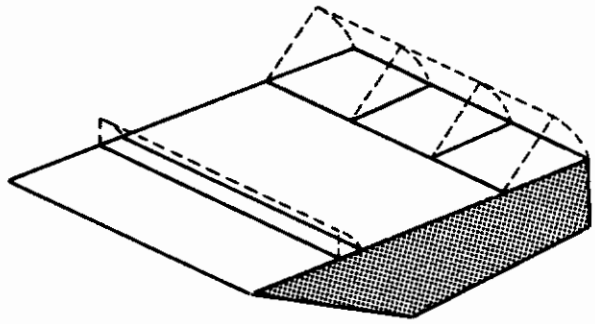

The models had square planforms and 25 percent chord trailing edge ramps. One of the models also had a forward ramp that could be deflected at angles up to 90° with respect to the flat plate surface. In addition to providing data for flows ahead of forward facing steps (or "spoilers"), the forward ramp provided data for examining leading edge effects. Further, it provided data for wider ranges of ramp aspect ratios and running length Reynolds numbers, Re_x. The ramp chord to plate length ratio was the same for the forward ramp as for the trailing edge ramps. For the same free stream conditions, the running length Reynolds numbers for the forward ramp data were one-third those for the trailing edge ramp data.

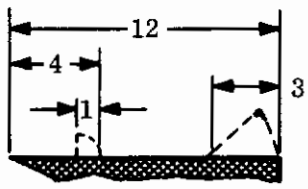

Evidence of the importance of Reynolds number effects is given by the sample forward ramp data shown in Fig. 2.

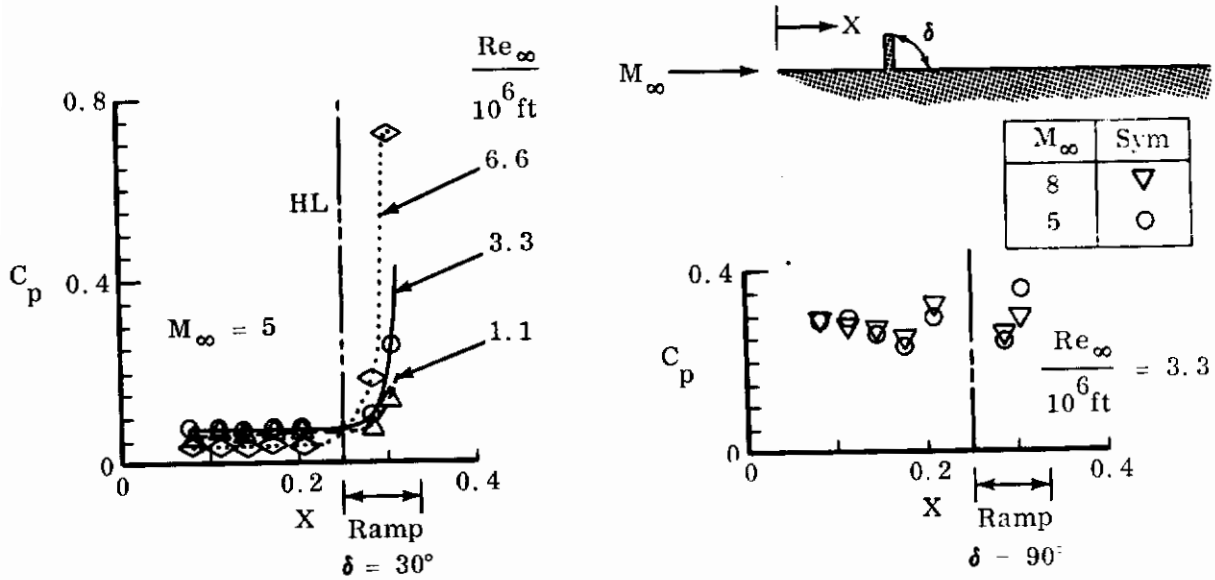

Figure 2. Centerline Pressure Distributions on Plate and Face of Forward Ramp (step) for $\alpha = 0$

Pressures measured on the flat plate and ramp surfaces were nondimensionalized with respect to free stream conditions and presented in standard coefficient form. The pressure coefficients are plotted versus X, the streamwise surface distance nondimensionalized with respect to the model length (see Fig. 26 , page 50). Based on the total model length (12 inches), the forward ramp hinge line is at X = 0.250 and its trailing edge is at X = 0.333. The pressures exceed the flat plate value ahead of the hinge line but do not reach their maximum values on the 30° ramp until near the ramp trailing edge. These separation effects become more pronounced for the thicker boundary layers (lower Re_∞ values) and higher pressure rises (larger ramp deflections). Indeed, the plate pressures in the separated flow region ahead of the forward facing step were essentially equal to those on the face of the step.

Pressure distributions for flows over full span, 30° trailing edge ramps are presented in Fig. 3. The pressure distributions and extent of the separated flow regions are affected markedly by changes in the free stream unit Reynolds numbers. Regarding the forward ramp data, the separation effects become more pronounced for the thicker boundary layers (due to either lower Re_∞ or higher M_∞ values). The separation point moves upstream with decreasing Reynolds number and reattachment is delayed. The inviscid wedge values (obtained from shock tables for 30° wedges) are not attained until considerably downstream of the hinge line.

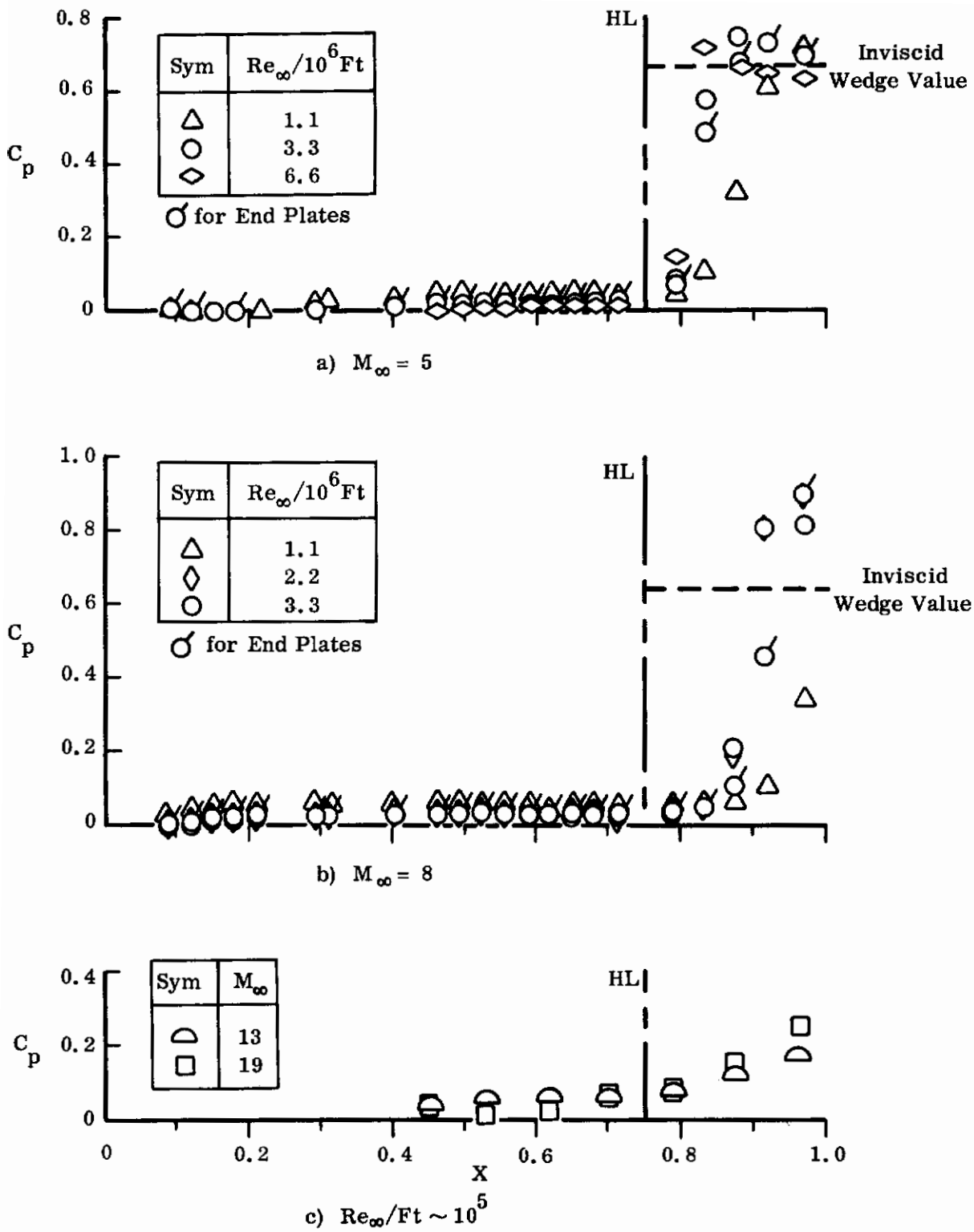

Figure 3. Pressure Distribution for Flows Over Full Span, 30° Ramps on a Flat Plate at $\alpha = 0$

For the same Reynolds number, the extent of separation increases with Mach number. Further, although the available variation in Re_∞ was smaller, the pressure distributions indicate the increased importance of Reynolds number effects with increasing Mach number. Thus, for the Mach 8 data, laminar separation near the plate leading edge was observed for Re_∞ /ft = 1.1 million, whereas transitional separation was observed for Re_∞ /ft = 3.3 million. Photographic evidence of this (but for a 5° model angle of attack) is provided by the shadowgraphs shown in Fig. 4.

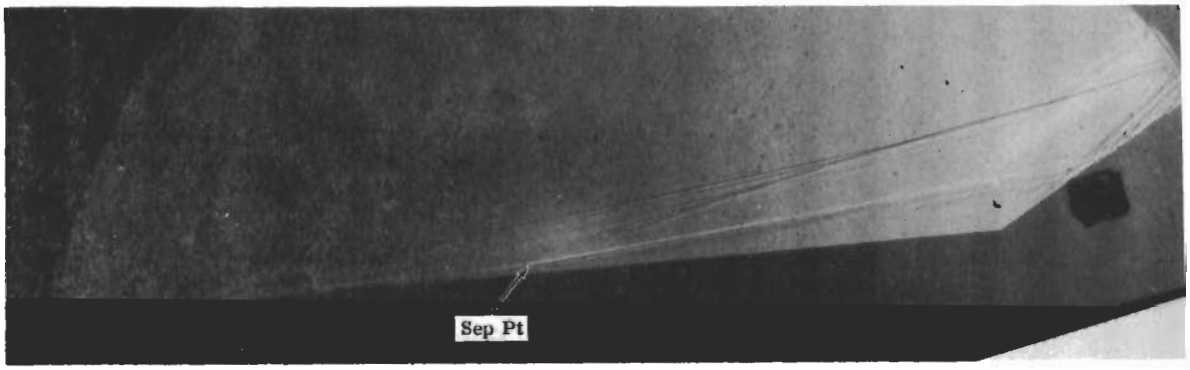

a) Re_∞ /ft = 1.1 Million

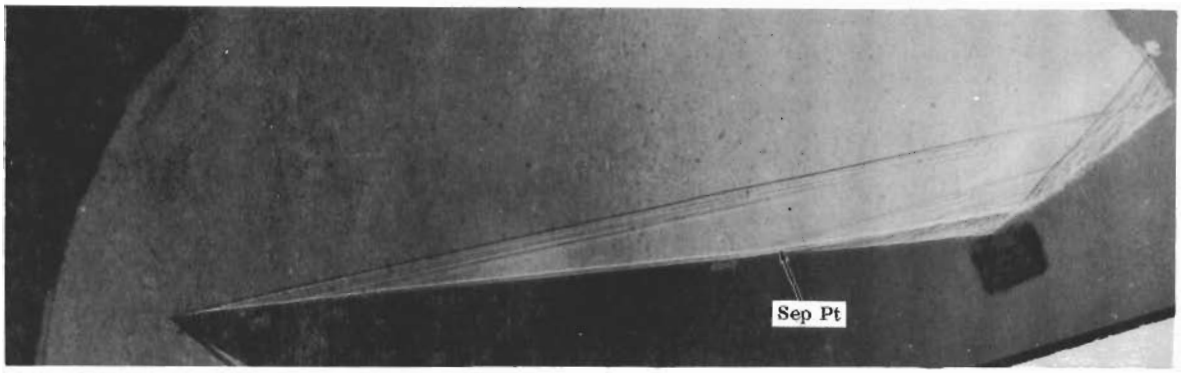

b) Re_∞ /ft = 3.3 Million

Figure 4. Shadowgraph Photographs for Mach 8 Flows Over a Full Span 30° Ramp on a Flat Plate at 5° Angle of Attack

Finite span effects are examined by comparing pressure distributions for full span trailing edge ramps with and without end plates and for a partial span trailing edge ramp (Figs. 3 and 5). The ramp and model geometry are described **on pages 47-52 herein (see also Fig. 1, page 2, for a photograph of the model with end**

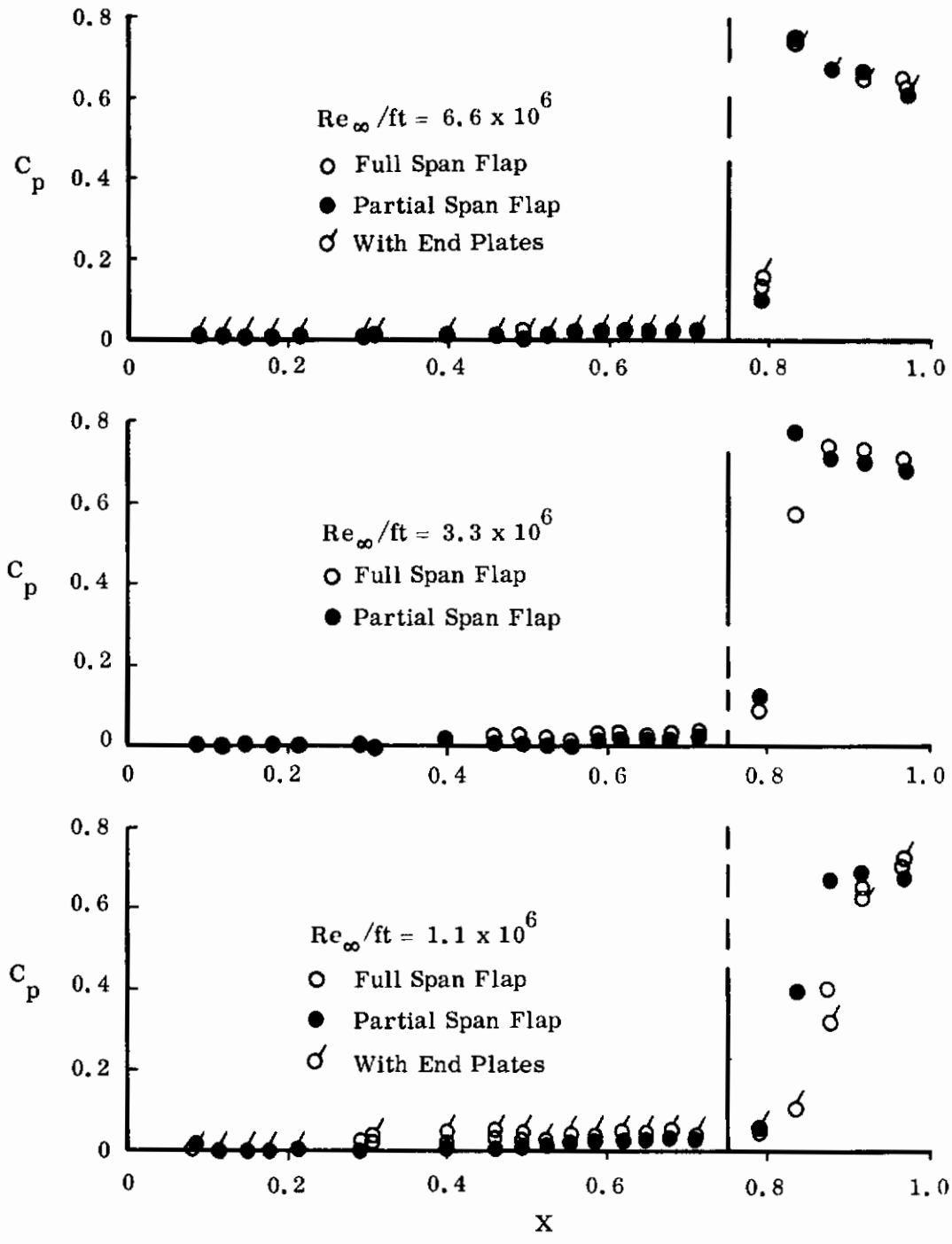

Figure 5. Pressure Distributions for Mach 5 Flows Over Full and Partial Span, 30° Ramps on a Flat Plate at α = 0

plates). The extent of separation is least for the partial span ramp and greatest when the full span ramp is end plated. Crossflow venting of the vortical reverse flow in the separated region ahead of the ramp is easiest for the partial span ramp but is essentially prevented by the end plates. These crossflow effects are more pronounced for the lower Reynolds numbers, higher Mach numbers, and higher pressure rises.

Indeed, for Mach 8 flows over 45° ramps, the end plates strongly influence the surface pressure distributions (see Fig. 6). The flow separates near the leading edge of the flat plate and doesn't reattach until near the ramp trailing edge. The end plates prevent venting of the separated reverse flow and delay reattachment. Thus, they substantially increase the amount of "trapped" flow in the separated region and lead to a considerably larger dividing streamline angle at separation. This results in the larger pressures measured on the flat plate surface. It is also indicated in Fig. 6 that the ramp pressures fall far below the estimated inviscid values (constant C_p values; the curves faired through the data points are only for clarity and do not represent analytical values). Indeed, with end plates, the force due to the ramp pressures may well be less than that due to the plate pressures upstream of the hinge line, with possible drastic consequences for the characteristics of ramp shaped controls on hypersonic vehicles.

Even when the model was pitched 5°, making the flat plate surface leeward, the end plates led to positive pressure coefficients on the plate surface. These pressures are comparable to those obtained at $\alpha = 0$ without end plates (Fig. 6). The inviscid wedge value of the ramp pressure coefficient was calculated using Prandtl-Meyer expansion for 5° from Mach 8 and then estimating the pressure rise due to a sonic wedge shock wave. As for the $\alpha = 0$ case, the end plates cause the pressures on the ramp surface to be far less than the inviscid values.

Without end plates, the maximum ramp pressures exceeded the inviscid wedge values in several instances (Figs. 6 and 7). In Fig. 7 the Mach 5 and 8 pressure data are compared for trailing edge, full span, ramps on flat plates at $\alpha = 0$ for various ramp angles. For ramp deflections of 30° and less, the pressure coefficient distributions ahead of the hinge line are insensitive to the change in Mach number. On the other hand, Mach number effects are quite pronounced on the ramp surface, especially near reattachment. The Mach 8 data presented in Fig. 7 for the 45° ramp were obtained from a different test run than those presented in Fig. 6. The repeatability of the data can be seen by comparing the pressure distributions in the two figures.

Very high pressures were measured near reattachment on the ramp surfaces when the model was pitched at positive angles of attack (flat plate windward). The possibility of high local loads at reattachment is due to the comparatively gradual compression of the flow through many oblique shock waves, thereby avoiding strong normal shock wave losses. Typical cases, for a 30° full span trailing edge ramp, are shown in Fig. 8 for both positive and negative angles of attack

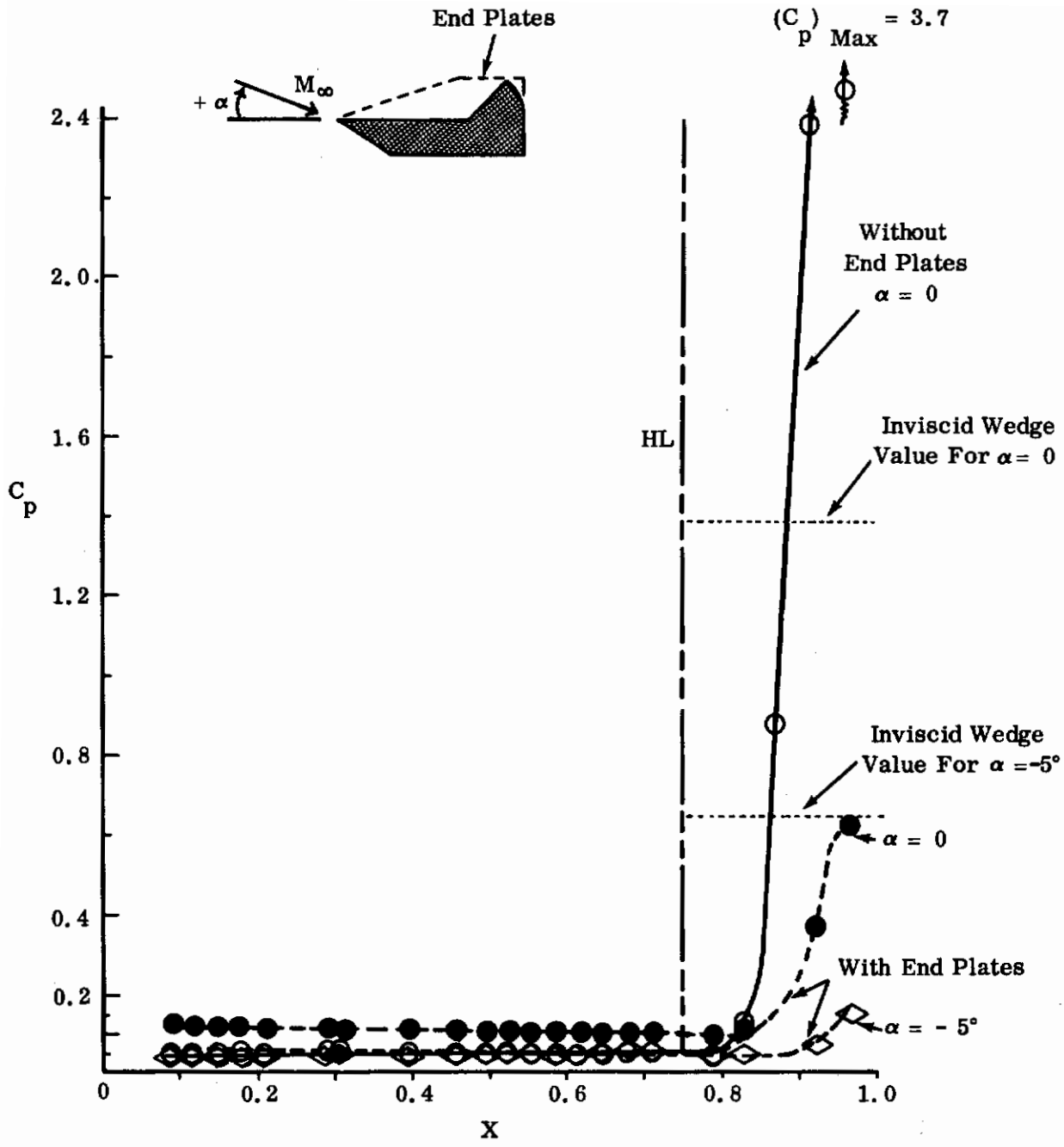

Figure 6. Centerline Pressure Distributions for Mach 8 Flows Over Full Span, 45° Ramps; Re_∞/ft = 3,300,000

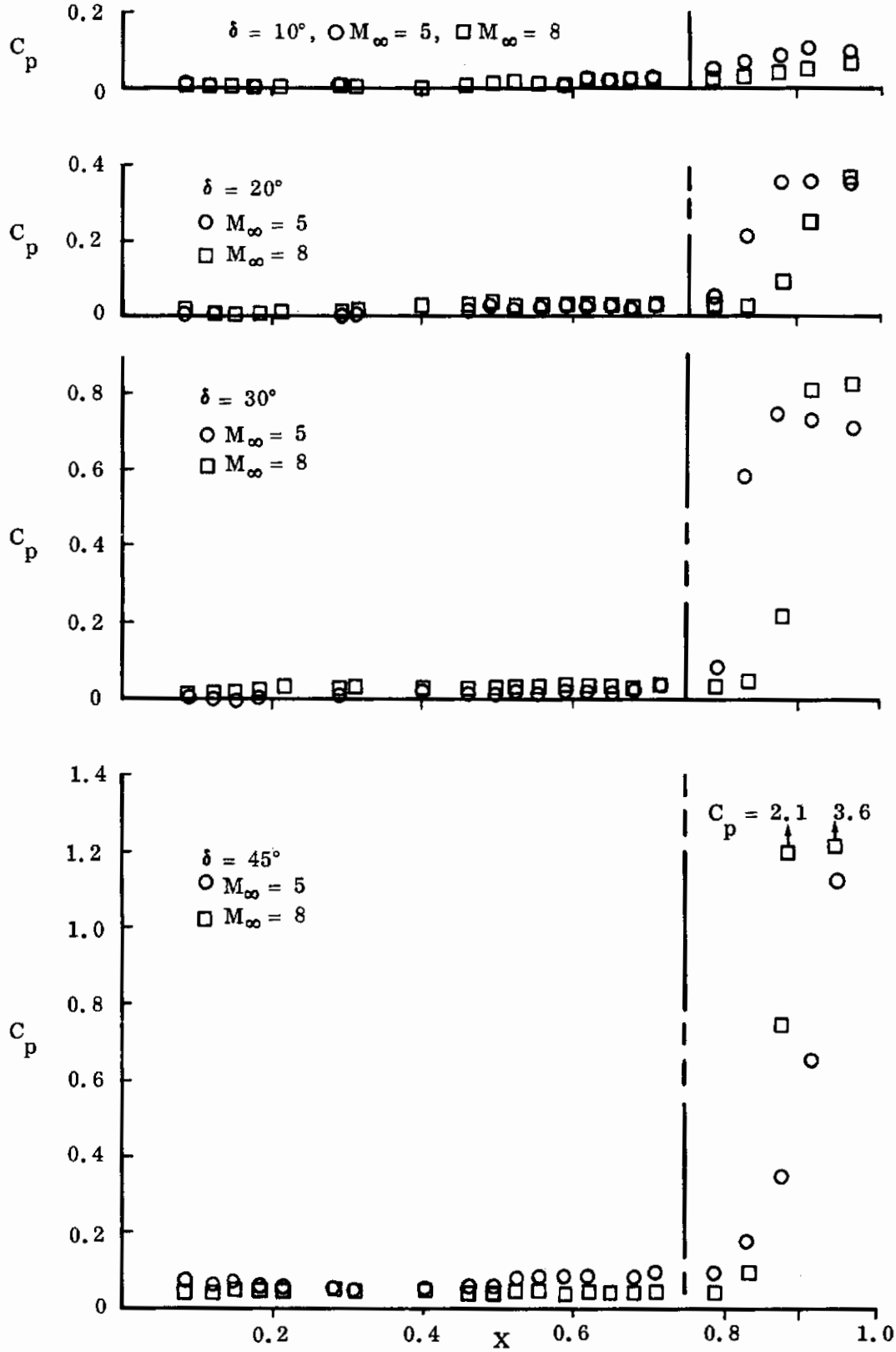

Figure 7. Pressure Distributions for Mach 5 and 8 Flows for Various Full Span Ramp Angles; $\alpha = 0$ and $Re_\infty/ft = 3,300,000$

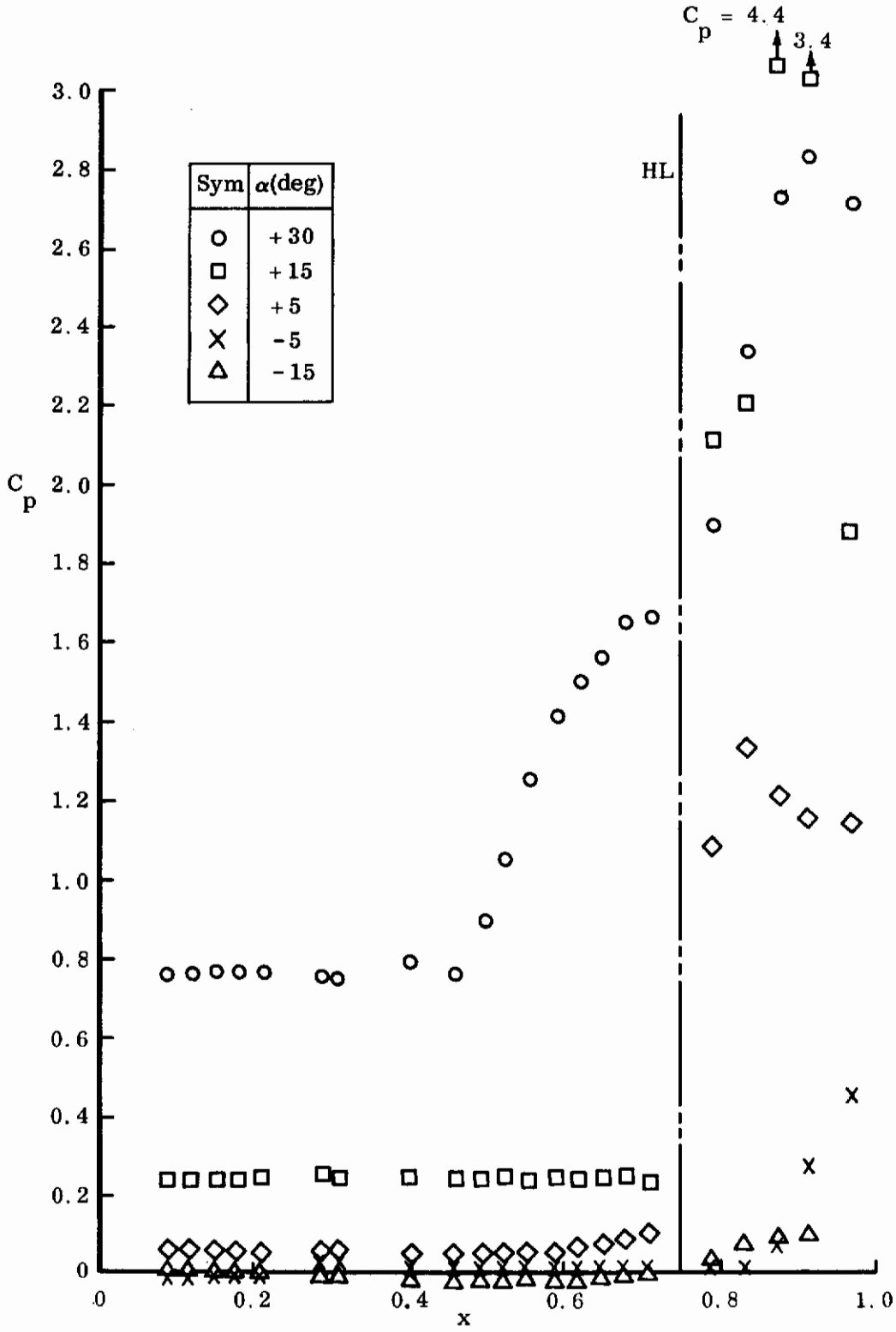

a) Mach 5 Data

Figure 8. Pressure Distributions for Flows Over Full Span, 30° Ramps for Various Angles of Attack for Re_∞ /ft = 3,300,000 (sheet 1 of 2)

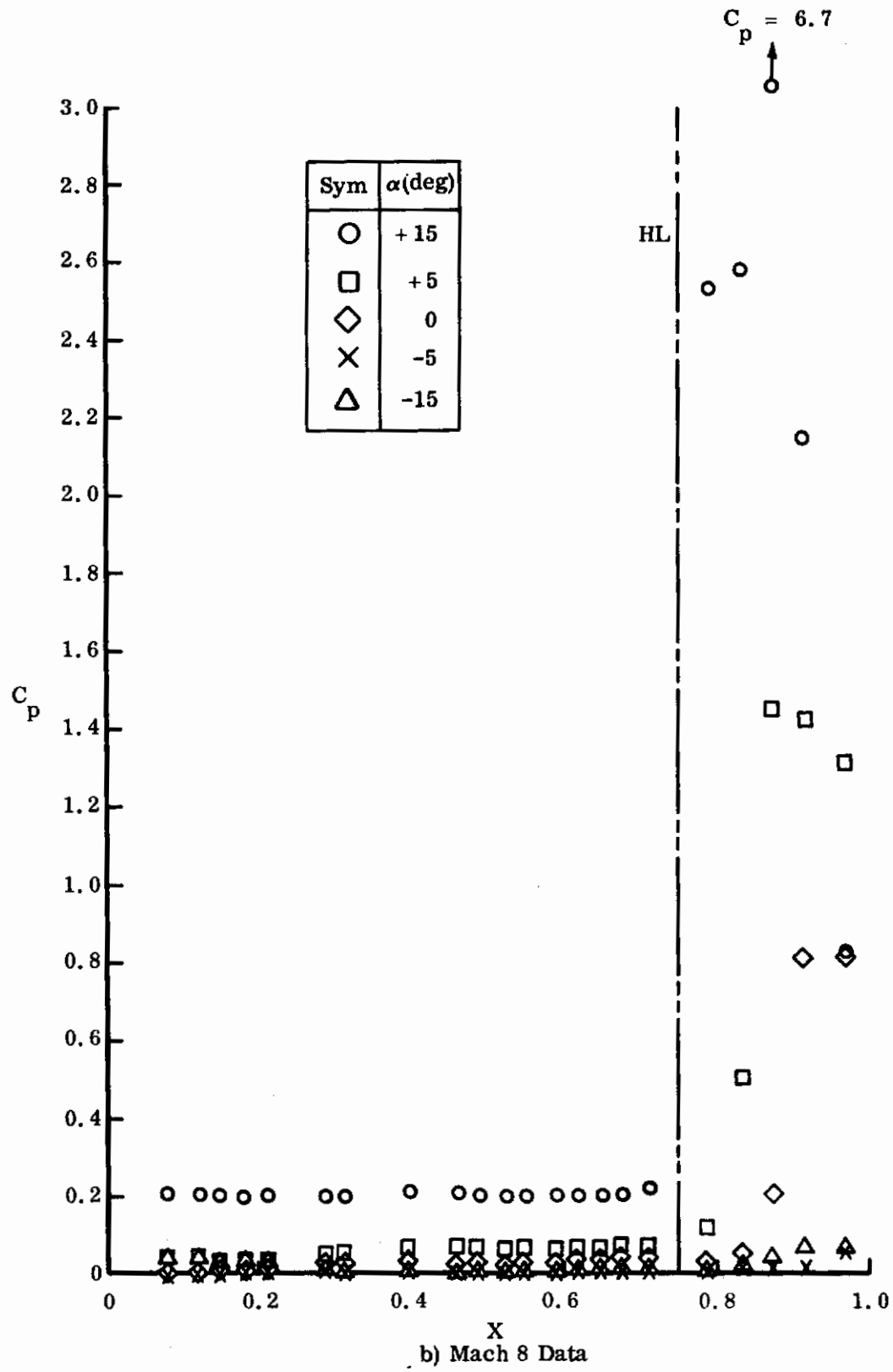

b) Mach 8 Data

Figure 8. Pressure Distributions for Flows Over Full Span, 30° Ramps for Various Angles of Attack for Re_∞/ft = 3,300,000 (sheet 2 of 2)

(referenced to the flat plate surface) for unit free stream Reynolds numbers of 3.3 million. Mach 5 data are presented in Fig. 8a and Mach 8 data are presented in Fig. 8b.

Sample heat transfer data, obtained for $M_\infty = 8$, 13, and 19, are presented in Fig. 9. The aerodynamic heating rates, $\dot{q}$ (BTU/ft^2 sec), are plotted versus the same nondimensional distance X as for the pressure coefficients. To obtain essentially centerline distributions for both the pressure and heat transfer data, it was necessary to offset slightly from the centerline both the pressure taps and thermocouples in the heat transfer models (see Fig. 26, page 52). Heating rates obtained for flows over 30°, full span, trailing edge ramps are shown in Fig. 9 for three free stream unit Reynolds numbers. The heat transfer rates decrease from their leading edge values to almost zero at the separation point, increase gradually within the separation zone and increase abruptly at reattachment. The heat transfer rates are very strongly dependent on Reynolds number values near reattachment. Reynolds number dependence for flat plates without ramps can be accounted for by presenting the data in terms of Nusselt number/ $\sqrt{Re_x}$, as done in the data reports (Refs. 5 and 7), but this parameter loses significance for the ramp data.

In addition to investigating flow separation effects on the aerodynamic heating rates, we investigated the effects of wall temperature on flow separation. This was particularly **desirable** because the heating rate distributions were obtained on essentially cold wall models whereas the corresponding pressure distributions were obtained on hot wall models (**see pages 41 through 60**). **Sample** data, obtained using an internally cooled model, **are** shown in Fig. 10 for two different wall temperature levels. Again, pressure coefficients are plotted along the center line of the flat plate and surface of a 30°, partial span, trailing edge ramp. Without cooling, the plate and ramp wall temperatures, T_w (°R), attained their equilibrium (zero heat transfer) values, T_{aw} (°R). The wall temperatures were reduced to about a third of these values with internal cooling. The wall temperature effects on pressure distributions are compared for three free stream unit Reynolds numbers. Additional data for examining wall temperature effects are readily available in Ref. 6.

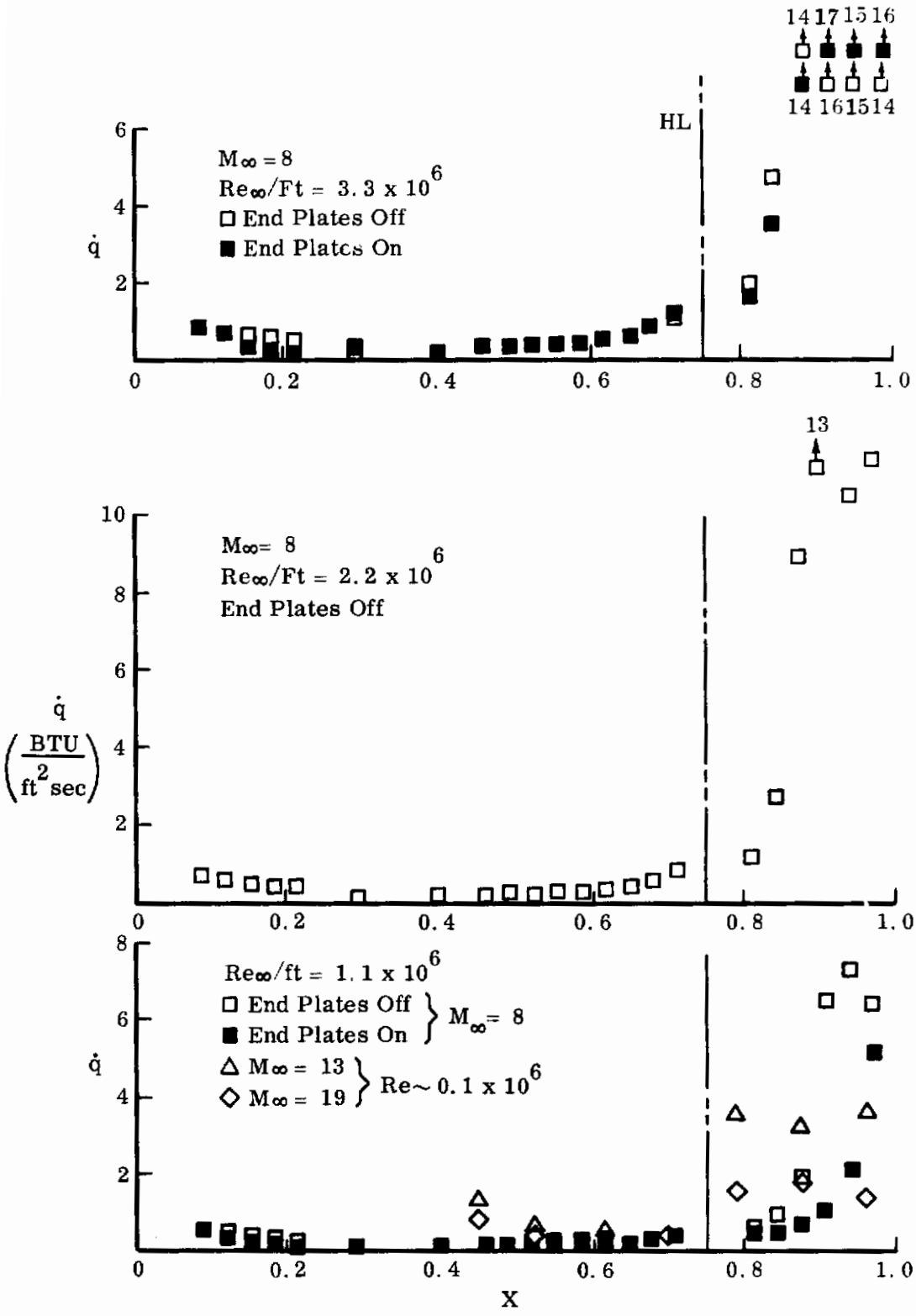

Figure 9. Aerodynamic Heating Rates for Flow Over Full Span, 30° Ramps on a Flat Plate at $\alpha = 0$

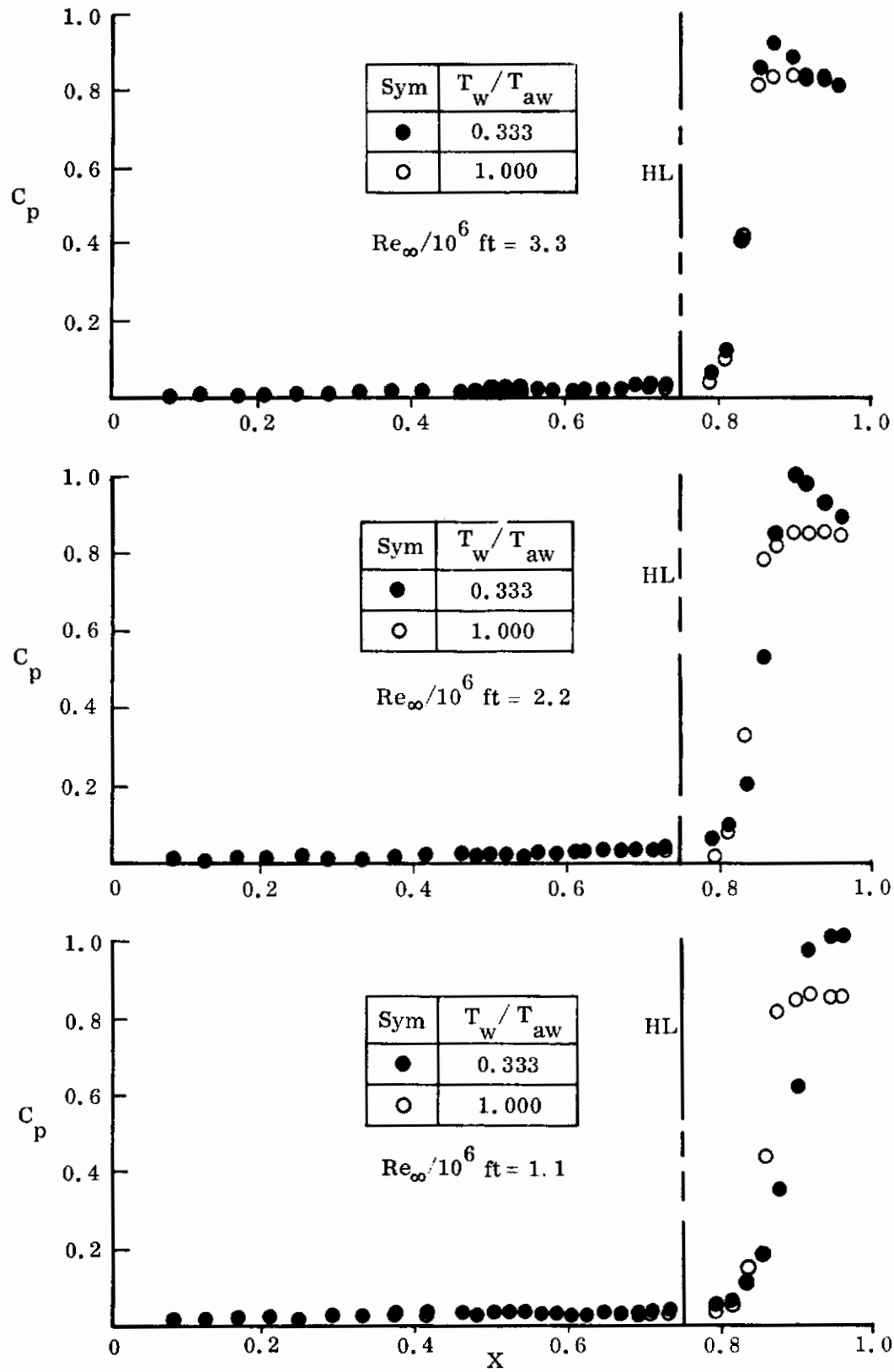

Figure 10. Wall Temperature Effects on Pressure Distributions for Mach 8 Flows Over a Partial Span, 30° Ramp on a Flat Plate at $\alpha = 0$

FLOWS OVER EXPANSION CORNERS AND DOWNSTREAM OF RAMPS

Further insight into the fundamental fluid processes responsible for flow separation was gained by investigating the causes of "breakaway" separation. This type of separation occurs at convex corners where the local, inviscid pressure gradient is favorable such as the flow breakaway from the leading edge of a leeward surface or from the corner of a rearward facing step (see sketch). Because the local pressure gradient is favorable, in the inviscid sense, there was controversy as to the cause of breakaway separation (Ref. 1).

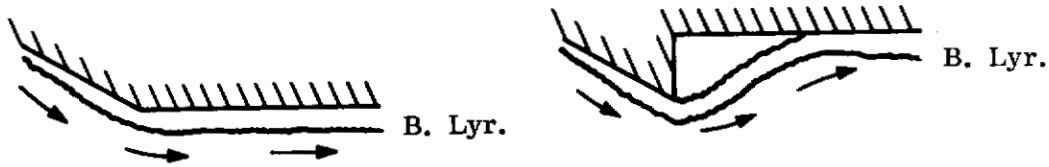

Our investigations of flows over expansion corners, downstream of ramps, and on leeward surfaces, indicate that separation will not occur without adverse pressure gradients. Thus, as for standard boundary layer separation, adverse pressure gradients are the prime cause of breakaway separation. However, the pressure rise responsible for breakaway separation can be far downstream of the separation point; its effects are propagated upstream through the subsonic portion of the boundary layer.

For example, flow separation from the leading edge of a leeward surface is attributed to the eventual downstream pressure rise required to recompress the flow at the trailing edge. This type of separation was investigated using the flat plate models with trailing edge flaps mentioned in the preceding section (see also Ref. 6, Part III). The flow was observed (through a ground glass shadowgraph viewing screen) as the model was slowly pitched through an angle of attack range, making the flat plate surface leeward, and then returned to zero. As the plate surface became more leeward, the separation point moved, comparatively rapidly, upstream to the sharp leading edge of the flat plate. Although rapid, the upstream movement of the separation point was continuous and, moreover, the process was reversible as the angle of attack was returned to zero. The procedure was repeated for different free stream Reynolds numbers (for $M_\infty = 8$) and pressure distributions were recorded at discrete angles of attack (Ref. 6). There was no sudden breakaway of the flow from the leading edge but rather a rapid extension of the separated flow region due to the pressure rise over the after portion of the model.

Separation behind rearward facing steps and ramps also can be attributed to the upstream propagation of adverse pressure gradients. Pressure rises at reattachment and our investigations of flows downstream of ramps are described after the following subsection. To assess the importance of adverse pressure gradient effects on breakaway separation, we investigated flows over simple expansion corners for which there were no downstream recompressions. In these cases, even for machined sharp expansion corners, there was no flow separation.

Flows Over Expansion Corners

Before our research into the problem, we had conjectured, primarily intuitively, that high speed flows could not negotiate sharp expansion corners without breaking away from the surface and forming at least a small bubble of separated flow immediately downstream of the corner. For supersonic flows over expansion corners the streamwise pressure gradient is negative and therefore favorable for attached boundary layers. However, the standard boundary layer assumption requiring that the surface curvature be small in comparison to the boundary layer thickness is violated at the sharp corner. Therefore, standard boundary layer methods are inapplicable and so, strictly **speaking, their indication that separation is caused by positive pressure gradients need not be true.**

Further, for flows over sharp expansion corners, there are large pressure gradients normal to the surface (in contrast to the standard boundary layer result $\partial p/\partial z = 0$). Thus, nondimensionalizing the curvilinear Navier-Stokes equations **(see Ref. 36, p.98)** and performing an order of magnitude analysis, the pressure variation across the boundary layer is found to be of the same order of magnitude as the pressure itself $[\Delta p = O(p)]$ for small corner radii $[r = O(\delta)]$. The normal momentum equation must be retained and $\partial p/\partial x$ cannot be replaced by dp/dx.

Indeed, in the attempt to apply momentum integral methods to the problem, both fourth (Ref. 36) and sixth (Ref. 37) degree velocity polynomials resulted in "bowed" or "popped" velocity profiles for $r < O$(running length of boundary layer). These profiles indicate velocities within the boundary layer exceeding those outside (sketch). **Bowed velocity profiles can be avoided by using exponential functions rather than simple polynomials (Ref. 38), but still it appears that the use of standard momentum integral methods for expansion corner flows should be limited to finite corner radii $r \gg \delta$.**

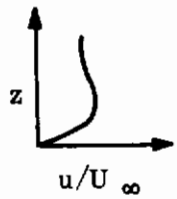

Abandoning standard boundary layer methods, simple approaches to the problem are to neglect or to avoid the sharp corner singularity. By assuming similar boundary layer profiles, displacement and momentum thicknesses and their ratios across the singularity can be calculated in terms of the inviscid flow conditions upstream and downstream of the corner. Of course, this masks the nature of the flow in the immediate vicinity of the corner. A similar approach makes use of flat-plate boundary-layer solutions upstream and downstream of the corner and joins them by ignoring wall shear in the vicinity of the corner (Ref. 39). The singularity is thus avoided by assuming a separated flow bubble (zero shear) that effectively rounds the sharp corner.

A more promising approach (in the hindsight of our experimental research), assumes that separation does not occur but that a new viscous sublayer starts on the downstream surface at the sharp expansion corner (Refs. 40 and 41). The upstream boundary layer is expanded inviscidly about the corner, both subsonic and supersonic layers, and superimposed on the new viscous sublayer. We applied the rotational characteristics method to the inviscid expansion of the supersonic portion of the shear layer and analyzed the flow field. Immediately downstream of the corner the shear layer velocity profiles are bowed. As expected, there are large, normal pressure gradients ($\partial p/\partial z > 0$); and the streamwise pressure gradients are favorable along every streamline in the flow field ($\partial p/\partial x < 0$).

Surface pressures were measured for flows over sharp and rounded expansion corners for various free stream Mach numbers and angles of attack (see **pages 47 through 52 herein and Refs. 5 through 8**). Steamwise pressure data along model center lines are presented in Figs. 12 through 14. The data are given in standard coefficient form, $C_p = (p - p_\infty)/q_\infty$, nondimensionalized with respect to free stream conditions (upstream of the wedge leading edge shock), and angles of attack are referenced to the flat plate surface downstream of the expansion corner (see Fig. 11). Because of the closeness of the data points (both C_p and X values, see Fig. 26), faired data curves are presented in this section for clarity; they do not represent

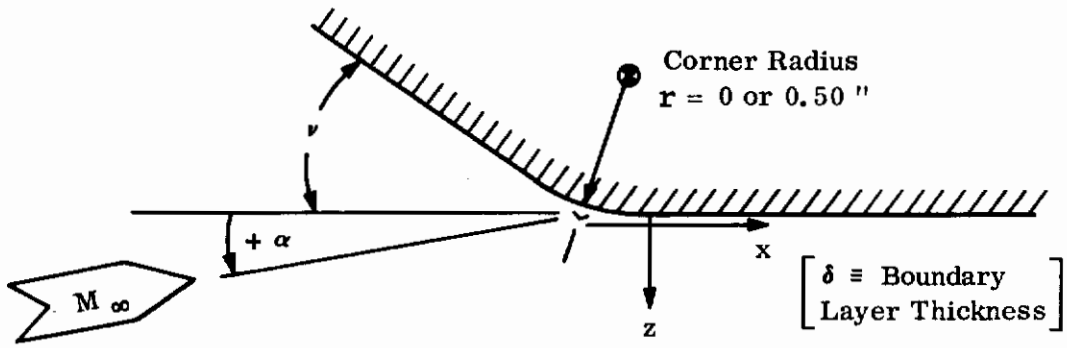

Figure 11. Nomenclature for Expansion Corner Flows

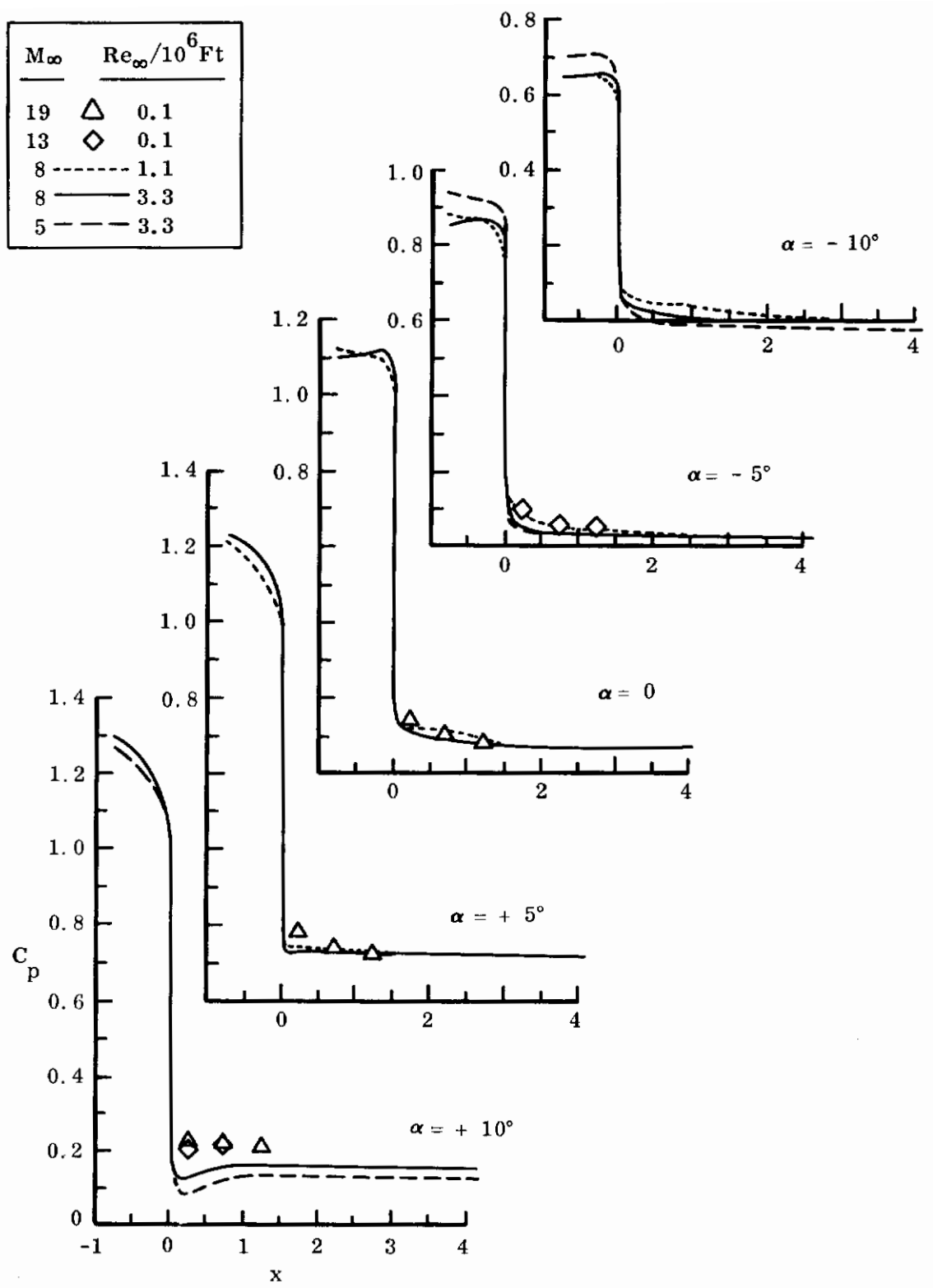

Figure 12. Pressure Distributions for Flows Over Sharp, 40° Expansion Corners

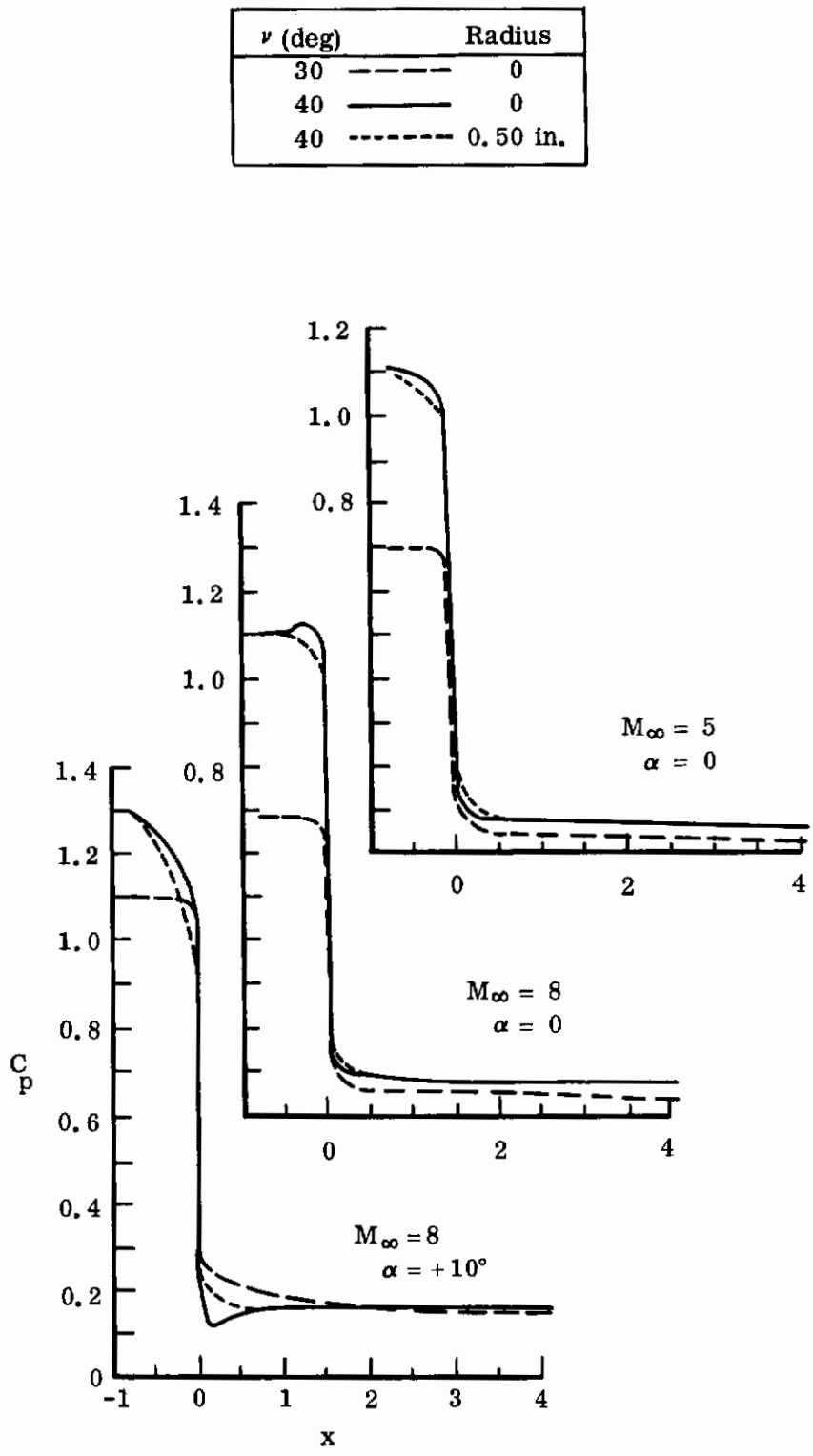

Figure 13. Expansion Corner Shape Effects on Pressure Distributions for $Re_\infty/10^6$ ft = 3.3

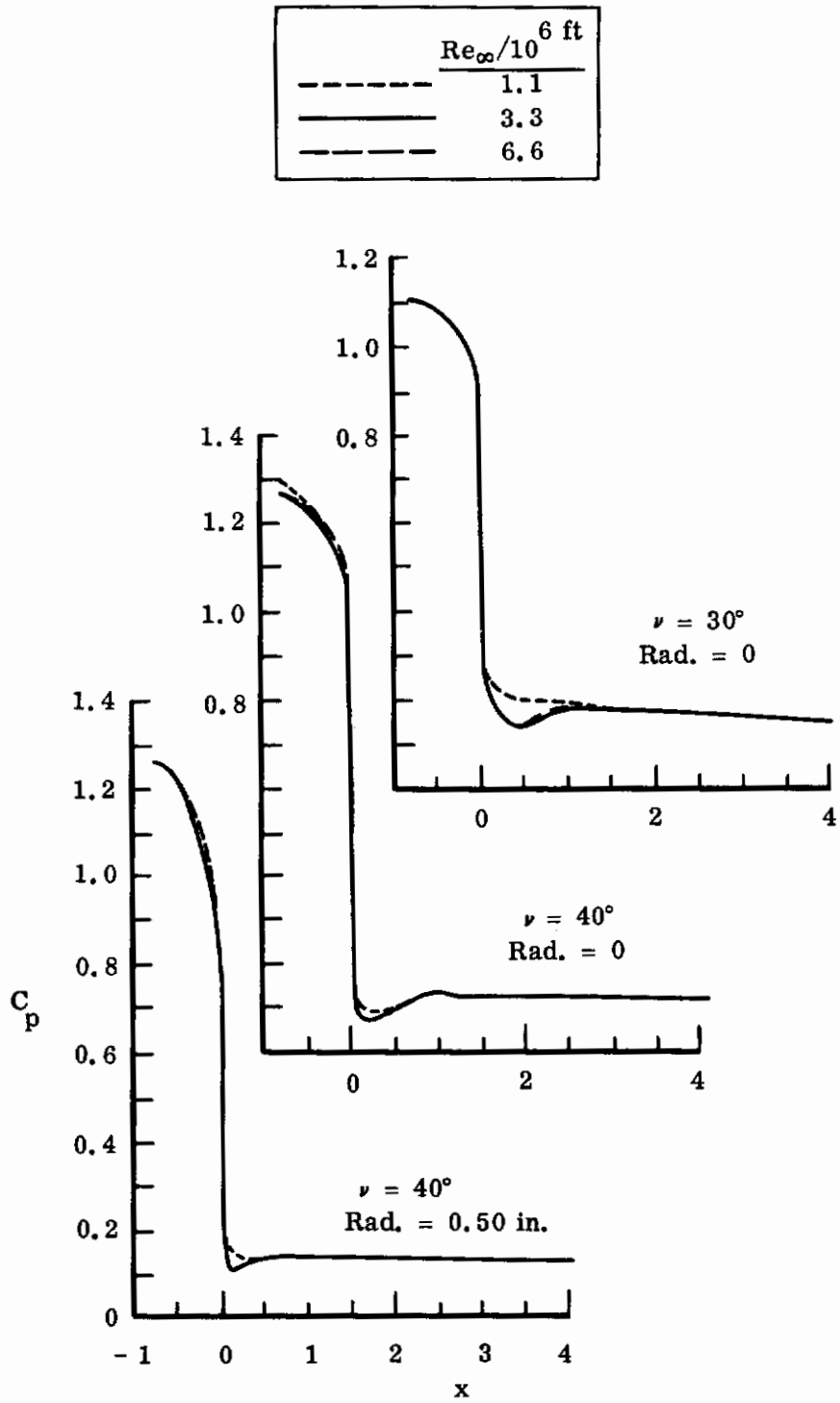

Figure 14. Reynolds Number Effects for Mach 5 Flows Over Expansion Corners for $\alpha = +10°$

analytical values.

The pressures measured downstream of the corners were slightly larger than those calculated by the rotational characteristics method described above, and these values, in turn, were slightly larger than those calculated using the simple, inviscid, shock expansion method. In all cases where the wedge leading edge shock was attached, the calculated values were quite close to the measured values downstream of the corner region.

In cases where the wedge leading edge shock is detached, there is a large drop in the pressure upstream of the corner. The measured pressures are less than those corresponding to sonic wedge flow. In some of these cases (for the higher Reynolds numbers), there is a characteristic dip in the pressure distribution immediately downstream of the corner (Figs. 12 through 14), followed by a recompression. For subsonic wedge flows there is a sonic line at the corner on the upstream surface. Expansion waves from the corner are reflected from the sonic line as compressions and are responsible for the recompressions in the figures. For very strong recompressions, like those on a flat-nosed plate, the adverse pressure gradient due to the recompression can cause a small separated flow bubble immediately downstream of the corner (Ref. 42, page 417 and 705). This again shows the dependence of separation on adverse pressure gradients.

Rearward and forward facing Stanton tubes at two stations (0.25 and 0.50 inches) downstream of the corners gave no evidence of any separation. For every test condition, every forward facing tube measured a higher total pressure than that measured by the corresponding rearward facing tube. Further, the rearward facing tubes gave pressures lower than the local surface static pressures. These results are the prime experimental evidence that there was no separation downstream of the sharp expansion corners.

Sample total pressures measured by the forward facing Stanton tubes are shown in Fig. 15. Although there were insufficient tubes to obtain boundary layer profiles (just three forward and three rearward facing tubes on each model, see "Experimental...Models" section and Refs. 5, 6 and 10, the data were sufficient to indicate that the boundary layer thicknesses downstream of the corners were substantially larger than those calculated immediately upstream of the corners.

The Stanton tubes didn't affect the downstream surface pressures, but did affect severly the aerodynamic heating rates measured at the same spanwise stations. These effects were limited to the wakes behind the tubes and did not extend inboard to the model centerlines. Sample centerline heating rate distributions downstream of the two dimensional corners are presented in Fig. 16. Heating rates downstream of axisymmetric corners (cone-cylinders) are presented in Ref. 41.

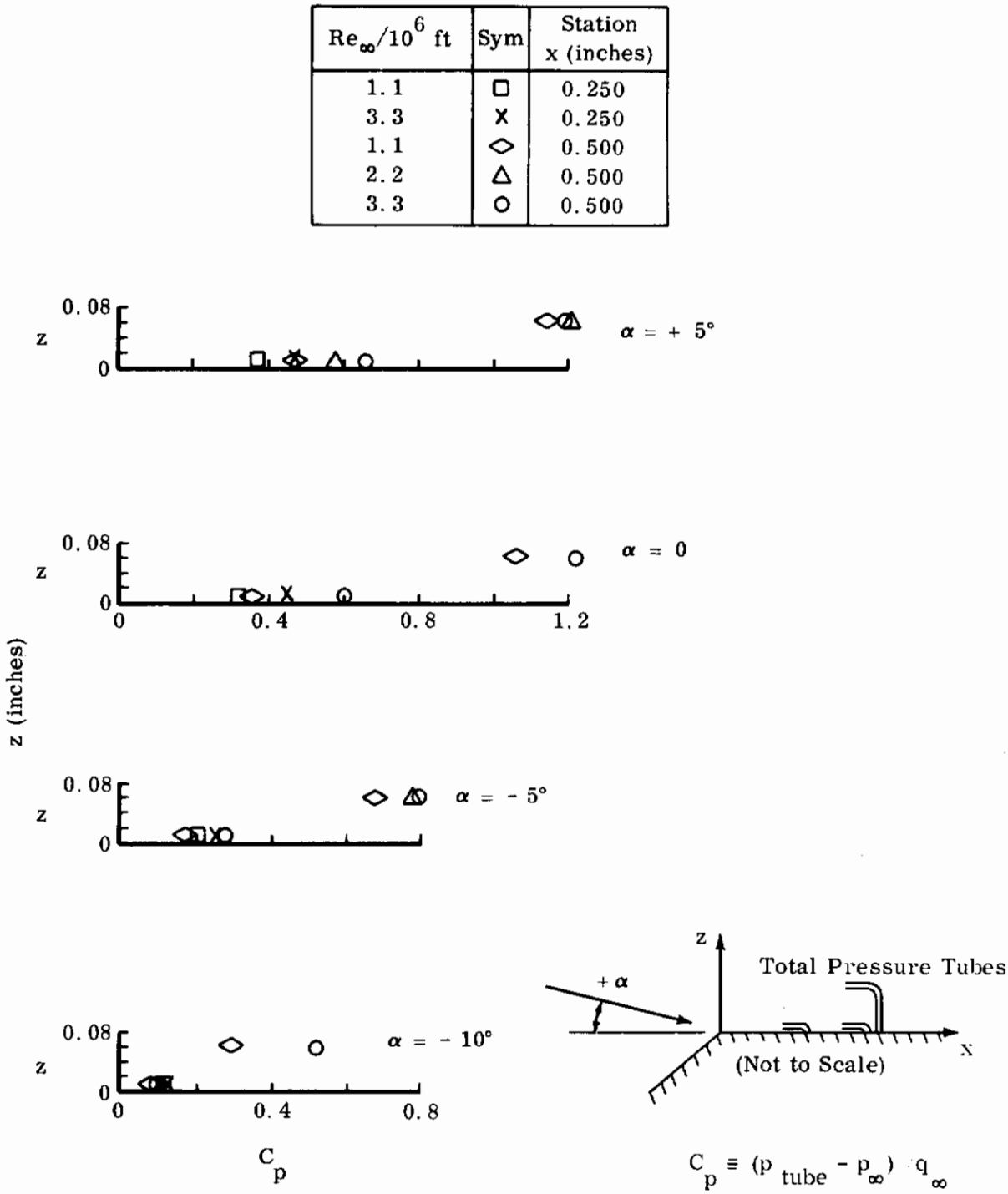

Figure 15. Pressure Coefficients in Boundary Layer at Two Stations Downstream of a Sharp, 40° Expansion Corner for $M_\infty = 8$

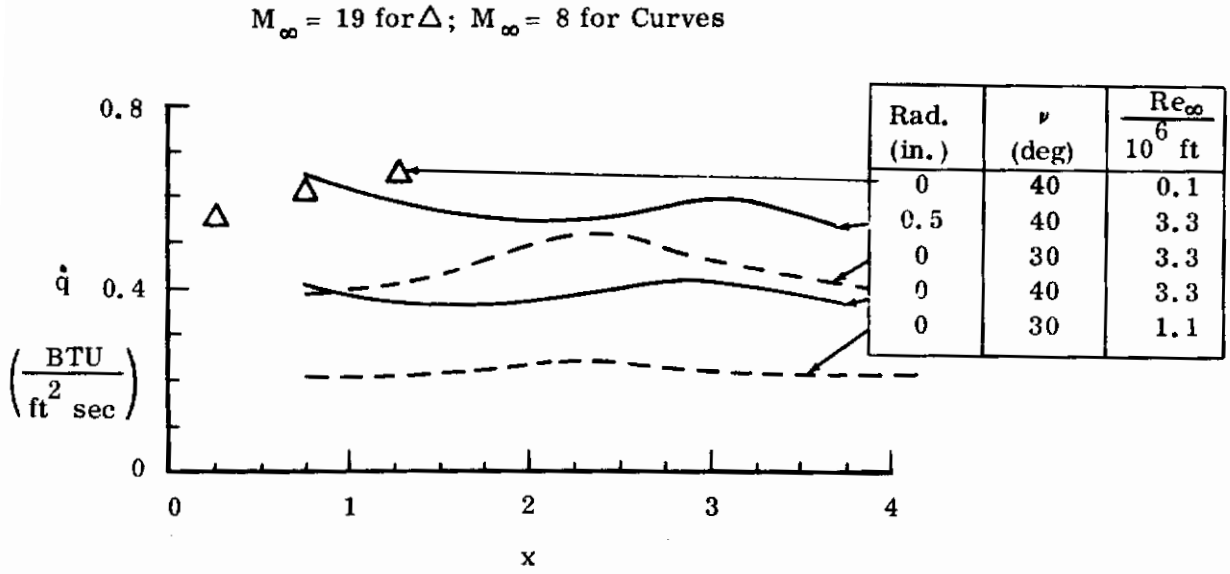

Figure 16. Heating Rates Downstream of Corners for $\alpha = 0$

Finally, in addition to the total pressure measurements and the distributions of surface pressures and heating rates, schlieren and shadowgraph flow photographs and high speed motion pictures showed no separation downstream of the sharp expansion corners. We must conclude that separation doesn't occur without adverse pressure gradients although, as for the flows described below, the pressure rises can be far downstream of the separation points.

Flows Downstream of Ramps

In addition to providing Re_x and aspect ratio effects for separation ahead of ramps (see preceding section), the forward flap on a flat plate model also provided data on the reattachment of flows downstream of ramps. As mentioned in the preceding section, the model was tested with and without endplates (see Fig. 1 and pages 47 through 52 for a more complete description of the model and forward flap). The nomenclature used here is indicated in the following figure, where X is the nondimensional distance downstream of the sharp leading edge. Reynolds numbers, Re_∞, are based on the one-foot length of the model and free stream conditions. Angles of attack and flap (ramp) deflections are positive when windward (as shown in Fig. 17).

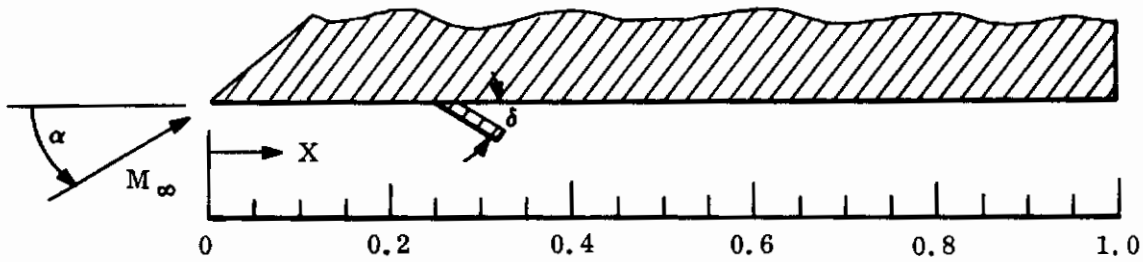

Figure 17. Nomenclature for Flows Downstream of Ramps

Pressures for $M_\infty = 5$ and 8, and aerodynamic heating rates for $M_\infty = 8$, were measured on the flat plate surface downstream of the flap for many angles of attack (up to 45°), and many flap deflections (up to 90°). Streamwise and spanwise distributions of all the data and schlieren flow photographs are presented in Refs. 5, 8 and 9; representative results are presented here in the following Figs. 18 and 19.

The flow separates from the trailing edge of the ramp-type flap and reattaches downstream on the flat plate surface. The extent of the separated flow region and the pressure rise at reattachment depend on several parameters: α, δ, M_∞, and Re_∞ (Fig. 18). For high surface angles of attack ($\alpha > 20°$), the downstream pressures are everywhere less than those recorded on the surface with no forward flap deflection. This can be attributed to model tip effects. However, at lower surface angles of attack, the pressures at reattachment considerably exceed those recorded for $\delta = 0$. These excess pressures depend on the flap deflection angle as well as on the stream flow conditions (compare Figs. 18a, b and c). The 30° flap leads to the highest excess pressures at reattachment whereas the 90° flap causes no excess pressure (similar to rearward facing steps, Ref. 31).

Except as noted in the first two parts of Fig. 18, the pressure distributions are those recorded along the centerline of the model without end plates. In most cases tested, there is no appreciable spanwise pressure variation across the center portion of the model; moreover, the pressure distributions downstream of the flaps are not significantly affected by end plates. The nondimensional $Y = 0.34$ spanwise location is two inches outboard from the model centerline.

Similar to flows over rearward facing steps (Ref. 31), the pressure drop in the separated flow region and the location of reattachment depend strongly on the laminar or turbulent character of the boundary layer (Figs. 18c and d). Turbulent boundary layers, associated with the higher Re_∞ values, lead to the greater pressure drops and reattachment upstream of that for laminar boundary layers.

Aerodynamic heating rates are substantially reduced in the separated flow region downstream of flaps but exceed the undisturbed, flat plate, values downstream of reattachment (Fig. 19b). As with the pressures, the heating rates downstream of flaps do not vary appreciably spanwise across the center portion of the model. However, the heating rates are more sensitive to end plate effects; a typical comparison showing end plate effects is drawn in Fig. 19c.

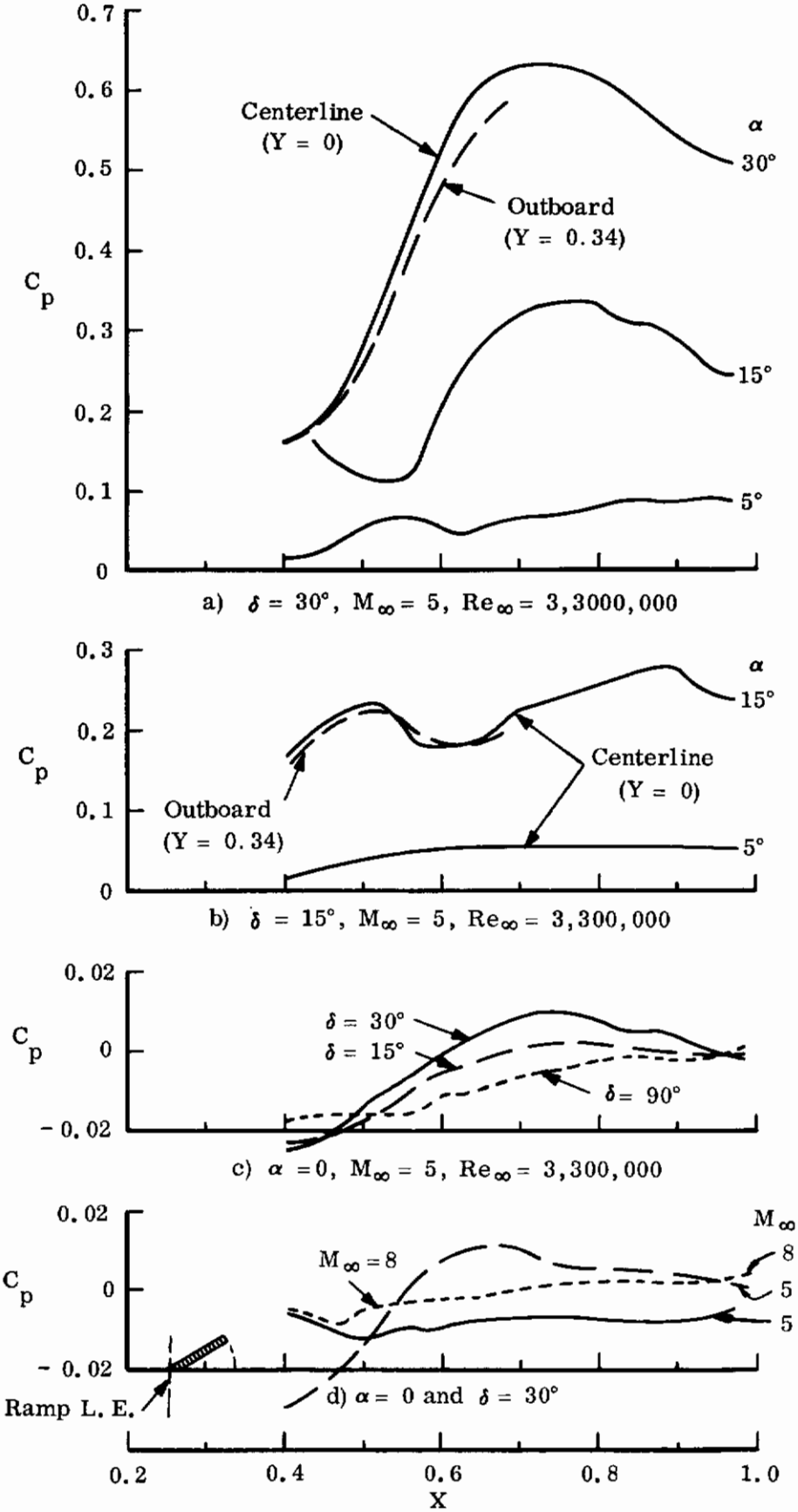

Figure 18. Pressure Distributions Downstream of Ramps

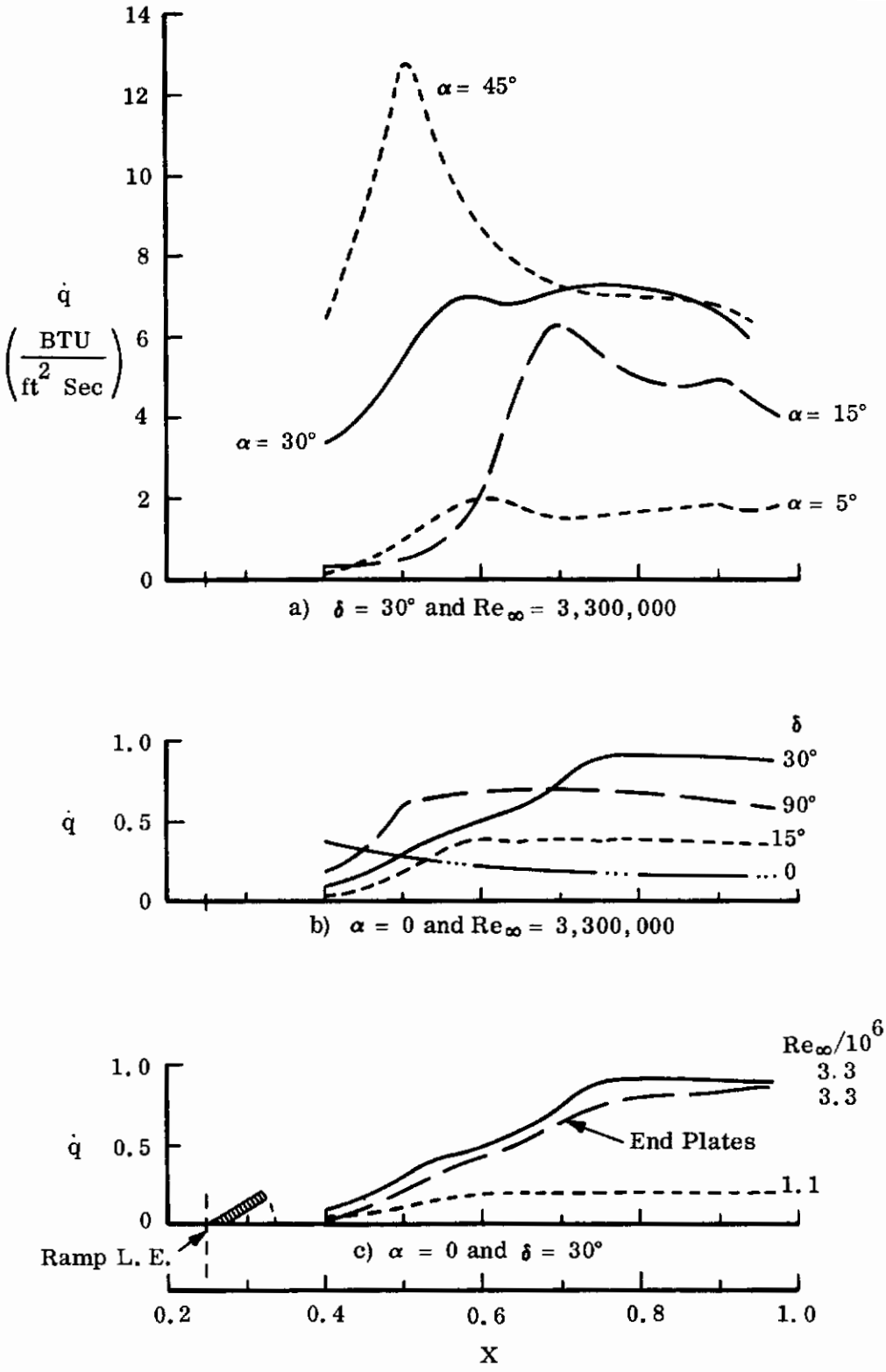

Figure 19. Heating Rates Downstream of Ramps for $M_\infty = 8$

FIN PLATE INTERACTION

The present understanding of the complicated flow in a streamwise corner region is poor in terms of a satisfactory theory, but for hypersonic free streams there are several rules and approximations that are helpful in predicting the observed effects. It appears that the dominant mechanism in fin plate interactions is always the separation of the plate boundary layer under the influence of the fin shock wave. There are three basic modes in which this separation can take place, and many combinations of them may be present in any given interaction flow.

The first mode occurs near the fin leading edge, where the thickness of the inviscid shock layer on the fin is very small relative to the natural length of the separated boundary layer on the plate. The pressure rise due to the fin shock is propagated upstream through the boundary layer and separation occurs far ahead of the fin. This mode has been observed on plates upstream of both blunt and sharp fins (see Fig. 20, parts a and b), although the detailed characteristics are different in the two cases. Three dimensional effects are always of first order importance in this mode, and there are no satisfactory methods for predicting the flow characteristics except for purely empirical correlations.

The second mode occurs when the fin shock layer thickness is comparable to the separation zone length measured normal to the local fin surface. The presence of the fin is an essential part of the structure of the separation zone in this mode, and the separation line on the plate is not in general parallel to either the fin or the fin shock (see Fig. 20, part c). A considerable amount of pressure and heat transfer data pertinent to the first and second modes was obtained for the investigation summarized herein (Refs. 7 through 11).

The third basic mode in which interaction separation can take place has been investigated theoretically and experimentally (Refs. 43 and 44). This mode occurs when the shock wave is sufficiently far from the fin so that the separated boundary layer on the plate can reattach without significant influences from the presence of the fin. In this mode the fin acts simply as a shock generator, and the problem reduces to the pseudo two-dimensional problem of a swept planar shock separating a boundary layer. The fin plate junction, far enough downstream of the leading edge, poses a streamwise corner boundary layer problem for the reattached flow downstream of the fin shock.

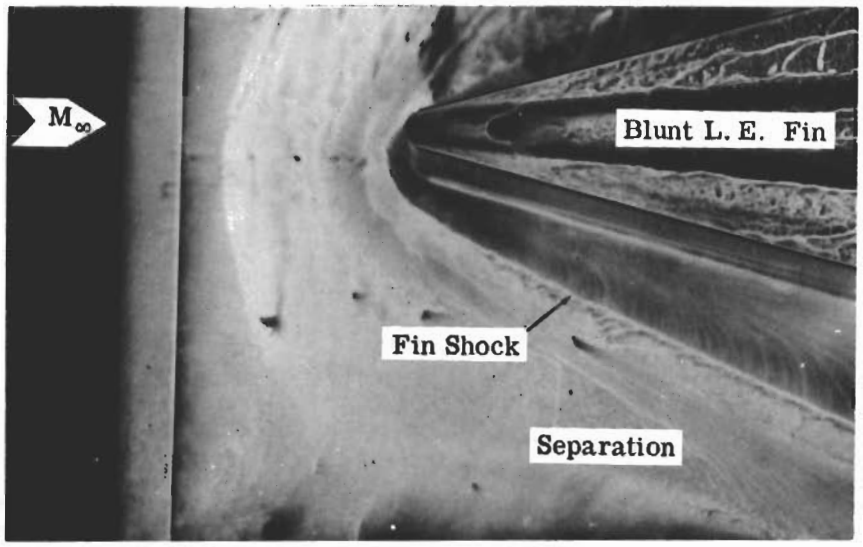

a) Flat Plate Parallel to M_∞, $\frac{Re_\infty}{ft} = 1,100,000$

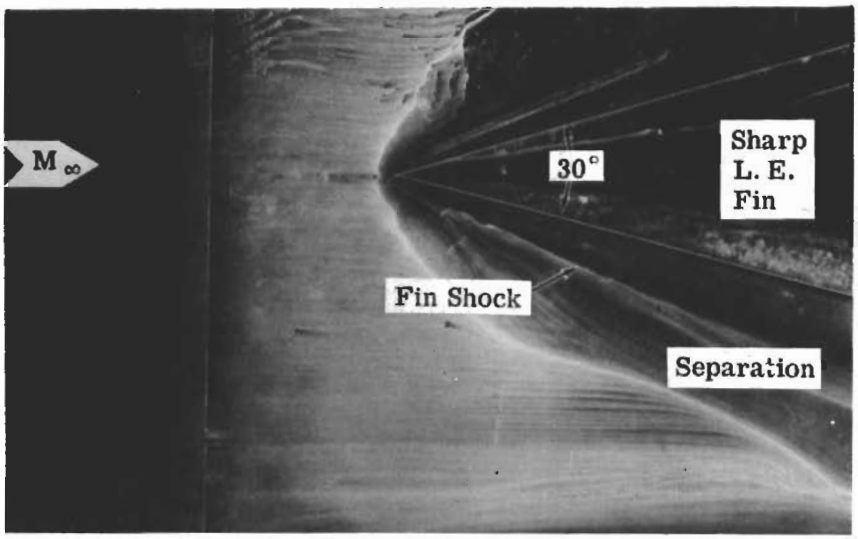

b) Flat Plate Parallel to M_∞, $\frac{Re_\infty}{ft} = 6,600,000$
(See Also Figure 22a)

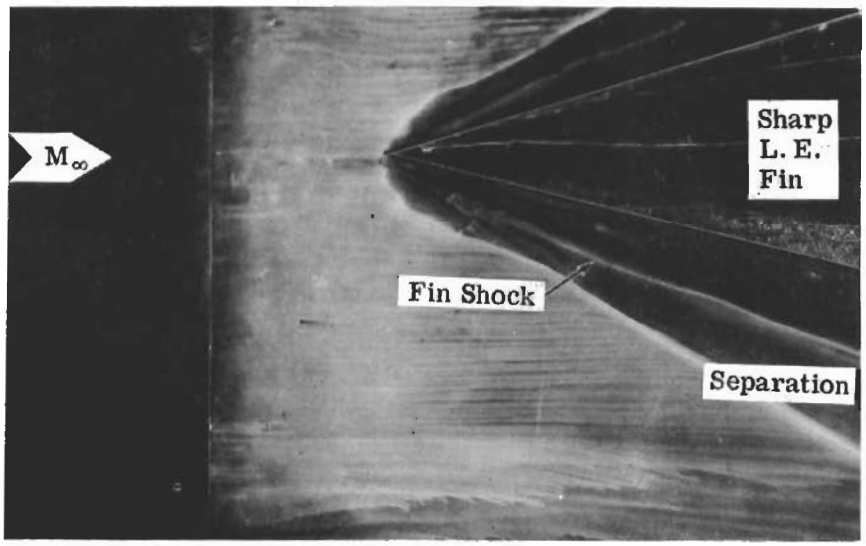

c) Flat Plate in Compression 5°, $\frac{Re_\infty}{ft} = 6,600,000$

Figure 20. Oil Film Flow Photographs of Fin Plate Interactions for $M_\infty = 5$

At hypersonic speeds the fin shock is close to the fin surface and generally the interaction cannot be split into separate incident shock and corner flow boundary layer problems. Thus the subject investigation was concerned primarily with the first two modes of fin plate interaction separation.

The oil film flow photographs of Fig. 20 present vivid evidence of the first and second modes of interaction separation caused by 30° wedge shaped fins mounted on a flat plate (see following section for model description). The high pressures on the blunt fin leading edge are propagated upstream through the plate boundary layer and cause separation far upstream of the fin (Fig. 20a). Indeed, the laminar boundary layer separates just downstream of the plate leading edge and is similar to the two-dimensional "free interaction" type of separation (see Refs. 10 and 11 for pressure distributions and profile schlieren photographs). The extensive region of separated flow ahead of the fin, characteristic of the first mode of interaction separation, is modified greatly for the sharp fin case shown in Fig. 20b. Although the region of separation is sharply reduced (in part due to the higher free stream Reynolds number), it is still predominantly three-dimensional over the forward portion of the model.

The extent of the first mode of interaction separation is seen to be limited to the sharp fin leading edge region in Fig. 20c. For this case the model was pitched 5° resulting in a somewhat lower speed flow over the flat plate. The major portion of the interaction is of the second mode described earlier. For this type of interaction the flow is generally conical in nature. The most promising theoretical approaches to the problem appear to be those based on crossflow plane analyses.

Pressure coefficient and heating rate distributions measured on the fin and plate surfaces at various steamwise stations (crossflow planes) are presented in Fig. 21. Coefficients are referenced to free steam conditions and the model angle of attack, α , is referenced to the flat plate surface. As indicated in the figure, the coordinate origin is at the intersection of the fin leading edge with the flat plate. Streamwise and fin spanwise (heightwise) stations are nondimensionalized with respect to the fin chord and height respectively. For the data presented in Fig. 21, the 30° wedge shaped fin had a sharp leading edge and an aspect ratio of 0.500 (see following section for model description).

The fin surface and inviscid shock locations and pressure coefficients (for a 15° flow deflection) are also indicated in Fig. 21. The pressure distributions on the plate surface resemble those measured in separated flow regions ahead of ramps. There are overpressures on the plate surface far outboard of the fin shock and generally the plate pressures do not reach the inviscid shock values until very close to the fin plate junction. On the fin surface the pressures increase somewhat from their values at the plate junction to values exceeding those given by two-dimensional inviscid shock

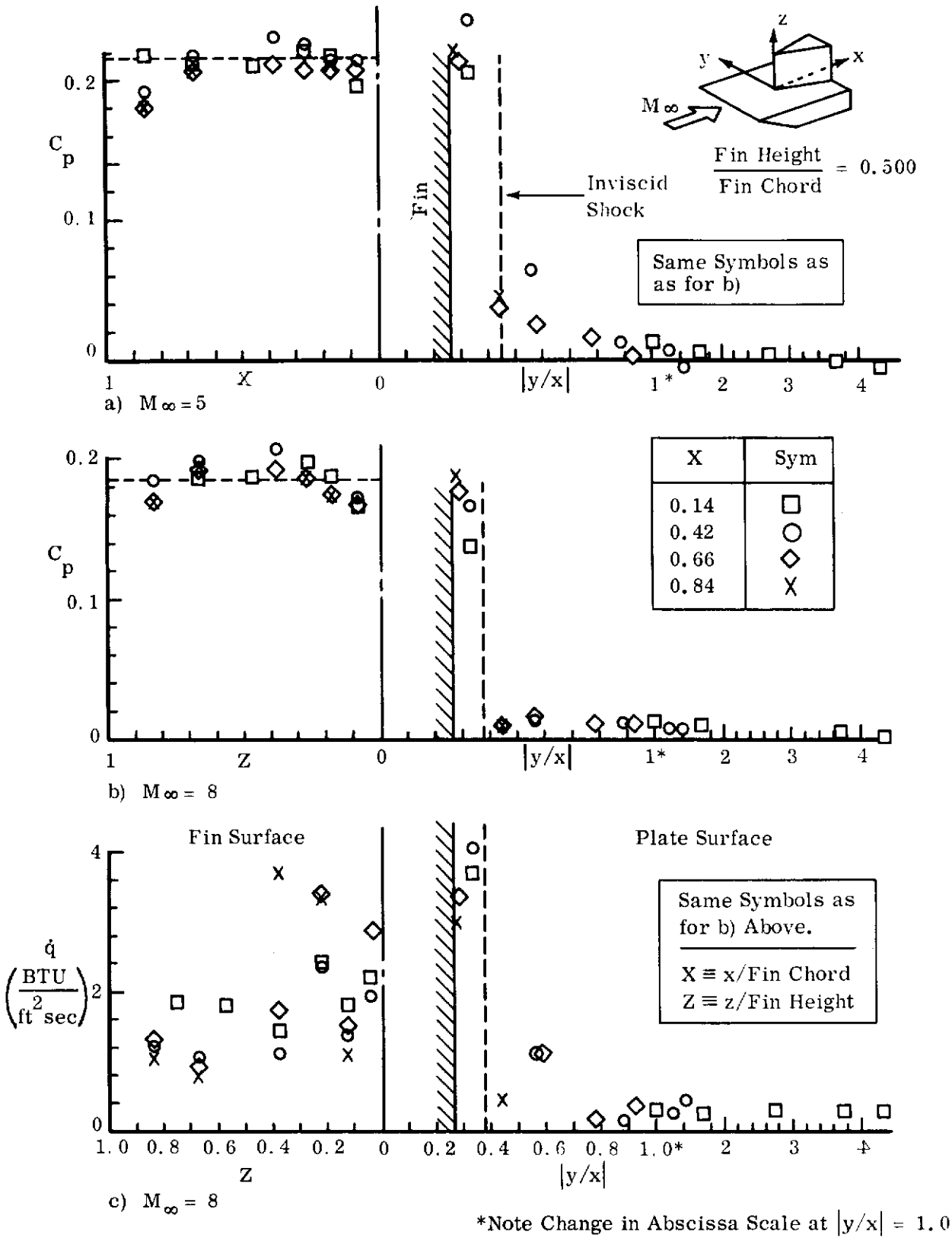

Figure 21. Fin Plate Interaction Pressures and Heating Rates at Various X Stations for Larger Fin (α = 0 and $Re_\infty/10^6$ ft = 3.3)

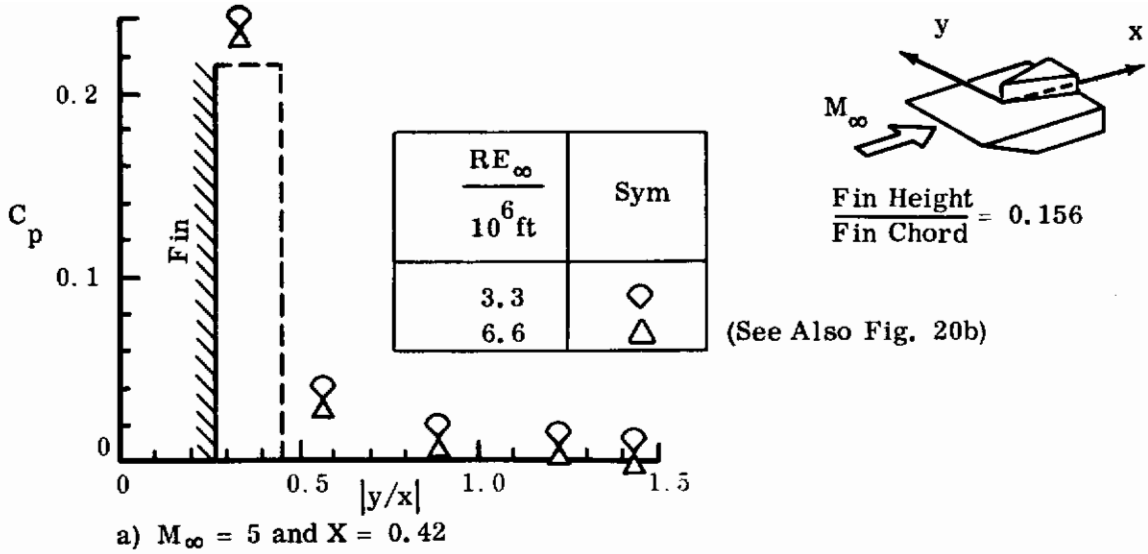

a) M_∞ = 5 and X = 0.42

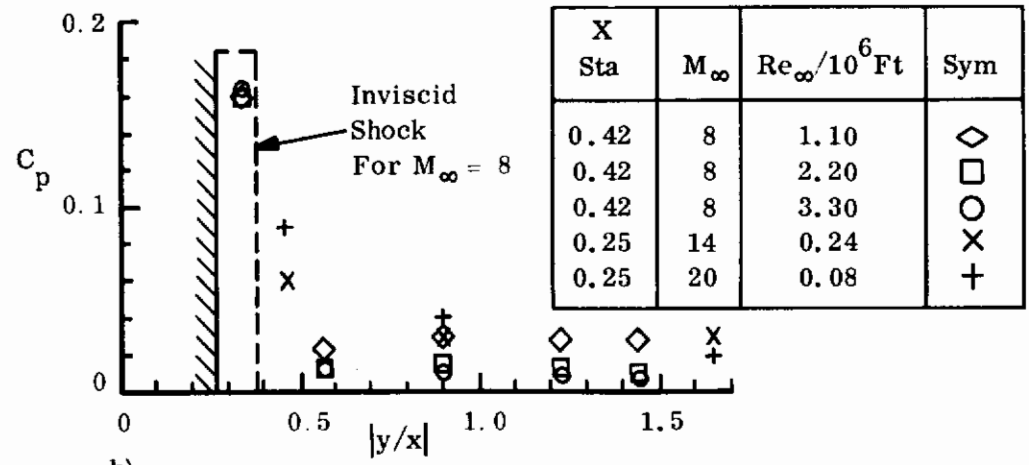

b)

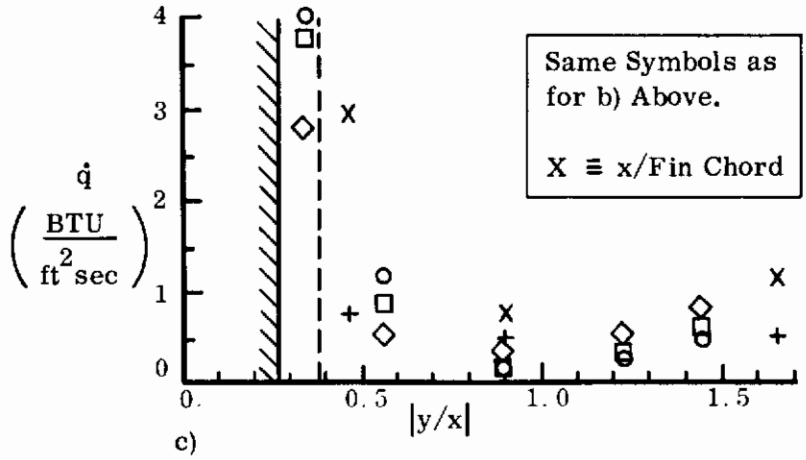

c)

Figure 22. Fin Plate Interaction Pressures and Heating Rates for Various M_∞ and Re_∞ for Smaller Fin (α = 0)

tables. These overpressures are attributed to the multiple shock compression of the flow in the interaction region and indicate the extent of the region. The interaction region is also marked by large aerodynamic heating rates, presented in Fig. 21c.

Mach and Reynolds number effects on the interaction pressures and heating rates are given in Fig. 22 for a 30° sharp leading edge fin with an aspect ratio of 0.156. Again similarly to two-dimensional separation ahead of a flap, the extent of separation and overpressures on the plate depend strongly on the boundary layer thickness. Particularly for the thicker boundary layers (larger M_∞ and smaller Re_∞ values), the pressure rise due to the fin shock is propagated far outboard and causes substantial overpressures over a large portion of the plate surface.

The data presented in Figs. 21 and 22 are representative of those obtained for the second mode of interaction separation described at the outset of this section. In many cases, particularly for fins with blunt leading edges, the interaction was predominantly three-dimensional in character (first mode). Although not amenable to theoretical analyses at present, pressures and heating rates were measured for a wide variety of flow conditions and can readily be used for engineering estimates (see following section and Refs. 7 through 11). Particularly noteworthy in this aspect are the high pressures and heating rates observed on the leading edges in the immediate vicinity of reattachment of the separated flow ahead of the fin. In some cases the peak values were more than three times larger than the stagnation values of the pressure and heating rate measured on the cylindrical leading edge outside of the interaction region (see sketch).

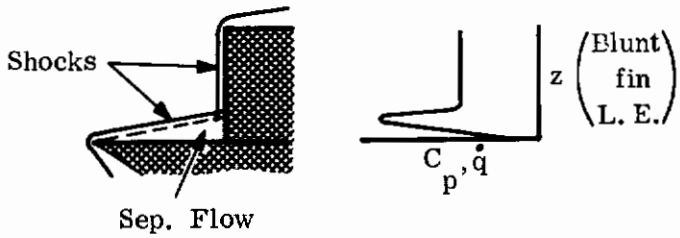

EXPERIMENTAL FACILITIES, TECHNIQUES AND MODELS

The wind tunnels and models used to obtain the experimental results presented herein are briefly described in this section. First, the over-all test program is outlined. The techniques used to obtain the data are then described along with the reduction and accuracy of the data. Finally, the models are described (see also Fig. 1 on page 2).

Tunnels and Ranges of Variables

Tests for the experimental portion of the program were conducted in the Grumman Hypersonic Shock Tunnel and at the AEDC von Karman facility. The particular AEDC wind tunnels used were the: 40-inch supersonic wind tunnel, 50-inch Mach 8 tunnel, and the Hotshot 2 hypervelocity tunnel. These facilities provided the Mach number and unit Reynolds number ranges shaded in the following altitude-velocity chart (Fig. 23). The test conditions fall within the so-called flight corridor whose upper and lower bounds are delineated, approximately, by the dotted hypersonic flight entry trajectories shown in Fig. 23.

Pressure and force data were obtained in the AEDC 40-inch supersonic tunnel for a nominal free stream Mach number of 5. The angle of attack ranges used for the various models are given in the following table. The table also lists the ranges of the unit free stream Reynolds numbers, sideslip angles, and control deflection angles. Oil film, schlieren flow photographs, and high speed schlieren motion pictures were taken. Pressure, heat transfer and force data were obtained in the AEDC 50-inch Mach 8 tunnel and shadowgraph flow photographs were taken for the configurations indicated in the table. Pressure data were obtained on just one configuration in the Hotshot 2 impulse-type, hypervelocity facility. Schlieren flow photographs were obtained and very high speed, color motion pictures were taken during the test runs when heat sensitive paint was applied to the model. More complete descriptions of this impulse type tunnel and the continuous flow tunnels mentioned above are readily available in the AEDC Test Facility Handbook (Ref. 45).

Limited pressure and heat transfer data were obtained in the Grumman Hypersonic Shock Tunnel for the Mach numbers and unit Reynolds numbers listed in the table. Interchangeable nozzle throat blocks are used for the different Mach number flows. Schlieren flow photographs were taken in addition to motion pictures showing the discolorization of heat sensitive paint applied to two of the models. Further descriptions of this tunnel are given in Refs. 7 and 22.

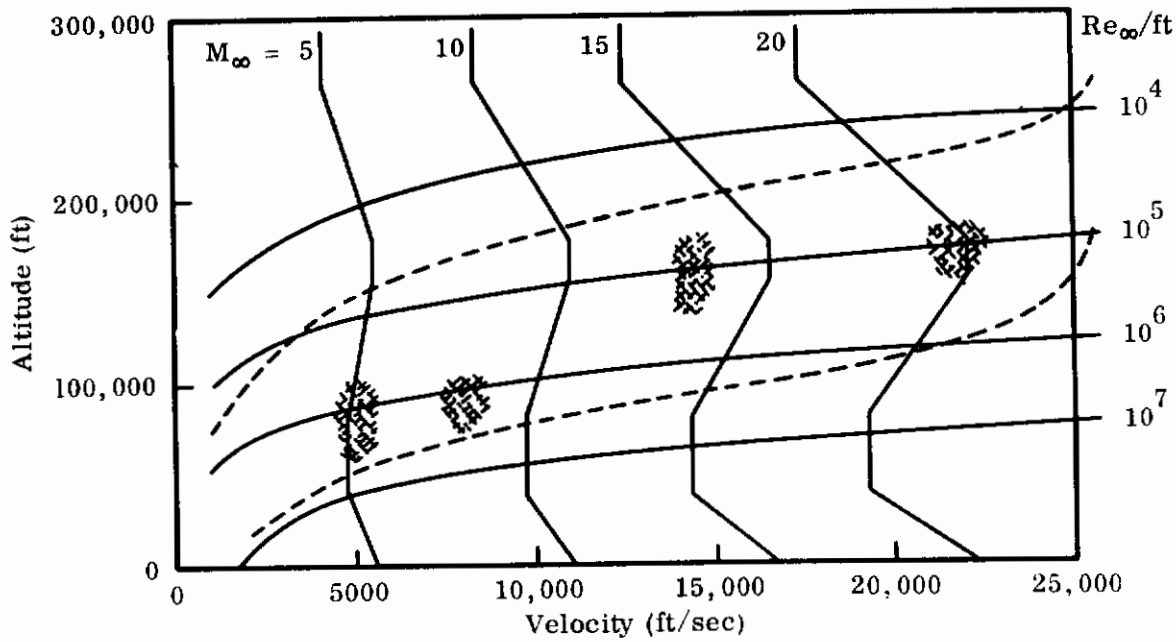

Figure 23. Altitude Velocity Chart with M_∞ and Re_∞/ft Test Ranges

Experimental Techniques and Data Reduction

All pressure data were reduced to standard coefficient form:

$$C_p = \frac{p - p_\infty}{q_\infty}$$

where p is the measured pressure, p_∞ is the free stream static pressure, and q_∞ is the free stream dynamic pressure.

The accuracy of the pressure measurements depends upon the particular facility and also the pressure level. For the Mach 5 data, pressures below 1.0 psia are measured to within ± 0.005 psia while the accuracy for the higher pressure measurements is ± 0.075 psia. Whence, depending upon the values of C_p and Re_∞, the pressure coefficient accuracy varies from about ± 0.009 to ± 0.020. Similarly for the Mach 8 data, pressure coefficient uncertainties vary, for example, from 0.004 for $C_p < 0.3$ and Re_∞/ft = 1.1 million, to 0.013 for $C_p = 2.0$ and Re_∞/ft = 3.3 million. Pressures obtained in the impulse type test facilities were estimated to be accurate to within 10 percent of their measured values. More thorough discussions of the pressure data accuracy are available in Refs. 10, 16, and 22.

TABLE I
OUTLINE OF TEST PROGRAM

Configuration	M_∞	$Re_\infty/10^6$ ft	α (deg)	β (deg)	δ (deg)	Data
flat plate with ramp shaped flaps; w. & w. o. end plates	5	1.1 to 6.6	-15 to 30	0	0 to 90	p & ph
	8	1.1 to 3.3	-15 to 45	0	0 to 90	p, HT & ph
	13	~0.1	-15 to 0	0	0 to 30	p, HT & ph
	19	~0.1	-15 to 30	0	0 to 45	p, HT & ph
flat plate with wedge shaped fins; sharp & blunt L.E. fins	5	1.1 to 6.6	-10 to 5	0	two different fin heights	p & ph
	8	1.1 to 3.3	-10 to 14	0		p & HT
	13	~0.2	0	0		p, HT & ph
	19	~0.1	0	0		p, HT & ph
delta wing - body combination with T.E. flaps; w. & w.o. tip fins & spoiler	5	2.3 to 5.0	-30 to 45	0	-40 to 40	F, p & ph
	8	0.8 to 3.3	-54 to 54	0	-40 to 40	F, p & HT
	19	~0.1	-30 to 30	0	-40 to 40	p & ph
pyramidal, triangular cross section, with T.E. flaps; w. & w.o. canards & ventral fin	5	0.7 to 6.6	-30 to 45	-2 to 14	0 to 40 (all flaps)	F, p & ph
	8	1.1 to 3.3	-54 to 54	-4 to 14	0 to 40 (all flaps)	F, p, HT & ph
	21	~0.1	-30 to 45	0	0 to 40	p, HT & ph

Notes: Angle of attack positive when flat plate surfaces windward. Sideslip angle is β and δ denotes flap deflections. F denotes 6 component force & moment data, p denotes pressure distributions, HT denotes heat transfer distributions, & ph denotes flow photographs.

Aerodynamic heating rates were obtained using the thin wall transient temperature technique. Cooling shoes were installed in the AEDC 50-inch Mach 8 tunnel. The model was pitched to the desired angle of attack while inside the cooling shoes. The shoes were then rapidly retracted and thermocouple temperatures recorded during the initial heating of the model. The cooling shoes were then closed, the model cooled to approximately 500°R , and pitched to the next desired angle of attack. In this manner, temperature histories were recorded for a set of test conditions while limiting the amount of heat absorbed by the model. The cooling shoes were then left retracted while the pressure data, which require several minutes to stabilize, were obtained at the same set of test conditions.

The aerodynamic heating rates, $\dot{q}$ (BTU/ft^{2}sec), are calculated from the temperature histories:

$$\dot{q} = \zeta \, abc \, (dT_w/dt)$$

where dT_w/dt (°R/sec) is the wall temperature rise rate; a (lbm/ft^3) is the density of the wall material; b (ft) is the thickness of the wall; c (BTU/lbm) is the specific heat of the wall material; and ζ is the correction factor for conduction effects and relates the measured heat transfer rates to the aerodynamic heating rates. For very thin walls, made possible by our innovation of the use of honeycomb sandwich panels (described in the following subsection), the temperature response is very rapid and conduction effects are negligible. To within the accuracy of the wall material properties and measured wall thicknesses, $\zeta = 1.00$.

The thin wall transient temperature method was also used to obtain the aerodynamic heating rates on the models tested in the Grumman Hypersonic Shock Tunnel. The temperatures measured by the thin film heat transfer gauges were converted by analogs and presented directly as heat transfer rates.

Six component force and moment data were obtained and reduced to standard coefficient forms for body oriented axes. Body axes were used in lieu of wind axes to facilitate the comparison of integrated pressure and force increments, and to facilitate determining control effectiveness.

The normal, axial, and side force coefficients are:

$$C_N \equiv \frac{\text{normal force}}{q_\infty S} \qquad C_A \equiv \frac{\text{axial force}}{q_\infty S}$$

and

$$C_Y \equiv \frac{\text{side force}}{q_\infty S}$$

where S is the reference planform area (see Table II). The pitching, yawing and rolling moment coefficients are:

$$C_m \equiv \frac{\text{pitching moment}}{q_\infty SL} \qquad C_n \equiv \frac{\text{yawing moment}}{q_\infty SL}$$

and

$$C_\ell \equiv \frac{\text{rolling moment}}{q_\infty SL}$$

where the reference length, L, is the planform virtual length and moments are taken about a point 0.60L downstream of the planform virtual apex on the longitudinal axis of the balance. The coefficients presented herein are those due to the total forces and moments measured; they are not corrected for base pressure effects. The sign conventions for the force and moment coefficients are given in Fig. 24. Angles of attack, α, are positive for nose up, and sideslip angles, β, are positive for nose left.

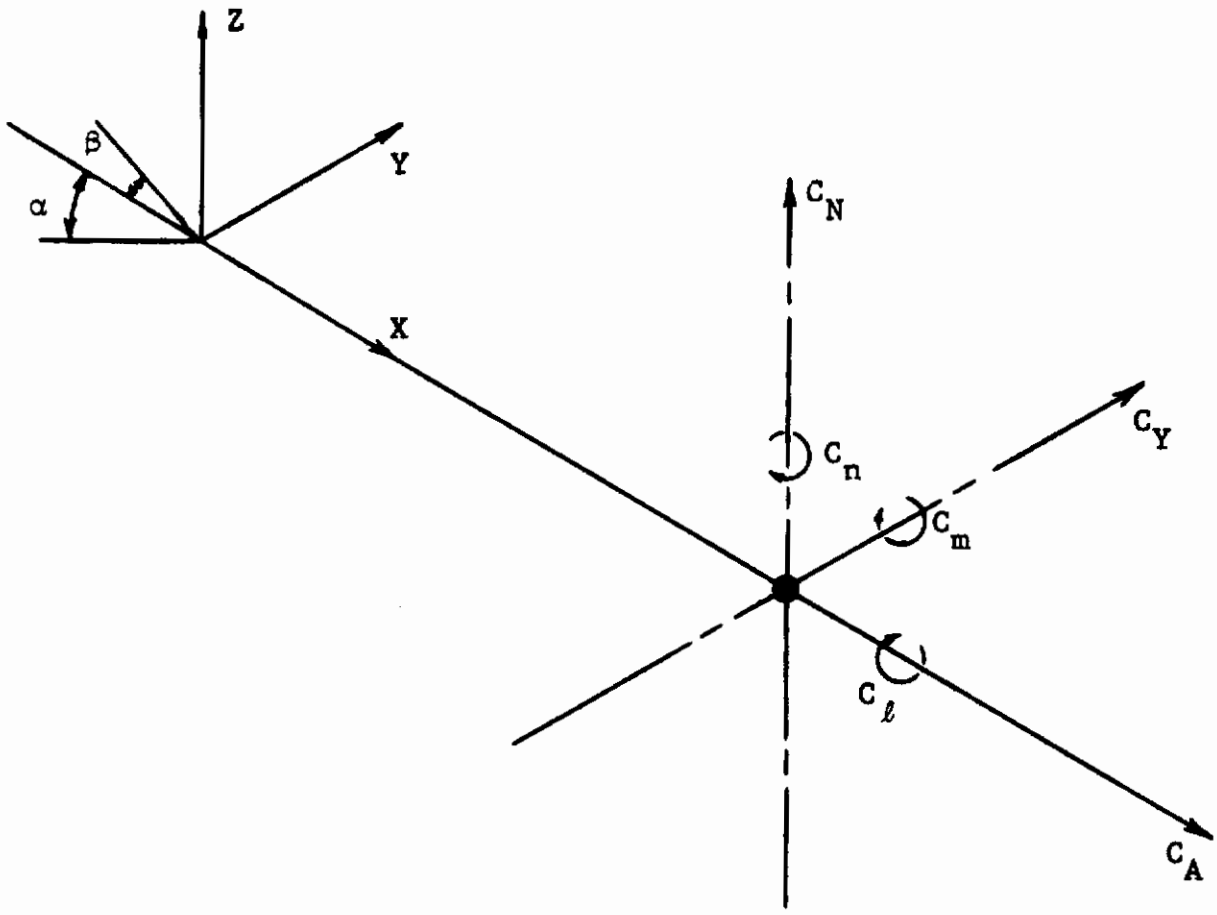

Figure 24. Sign Conventions for Force and Moment Coefficients

The total forces and moments were obtained using an AEDC water cooled balance. The same balance was used in both continuous flow wind tunnels for both force models. The uncertainties in the force and moment coefficients obtained from the balance measurements are shown in the following table for both models for the nominal values of the Mach 5 and Mach 8 free stream dynamic pressures. The uncertainties in the coefficients vary inversely with the q_∞ values, and can be calculated for the different free stream Reynolds numbers by dividing the tabulated uncertainties by the ratio of the q_∞ values for the different free streams. Reference areas and lengths for both force models are given in Table II.

TABLE II
FORCE AND MOMENT COEFFICIENTS

	Reference Areas and Lengths	
	delta wing - body	pyramidal configuration
S	191.2 square inches	157.6 square inches
L	18.2 inches	20.8 inches

	Uncertainties in Coefficients*			
	delta wing - body		pyramidal configuration	
	Mach 5 (q_∞ = 1.81 psia)	Mach 8 (q_∞ = 2.56 psia)	Mach 5 (q_∞ = 1.81 psia)	Mach 8 (q_∞ = 2.56 psia)
C_N	± 0.0039	± 0.0154	± 0.0080	± 0.0174
C_A	± 0.0021	± 0.0033	± 0.0020	± 0.0037
C_Y	± 0.0029	± 0.0077	± 0.0052	± 0.0087
C_m	± 0.0016	± 0.0044	± 0.0016	± 0.0043
C_n	± 0.0010	± 0.0022	± 0.0010	± 0.0021
C_ℓ	± 0.0003	± 0.0004	± 0.0002	± 0.0004

*Due to error spread in balance readings for Mach 5 and repeatability spread in data for Mach 8 (Refs. 15 and 21).

Normal loads and hinge and twisting moments were measured on one of the remotely controlled trailing edge flaps on the pyramidal configuration. The water cooled flap balance and accuracy of the measured flap loads are described in Ref. 23, wherein the flap force and moment data are presented.

As described in the following subsection, remotely controlled flaps were used for several of the models. Flap deflections, for the remotely controlled flaps, were set using Leeds and Northrup indicator readings of potentiometers connected to the flap drive screws. The flap settings were checked frequently using a surveyor's transit and were estimated to be accurate to well within a quarter of degree.

Several photographic techniques were used as aids in determining regions of separated flow and in interpreting the measured pressures and aerodynamic heating rates. Virtually all of the better flow photographs obtained are reproduced in the various data reports (Refs. 5 through 23).

Profile schlieren and shadowgraph photographs were useful in indicating boundary layer thickness, transition, separation and the accompanying shock wave patterns. Schlieren motion pictures, when reviewed at a much reduced speed, showed that separated flows were stable.

Charring of a thin coat of ordinary white enamel paint, sprayed on the Hotshot 2 model, clearly indicated regions of high aerodynamic heating rates. However, only marginal results were obtained from paint tests in the Grumman Hypersonic Shock Tunnel. A slight discoloration occurred, rather than decisive charring, probably due to the much shorter durations of the shock tunnel flow and consequent less total heat flow per test run (Refs. 7 and 10).

Oil film flow photographs were obtained in the AEDC 40-inch supersonic tunnel. A thin film of oil, which was fluorescent under ultraviolet light, was sprayed on the model at the outset of a test run. The tunnel flow was started and the fluorescent oil film observed as the desired tunnel flow conditions were reached. When the oil film flow pattern had become established, and steady, it was photographed. The model angle of attack, or flap deflection, was then changed to the next desired setting and the new oil film flow pattern photographed when it became established. This was repeated for several different test conditions before a major portion of the oil had evaporated or blown downstream off the surface of the model (Refs. 11 and 23).

Model Descriptions

As indicated at the outset of this section, and in Fig. 1 on page 2, flows over four basic configurations were investigated: a flat plate with ramp shaped flaps, another flat plate with wedge shaped fins, a delta wing body combination, and a pyramidal configuration having a triangular cross section. Eleven wind tunnel

models, each having several geometric variations, were required: seven for the continuous flow tunnels, one for Hotshot 2, and three for the Grumman Hypersonic Shock Tunnel.

Four models for the continuous flow tunnels were instrumented for both pressure and heat transfer measurements. Our innovation of the use of honeycomb sandwich construction for the planar portions of these models avoided many of the usual problems associated with thin wall heat transfer models and led to exceptional accuracy in the heat transfer data (Refs. 2 and 3).

The honeycomb sandwich panels are composed of 1/4 inch thick, stainless steel honeycomb having 3/8-inch cells, sandwiched between 0.018-inch-thick stainless steel sheets. The honeycomb webs were just 0.002 inches thick and were perforated to ensure pressure equalizaton. Thermocouples were spot welded to the inner surface of the outer wall of the honeycomb sandwich in the middle of individual honeycomb cells. These panels permitted the use of considerably thinner walls without buckling than those possible with standard "thin wall" models or those obtained by milling local thin spots in thick wall models. Thus response time was faster, conduction effects were greatly reduced, and the heat absorbed by the model was minimized (thereby substantially reducing the cooling time required). Further, the wall heated more uniformly, subject only to the distribution of aerodynamic heating rates, and local hot spots and large heat sinks were avoided.

To make optimum use of the continuous wind tunnel test time and eliminate time consuming shut downs required for minor model changes, the aerodynamic control surfaces on several of the models were remotely actuated. A specially designed water cooled actuator housing was fabricated and used interchangeably for the three pressure and heat transfer models having moveable control surfaces. The housing was attached to the base of the model and then the entire model-housing unit was sting mounted (see Fig. 25a). The housing contained three each: drive screws, motors, and linear potentiometers (see Fig. 25b).

Three flat plate models with ramp shaped flaps were used. The models had machined sharp-leading edges, square planforms, and their lower surfaces formed 40° expansion corners. Two models, for the Mach 5 and 8 tests, had 12-inch-square planforms while the third model, tested in the Grumman Hypersonic Shock Tunnel, had a 6-inch-square planform. Line drawings of the larger models, showing instrumentation locations and flap geometry, are given in Fig. 26.

One of the larger models, instrumented for both pressure and heat transfer measurements, had three sets of remotely controlled flaps: a forward flap with 90° travel, an essentially full span aft flap with 45 degree travel, and a partial span aft flap with 45 degree travel. A photograph of this model, with end plates attached, is shown in Fig. 1, page 2. The expansion corner formed by the intersection of the lower surfaces of the model had replaceable sharp and

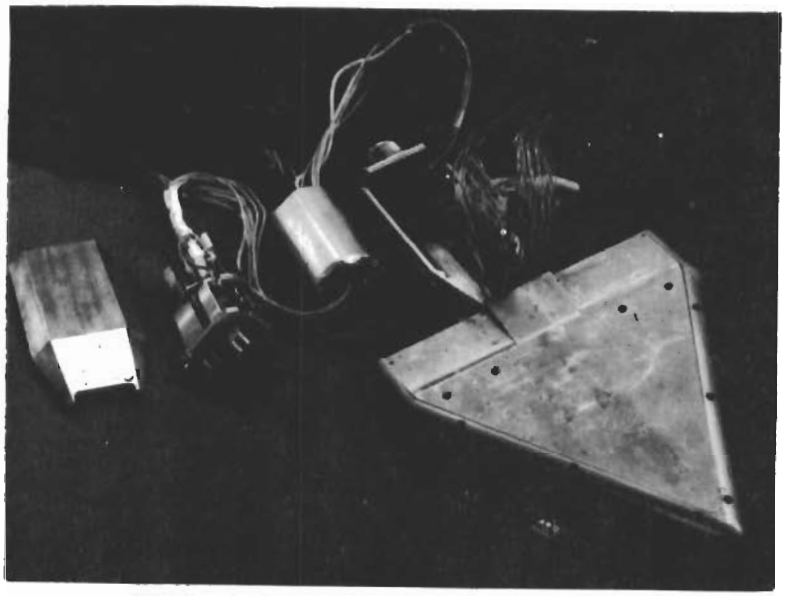

a) Actuator housing parts behind wing body model

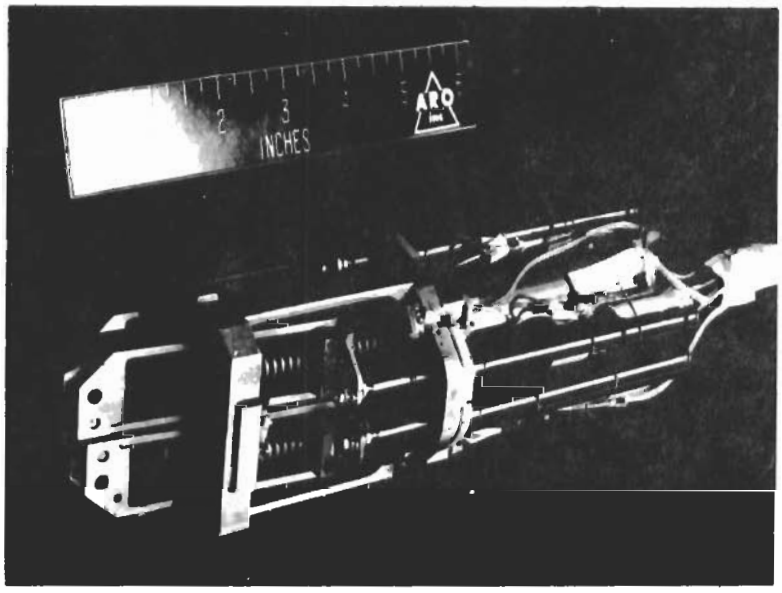

b) Drive screws, motors, and potentiometers

Figure 25. Water Cooled Actuation System for Remotely Controlled Flaps

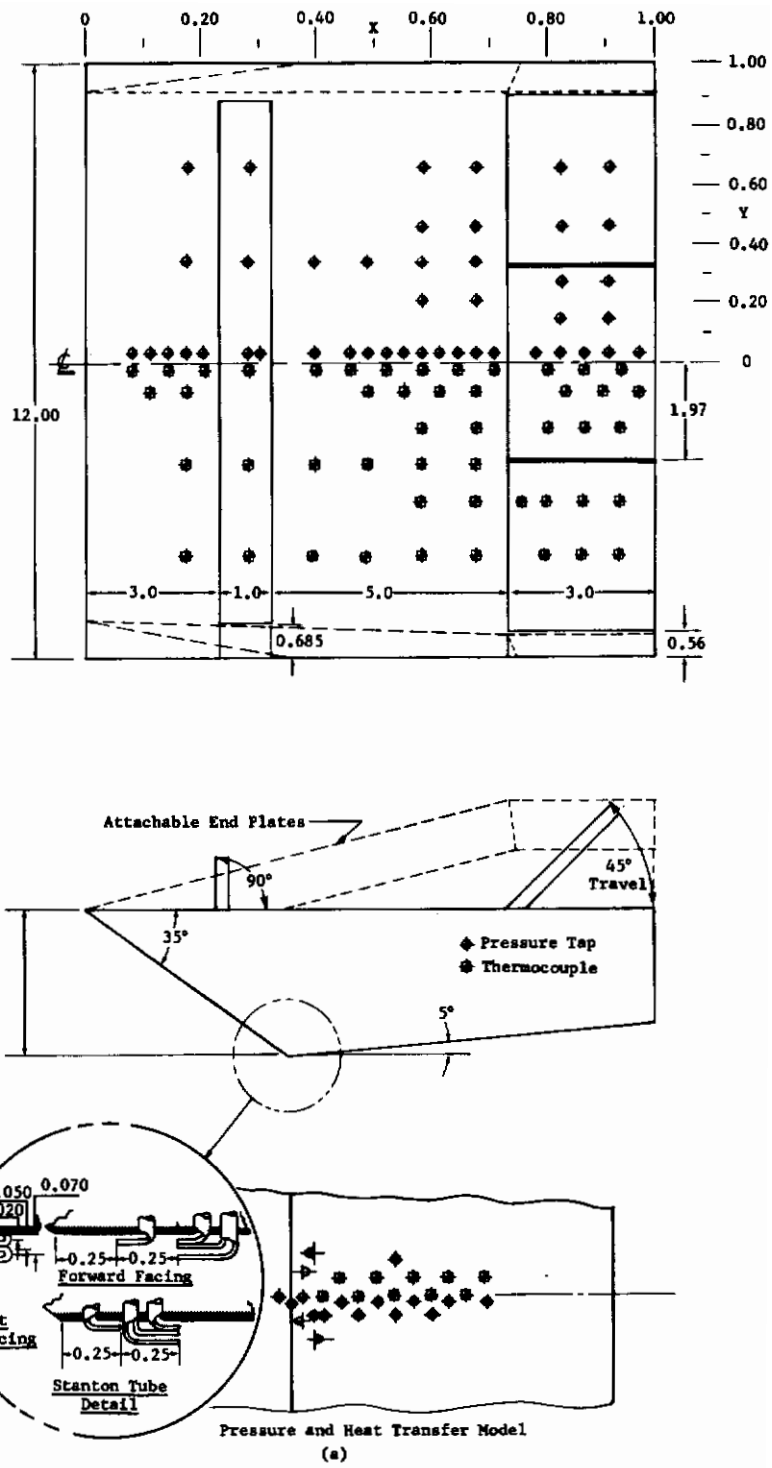

Figure 26. Line Drawings of Flat Plate Models with Ramp Shaped Flaps

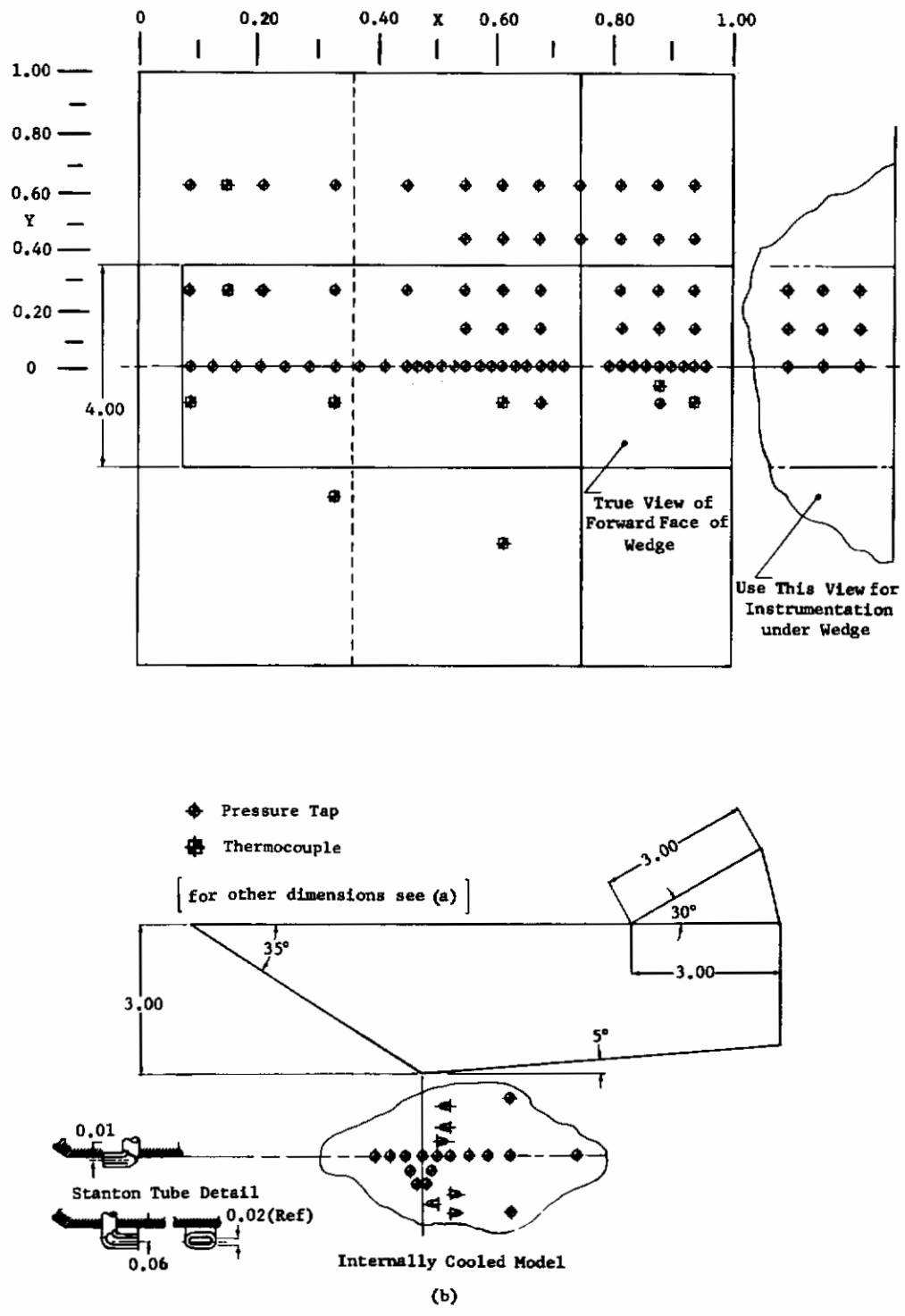

Figure 26. Line Drawings of Flat Plate Models with Ramp Shaped Flaps

1/2-inch-radius corners. The expansion corner instrumentation was similar to that for the larger flat plate fin model (Fig. 27).

The other model shown in Fig. 26 was internally cooled by a mixture of low temperature oxygen and nitrogen. The model had attachable full span, 25 percent chord, trailing edge flaps having ramp angles of 10, 20, and 30°; and an attachable partial span, 30°, trailing edge flap that was also internally cooled. The coolant was supplied to settling chambers in the basic model and in the ramp and was then passed through channels adjacent to the flat plate and ramp surfaces. Because of its high thermal conductivity, the coolant channels were fabricated of thick berrylico sheet in the attempt to maintain as unifrom a wall temperature as possible. As shown in Fig. 26, both the upper and lower surfaces of the model had comparatively dense streamwise pressure instrumentation. Six total pressure, forward and rearward facing, Stanton tubes were mounted at two stations downstream of the sharp expansion corner.

The Grumman Hypersonic Shock Tunnel model had 15°, 30°, and 45°, full span, 25 percent chord trailing edge ramps. It was instrumented with 10 pressure gauges and 10 heat transfer gauges. As for the larger pressure and heat transfer model, the inboard pressure and heat transfer instrument distributions had to be offset slightly from the model centerline (Fig. 26a). Further descriptions of these flat plate models with ramp shaped flaps are available in Refs. 5 through 7.

Fin plate interactions were investigated using two flat plate models with 30°, total angle, wedge shaped vertical fins mounted on their upper surfaces (see Fig. 1, page 2, and Fig. 27). Pressures and aerodynamic heating rates were measured on both the plate and fin surfaces of both models. The larger model had a 12-inch-square planform. The lower face of the model intersects the flat plate upper surface at 30°; both the leading edge and the 30° expansion corner on the lower surface are machined sharp. The lower surface instrumentation is similar to that for the pressure and heat transfer model shown in Fig. 26a). A total of four fin configurations were mounted on the upper, flat plate surface of the model: "small" and "large" fins with sharp and blunt leading edges. The sharp leading edge fins have 8 inch chords which are reduced by about 8 percent for the 0.25 inch radius blunt leading edges. The height of the "small" fin is 1.25 inches and that of the "large" fin is 4.00 inches.

The other fin plate interaction model, tested in the Grumman Hypersonic Shock Tunnel, had a 6-inch-square planform and 4-inch-chord, sharp leading edge, fins geometrically similar to those on the larger model. Further descriptions of the fin plate interaction models are available in Refs. 7, 10, and 11.

Three models of the clipped delta wing body combination were required for the force, pressure and heat transfer data for a "typical" hypersonic winged re-entry configuration. A rear view photograph of the model mounted in the AEDC 50-inch Mach 8 tunnel is shown in

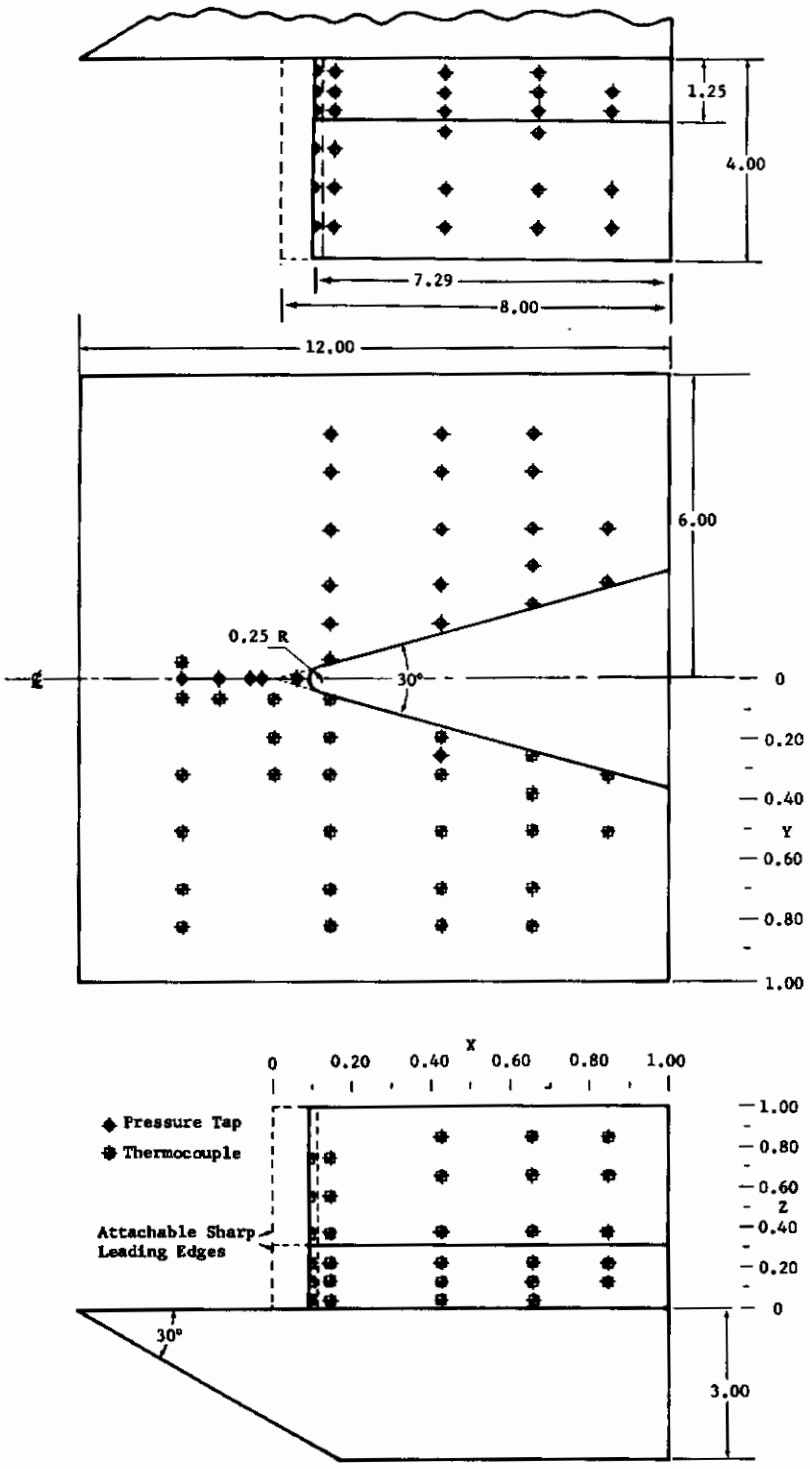

Figure 27. Line Drawing of Fin Plate Interaction Model

Fig. 28. The actuator housing for the flap drives and controls is evident immediately behind the model. The basic pressure and heat transfer model consists of a spherically capped cylindrical cabin mounted on top of a blunt delta wing with 60° sweepback. The delta wing has clipped tips and a thickness equal to 10 percent of the virtual length of the model. The cabin height is equal to the wing thickness.

Figure 28. Photograph of Winged Re-entry Configuration in the AEDC 50-Inch Mach 8 Tunnel

The model has three, remotely controlled, trailing edge flaps; two outboard "aileron type" flaps, extending from the cabin-wing junctions to the shoulders of the cylindrical wing tips, and one "split" flap on the lower surface of the wing, extending spanwise between the outboard flaps. The flaps are rectangular and have chords equal to 15 percent of the virtual length of the model. Each flap is individually controllable; the outboard flaps have a travel of ± 40° and the center flap on the lower surface has a travel of +20°. Flap deflections are defined positive for downward deflections of the flap trailing edges.

The model has attachable tip fins, a trailing edge spoiler, and an attachable conical fairing for the spherically capped cabin. The fins are attachable to the cylindrical wing tips of the model and have cylindrical leading edges with 50° sweepback. The spoiler is attachable to the lower surface of the model, spanning the distance between the tip fins, and has a height equal to the vertical projection of the trailing edge flaps when deflected 20°. The instrumentation locations are indicated in Fig. 29.

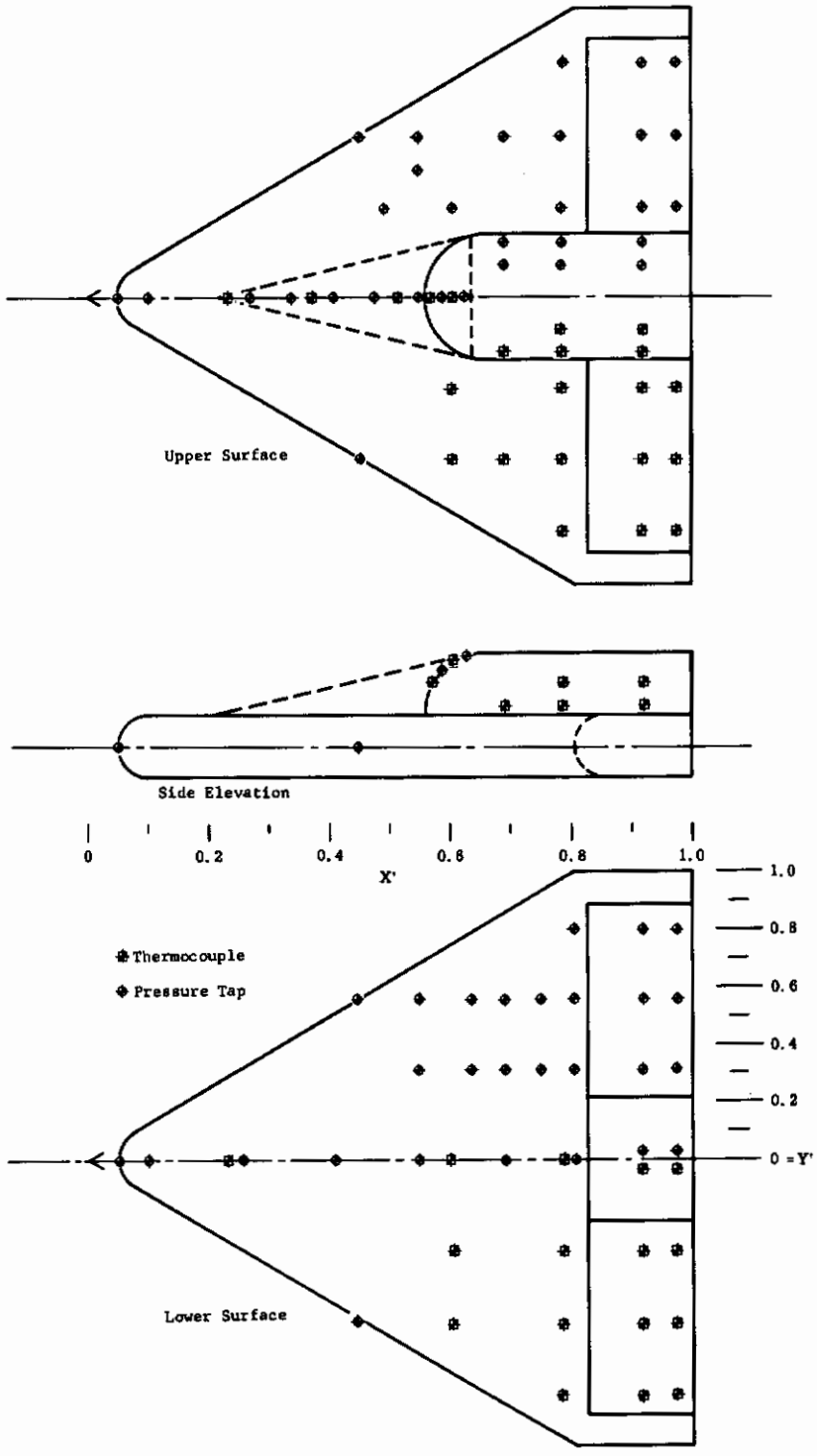

Figure 29. Line Drawings of Winged Re-entry Pressure and Heat Transfer Model

The pressure and heat transfer model was limited to a 12 inch span to fit inside the cooling shoes for the AEDC 50-inch Mach 8 tunnel. A geometrically similar model, but with a 16.8 inch span, was used to obtain six component force and moment data in the continuous flow wind tunnels. As indicated in Fig. 30, the balance cavity extended into the conical cabin fairing and all force data were obtained for this conical cabin configuration.

Three water cooled electric motors were contained within the force model and used to control the aileron-type trailing edge flaps and the movable apex of the delta wing. Attachable tip fins, full span +20° trailing edge flap, and trailing edge spoiler were provided.

A third geometrically similar model, having a 9-inch span, was tested in the AEDC Hotshot 2 hypervelocity facility. Further descriptions of these wing body models are given in Refs. 12 through 14, 16, and 18.

Finally, three models of the pyramidal configuration were required for the force, pressure, and heat transfer data. The configuration has a triangular cross section with 35° dihedral angles (see Fig. 1, page 2). The lower surface of the model is a blunt delta wing with 70° sweepback. The planar portions of the dihedral surfaces are right triangles and are connected by a cylindrical segment that forms the model's ridge line. The three cylindrical leading edges and the spherical nose have the same radius (also the same as for the wing-body configuration). The cross sectional shape is the same as one of the ASD-General Applied Sciences Laboratory pyramidal models tested in the AEDC Hotshot 2 hypervelocity facility (Ref. 46).

A photograph of the pressure and heat transfer model in the AEDC 40-inch supersonic tunnel is shown in Fig. 31. Again, the same flap actuator housing as used for the models described earlier, is evident immediately behind the model. The model has four, remotely controlled, trailing edge flaps, one on each dihedral surface, and two on the lower surface that are actuated as a pair. The flaps have rectangular planforms, and their hinge lines are parallel to the base of the model (perpendicular to the ridge line). The chords of the remotely controlled flaps are 15 percent of the virtual length of the model. The flaps are deflectable at angles between 0° and 40°, measured in the planes normal to the flap hinge lines. In addition to the remotely controlled flaps, one pair of instrumented flaps having a set deflection of 20° and a chord equal to 25 percent of the model reference length are attachable to the lower surface of the model.

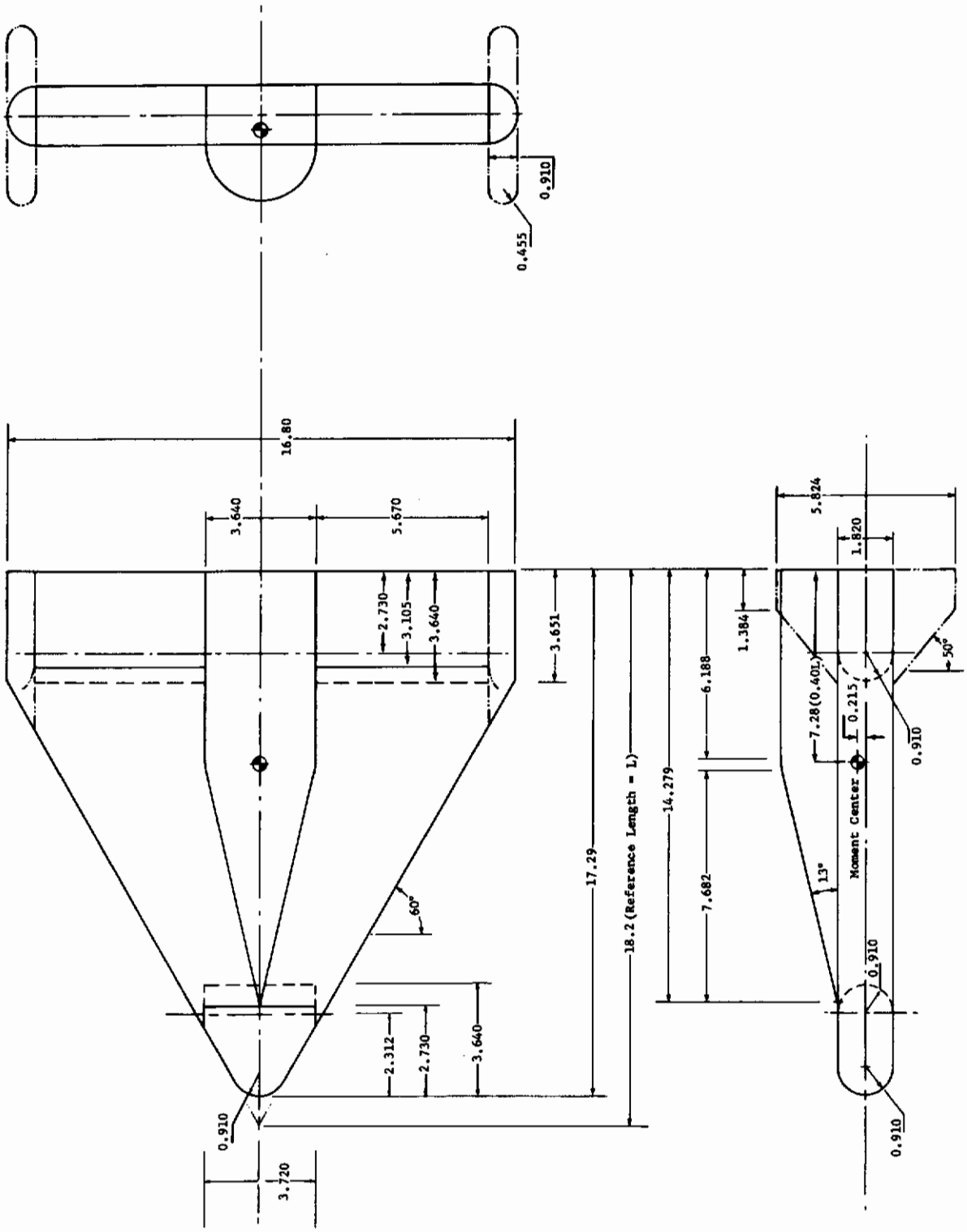

Figure 30. Force and Moment Model of Winged Re-entry Configuration

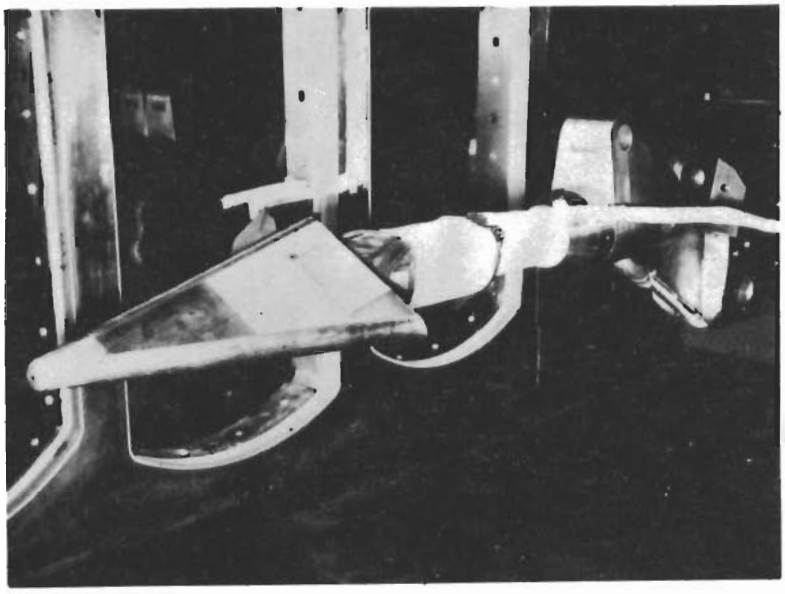

Figure 31. Photograph of Pyramidal Configuration in the AEDC 40-Inch Supersonic Tunnel

The model has attachable canards (Fig. 1, page 2) that have cylindrical leading edges and 45° sweepback. A ventral fin is attachable on the lower surface of the model between the trailing edge flaps; it can be set at fin (or rudder) deflection angles of 0° or +15° (trailing edge left), and has a chord equal to 15 percent of the model reference length. Instrumentation locations are indicated in Fig. 32.

The flaps on the dihedral surfaces of the force model (Fig. 33) were remotely controlled using water cooled motors and potentiometers contained within the model. The lower surface flaps were individually attachable (sideslip force data were obtained for asymmetric lower flap settings). The upper surface, port dihedral flap is supported by a force balance beam which is instrumented for flap normal force, hinge moment, and twisting moment; flap loads are presented in Ref. 23.

Finally, pressure and heat transfer data were obtained on a geometrically similar model in the Grumman Hypersonic Shock Tunnel. The model had a six-inch span and only 40° flaps were tested. Further descriptions of these models are given in Refs. 19 through 23.

Sample data obtained on the wing body and pyramidal configurations are presented in the following section.

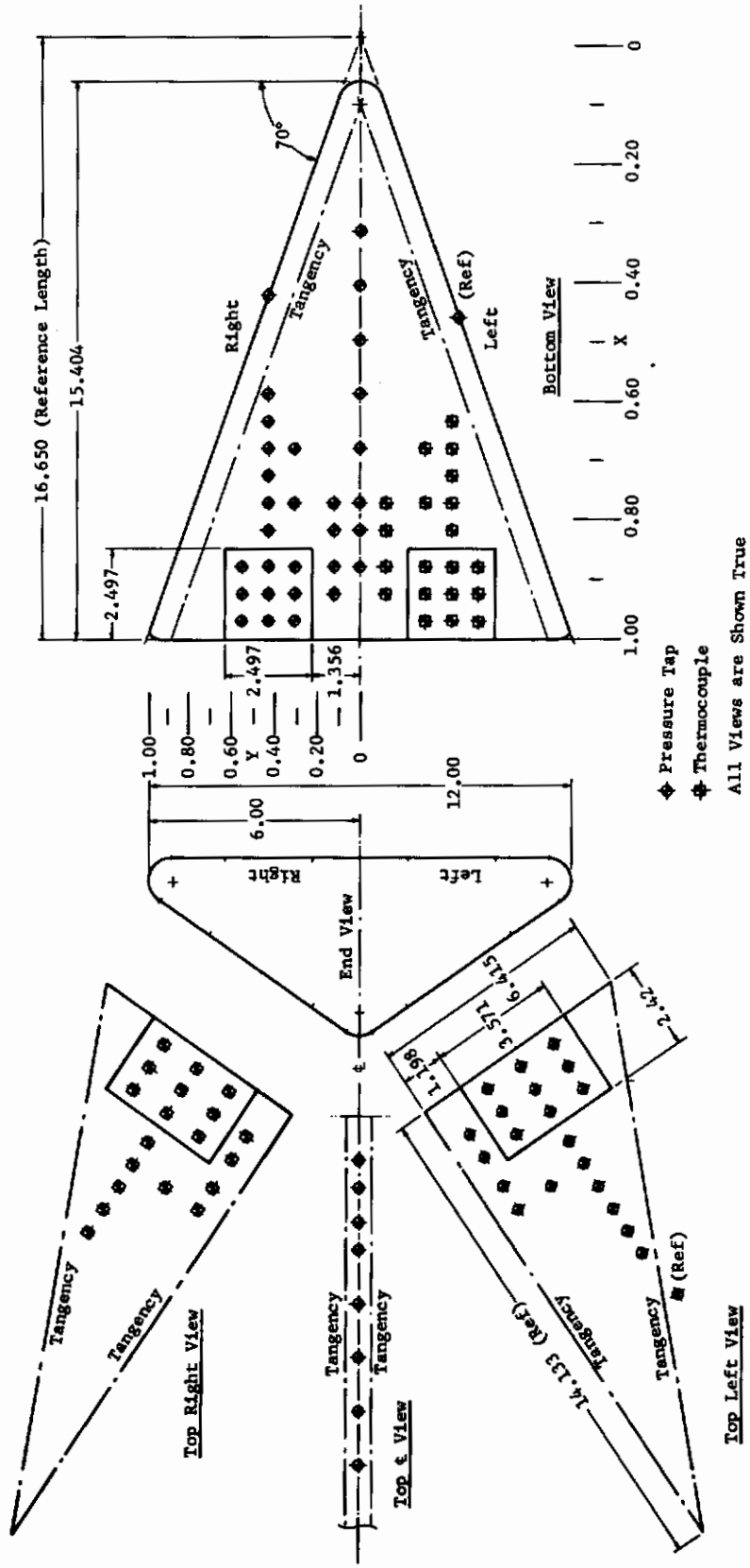

Figure 32. Line Drawing of Pyramidal Configuration Pressure and Heat Transfer Model

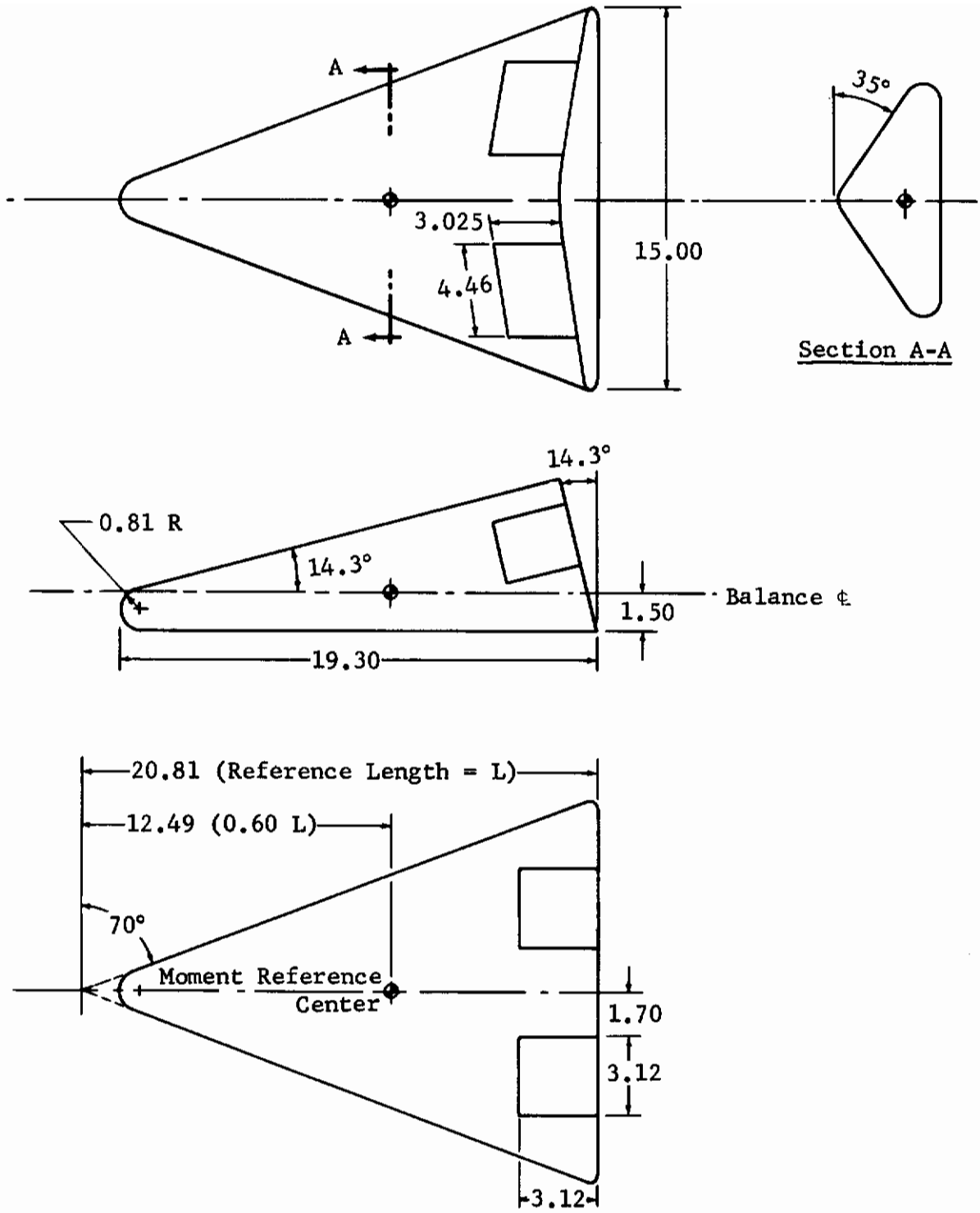

Figure 33. Force and Moment Model of Pyramidal Configuration

HYPERSONIC AERODYNAMIC CONTROLS

Controls are required to provide maneuvering capability for flight vehicles and can also be used to supply the aerodynamic stability and trim necessary to maintain an equilibrium flight trajectory. The most economical and straight-forward type of control for a vehicle flying in the atmosphere is usually an aerodynamic surface, but the application of aerodynamic control surfaces to hypersonic flight vehicles presents many formidable problems. For flight at very high altitudes, thick boundary layers and low dynamic pressure may render aerodynamic controls ineffective; extensive separated flow regions induced by deflected controls can alter the aerodynamic load distribution and stability characteristics throughout the flight regime. The over-all stability problems are aggravated by the large ranges of speed and angle of attack encountered by hypersonic flight vehicles. Further, these vehicles, as envisioned to present, tend to have compact geometries and therefore require high control loads to produce useful moments about the center of gravity.

Although innumerable control configurations are possible, the general problem areas can be investigated using a limited number of different types of controls on simplified configurations. Thus, the models described in the preceding section were used only as carriers for a wide assortment of aerodynamic controls and are not proposed as actual flight configurations. They served to generate different types of hypersonic flow interactions and provided information on control characteristics and effectiveness. The data obtained on the typical hypersonic flight configurations are readily available in a series of Air Force reports (Refs. 9 through 23, see Fig. 1, page 2). The reports contain plots of all the pressure, aerodynamic heating rate, force, moment, and flap load data, and also many flow photographs.

This section contains selected data from the broad experimental program on the effectiveness of aerodynamic controls for hypersonic flow conditions. Representative results are presented for trailing edge flap type controls. The term "flap" is used herein to denote controls with a general type of geometry, rather than their function. Thus, trailing edge elevators, ailerons, or elevons are all referred to as flaps. Results for the other aerodynamic controls tested and salient aspects of the data are discussed qualitatively.

We also present, in the Appendix, a synopsis of the information on hypersonic aerodynamic controls available in the literature. For a number of these reports we present, in tabular form, information on the control tested, the vehicle configuration, the test conditions, and the data obtained. The remainder of the reports listed in the Appendix will also be of great interest to those working in the field of hypersonic aerodynamic controls.

Delta Wing Body Combination

Partial and full span flaps were tested on the trailing edge of a blunted, 60° sweepback, delta wing with clipped tips and an overslung body (see preceding section). The partial span flaps were independently operated (travel angle of ±40°), and data were obtained for both symmetric and asymmetric flap settings. The wing apex was deflectable (travel angle of ±20°). The model also had an attachable trailing edge "spoiler" (used in this case to generate pressures, like a +90° flap).

The basic wing-body combination provides controls information for configurations having either overslung or underslung bodies. For convenience we have chosen the overslung body configuration as our reference and we have defined the coordinate system and control deflection angles with reference to this basic configuration (positive control deflection angles increase C_N for $\alpha \approx 0$). Thus the positive angle of attack regime for the overslung body provides the aerodynamic data for the underslung body at negative angles of attack. The sign of the flap deflection angles, for the underslung body case, must be reversed so that both cases are viewed in the same reference system. This definition fixes the flat plate surface of the wing as the lower surface for the results presented herein. The angle of attack is positive when the flat plate surface is windward. The static longitudinal aerodynamic characteristics at Mach 5 and 8 of this basic configuration are shown in Figs. 34 through 36. Increments due to symmetric deflections of the trailing edge flaps are presented in each figure. Fig. 34 also presents the angle of attack for zero normal force and Fig. 35 presents the trim angle of attack; these are presented as functions of the flap deflection angle.

The flaps are effective in producing force increments through the entire angle of attack range and are most effective when deflected into the incident flow. The normal force increments increased with angle of attack for positive flap deflections at positive angles of attack and negative flap deflections at negative angles of attack up to angles of attack of about +30° and -30°, respectively. Beyond these angles of attack the incremental normal force coefficients decreased with increasing angle of attack. At high angles of attack and large flap deflection angles, the flap is almost normal to the flow and contributes little to the normal force coefficients. The geometric effects can be seen by comparing the curve of ΔC_N for $\delta_L = \delta_R = 20°$ and 40°. For the 20° flap deflection case, the peak ΔC_N occurs at $\alpha \approx 40°$, while for the 40° flap deflection case, the peak ΔC_N occurs at $\alpha \approx 25°$. It is also noted that the flaps produce incremental normal force coefficients through the entire angle of attack range, even when they are deflected out of the flow (Fig. 34); in part this is due to the pressure relief on the windward side of the model.

With the moment reference center at 60 per cent of the virtual root chord the basic configuration was statically stable at Mach 5 and 8 for the middle portions of the angle of attack ranges for all flap deflections tested (Fig. 35). Based on the trim angles obtained

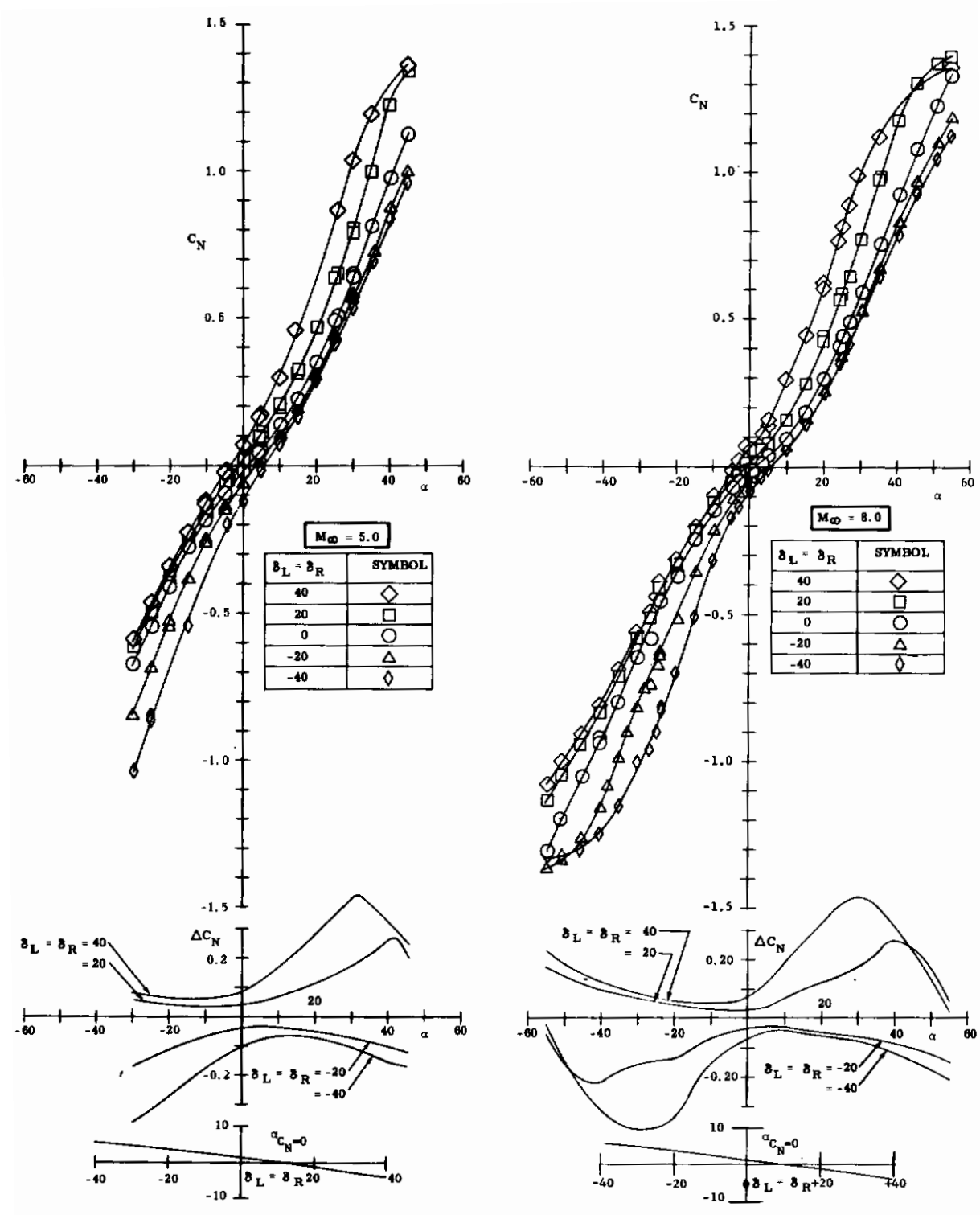

Figure 34. Normal Force Coefficients for Delta Wing Body Combination with Symmetric Flap Deflections

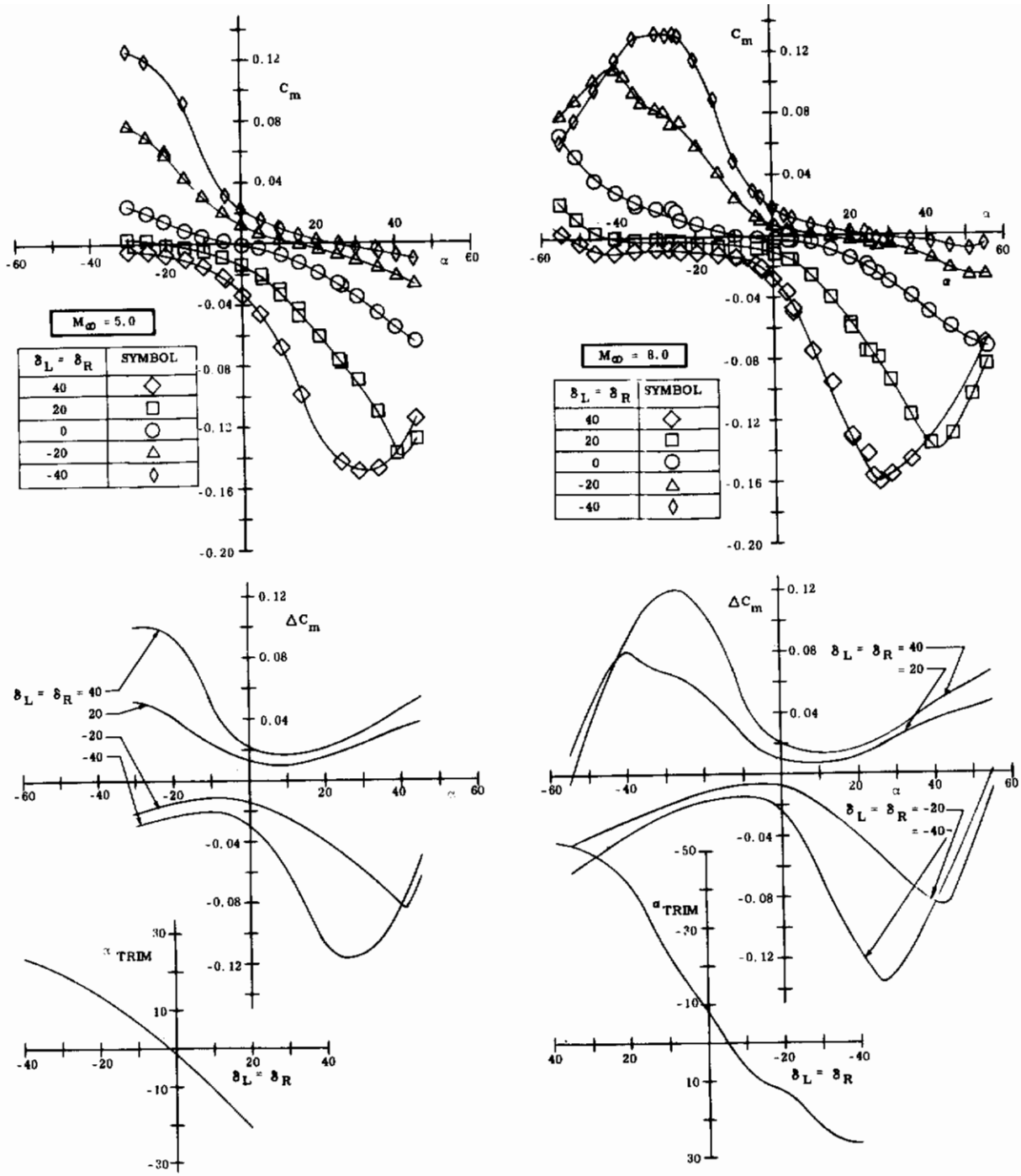

Figure 35. Pitching Moment Coefficients for Delta Wing Body Combination with Symmetric Flap Deflections

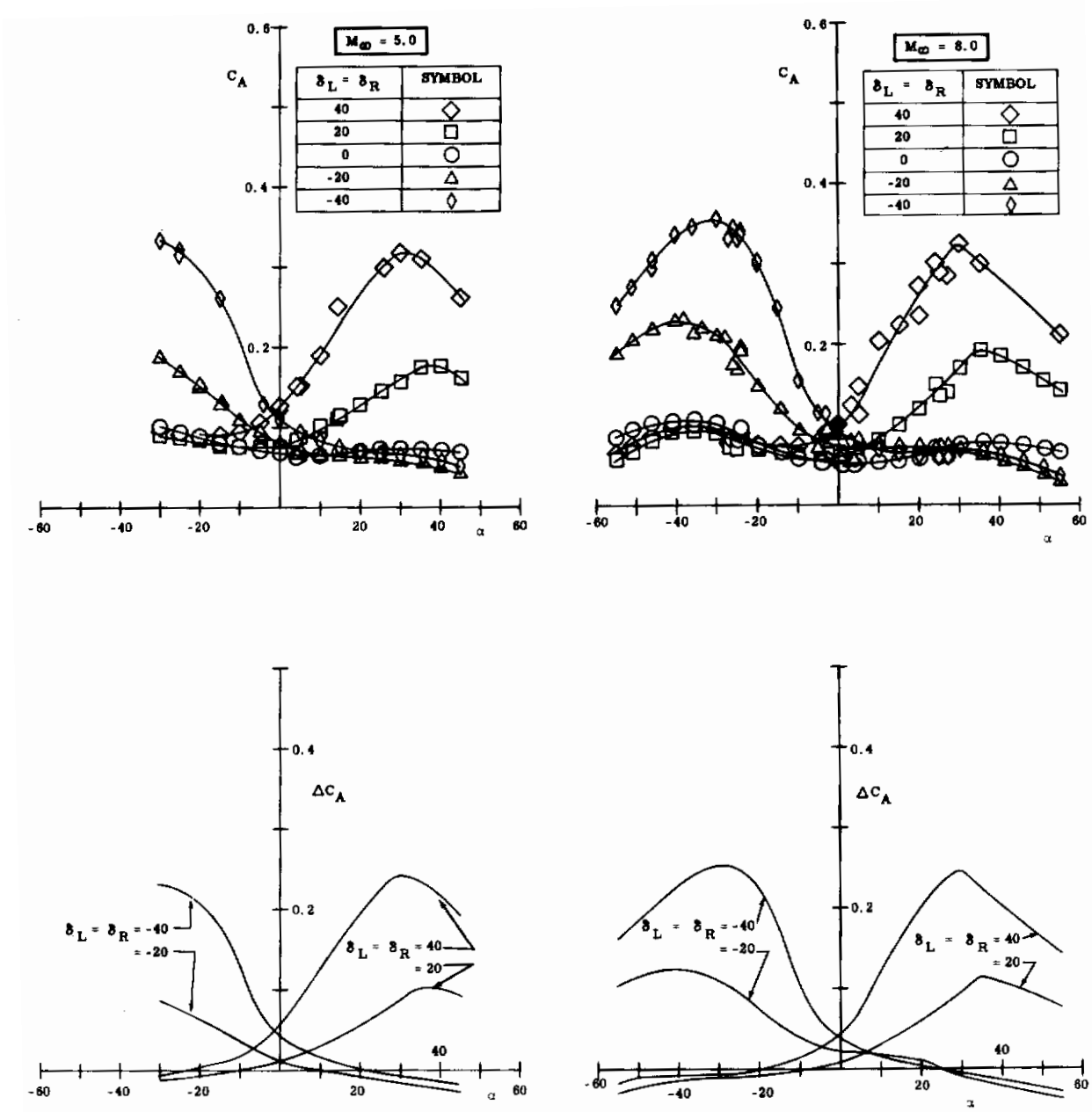

Figure 36. Axial Force Coefficients for Delta Wing Body Combination with Symmetric Flap Deflections

at Mach + it is believed that a trim point would be found at Mach 5 for the 40° flap deflection if the tests had been extended to higher negative angles of attack. Although trim points were found for all flap deflection angles at Mach 8 there are large ranges of angle of attack where the stability of the configuration, using these flaps, varies from marginal to neutral.

Strong pitch-up (indicated by a decrease in restoring moment negative at $+\alpha$ and positive at $-\alpha$), is observed when the flaps are deflected into the flow. The angle of attack at which pitch-up occurs is strongly dependent on the flap deflection angles. This dependency is caused by the extensive separated flow areas induced by large flap deflection angles. This flow separation tends to limit the pressure rise on the flap but induces a strong pressure rise on the wing forward of the flap hinge line. The forward movement of the center of pressure, due to this effect, sharply decreases the pitching moments.

In the angle of attack range where the flaps are deflected into the flow, and prior to the onset of pitch-up, these flaps are effective generators of restoring moments for both the overslung and underslung configurations. Due to the marginal stability when the flaps are deflected out of the flow, the trim points are not well defined.

The axial force coefficients, and the incremental changes due to symmetric flap deflections, for Mach 5 and 8 flows, are presented in Fig. 36. As expected, the axial force increments induced by the flaps are positive and large when they are deflected into the incident flow and small, or negative, when they are retracted out of the flow. These negative increments imply a reduction of the axial force coefficient by the retraction of a sector of the wing from a high pressure area. This same effect can be seen in the normal force coefficients.

The addition of tip fins to this configuration produced increases in the normal force coefficients and the axial force coefficients at both Mach 5 and 8. The effectiveness of the flaps increased in the presence of the tip fins. The slope of the resulting pitching moment curve increases and the extent of the marginal stability range was decreased. The presence of the fins narrowed the latitude of trim angles associated with flap deflection. These effects are illustrated in the following sketch.

Comparisons were obtained between the partial span trailing edge flaps and a full span flap for a flap deflection angle of $+20^{\circ}$. A full span spoiler, having the same height as the $+20^{\circ}$ flap, and a deflectable apex were also tested (see preceding section for further

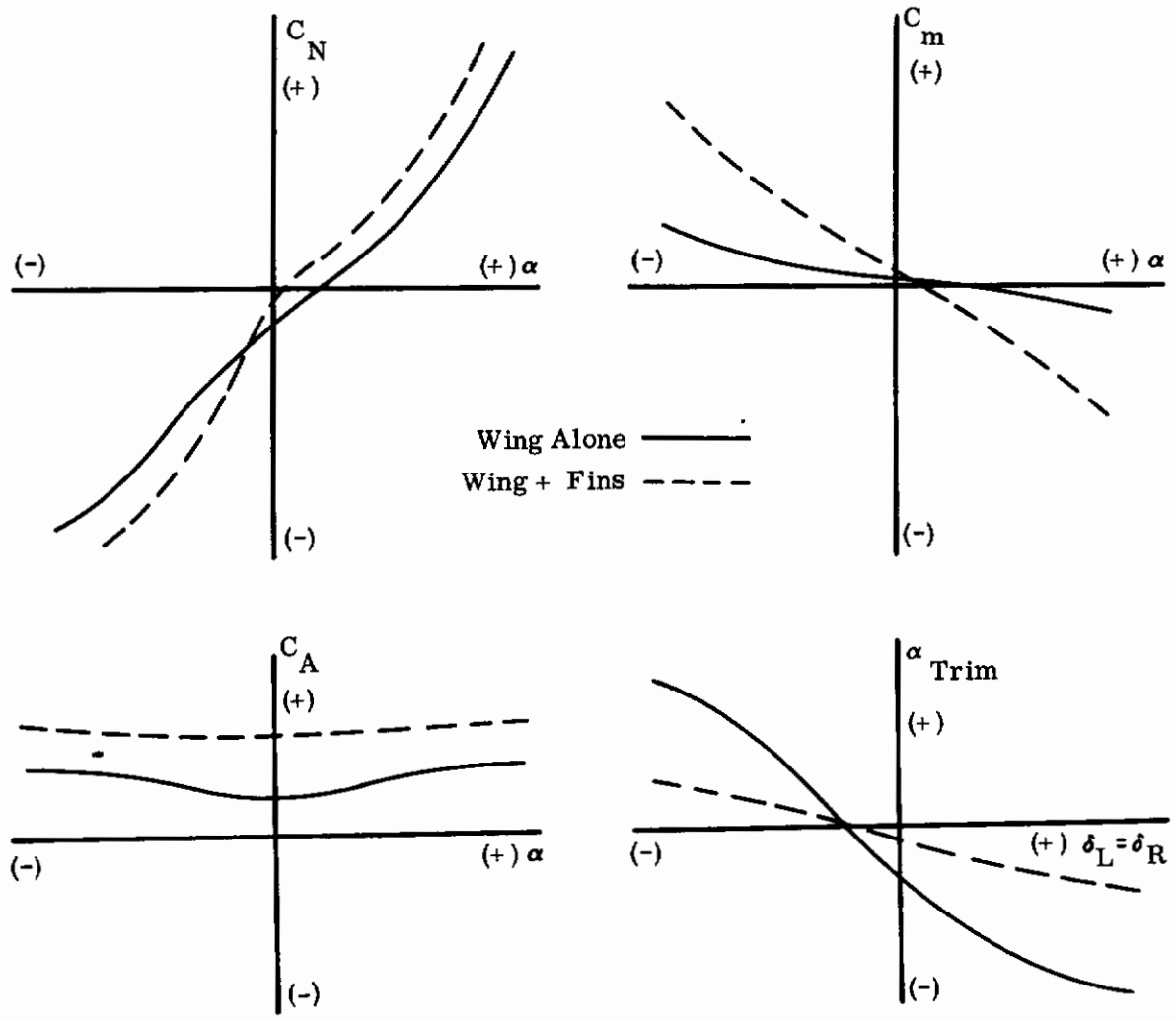

Delta Wing - Fin Effects

description of these controls). As shown in the following sketches, the added control surface area of the full span flap produced positve normal and axial force increments and stronger restoring moments. The full span spoiler was effective in producing increments of normal force and restoring pitching moment when it was exposed to the flow. The effectiveness, approximately the same as the full span flap, increased with increasing angle of attack in the angle of attack range of 0° to $+25^{\circ}$. It also produced increases in the axial force coefficients. The deflectable apex, although it produced slight increments in normal force and pitching moments, was not as effective as the other controls investigated.

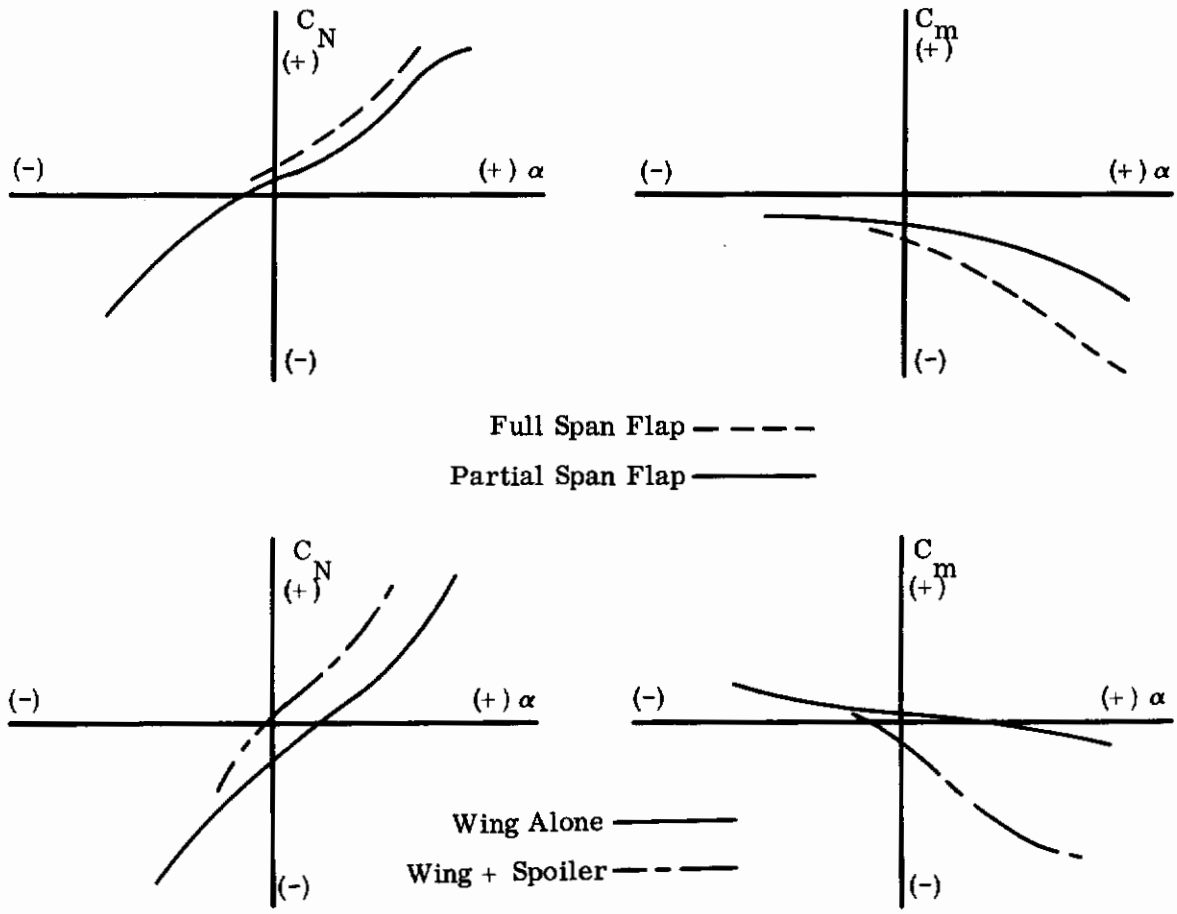

Delta Wing - Full Span Flap - Spoiler Effects

The lateral and directional characteristics of the aileron type flaps on the basic configuration are shown in Fig. 37. The aileron controls are effective over the range tested whether they are deflected separately or differentially. Around $\alpha \approx 0$, the individually deflected flaps produce lower rolling moments and higher, adverse, yawing moments than the differentially deflected flaps. As the angle of attack is increased, and one of the differentially deflected flaps is shielded by the wing, the differences in response of both types of roll control diminish. The effectiveness increased with increasing control deflection and increasing angle of attack. The adverse yawing moment also increased with increasing control deflection and angle of attack with the exception of the region around $\alpha \approx 0$ where differential flap deflections tended to minimize the adverse yawing moments. When both flaps are exposed to the flow they produce opposite (cancelling) yawing moments except for the interference loads induced on the body that are generally quite small. The addition of the fins had little effect on the yawing moments ($\beta = 0$) but did, in general, increase the rolling effectiveness.

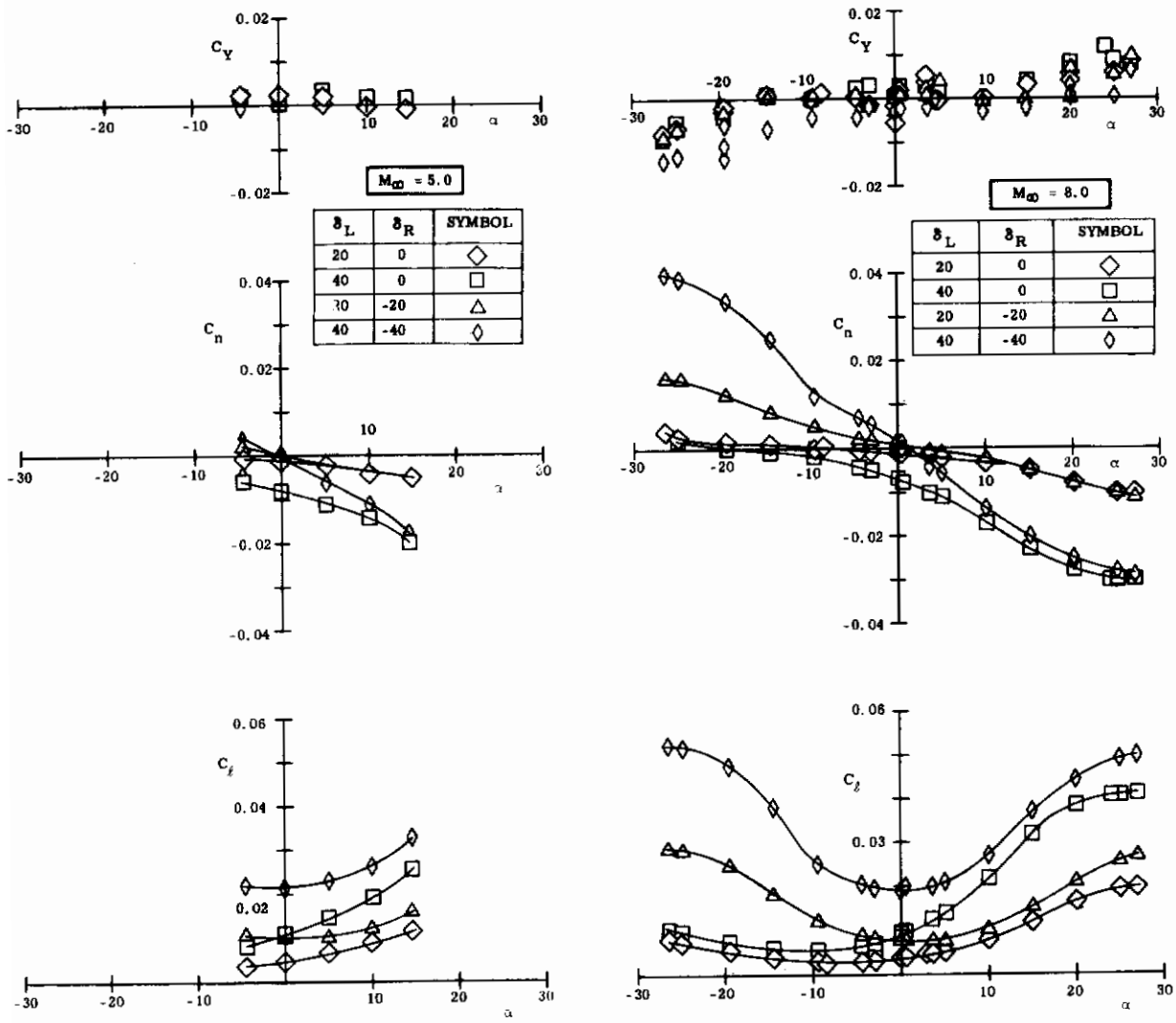

Figure 37. Lateral and Directional Characteristics for Delta Wing Body Combination with Asymmetric Flap Deflections

We have also included a group of pressure and heat transfer distributions in order to provide a better understanding of the effects of control deflection and angle of attack on the aerodynamic characteristics of the vehicles (Fig. 38). These distributions are representative of those obtained at Mach 5 and 8 and do not necessarily indicated the peak values that were induced by interference effects. For comparison purposes we have also included sample Mach 19 data. The complete pressure and heat transfer distributions can be found in Refs. 9 through 17, a few of the results are summarized here. Evident immediately is that control deflections produce large increases in pressure and heat transfer on the control itself. Moderate deflection angles and angles of attack ($\alpha \rightarrow 20^{\circ}$, $\delta \rightarrow 20^{\circ}$) do not induce extensive separation forward of the hinge line. Large flap deflections induce separation far forward of the hinge line at all angles of attack while at high angles of attack all flap deflections tested induced strong separation effects forward of the hinge line. These observations on the pressure distributions explain the increased control effectiveness in the low and intermediate angle of attack and control deflection ranges (due to pressure increase on controls that are aft of the moment center), and the decrease in effectiveness at high angles of attack (due to pressure decrease on flap and pressure increases on wing forward of moment center).

The heat transfer data, presented in Fig. 38, show extreme heating rate values on the flaps at high angles of attack and large deflection angles. In some cases the measured values exceeded those calculated at the blunt nose stagnation point. This heating problem is a major stumbling block to the design of hypersonic aerodynamic controls.

Pyramidal Configuration

Trailing edge flaps were also tested on the blunt pyramidal configuration described in the preceding section (Fig. 33). The lower surface, a 70° sweptback delta, and the upper (dihedral) surfaces, have 15 percent root chord trailing edge flaps. Angle of attack is referenced to the lower, delta wing, surface and is positive when this surface is windward. The dihedral surfaces are aligned with the flow, and their flap hinge lines are perpendicular to the flow, at a model angle of attack of 14.3°. Flap deflection angles, whether for the upper on lower surfaces, are positive when deflected away from the surface.

The static longitudinal aerodynamic characteristics of the basic pyramidal configuration are shown in Figures 39 through 41. The experimental data are presented and also the increments due to symmetric deflections of the upper or lower flaps. The angles of attack for zero normal force and the trim angles of attack are presented as functions of the flap deflection angles in Figs. 39 and 40.

As for the wing-body combination, the flaps were effective in producing useful normal force increments and restoring pitching moments when deflected into the incident flow. When, however, the flaps were shielded by the body they were ineffective as controls.

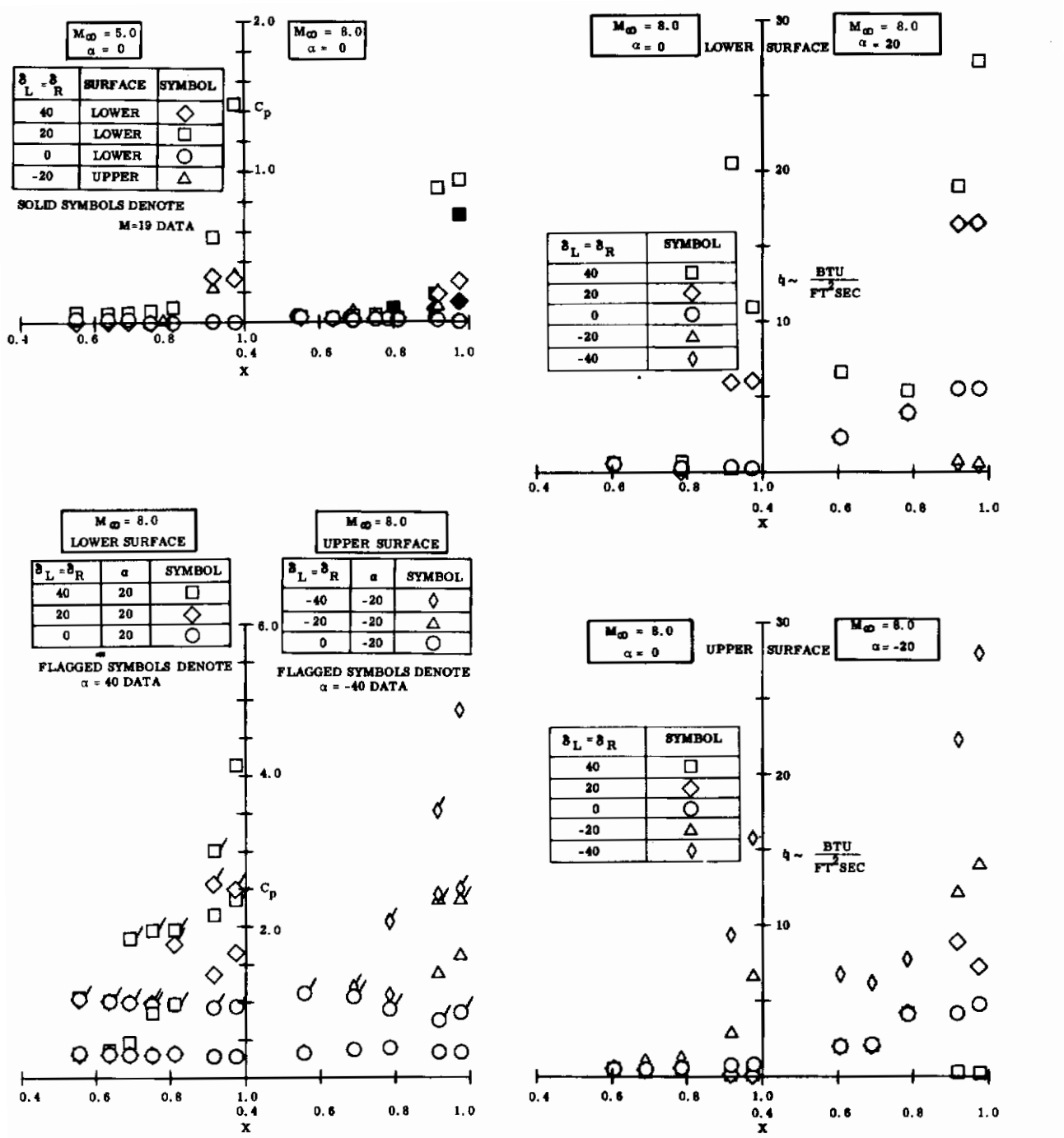

Figure 38. Typical Pressure and Heat Transfer Distributions Along Flap Centerline for Delta Wing Body Combination

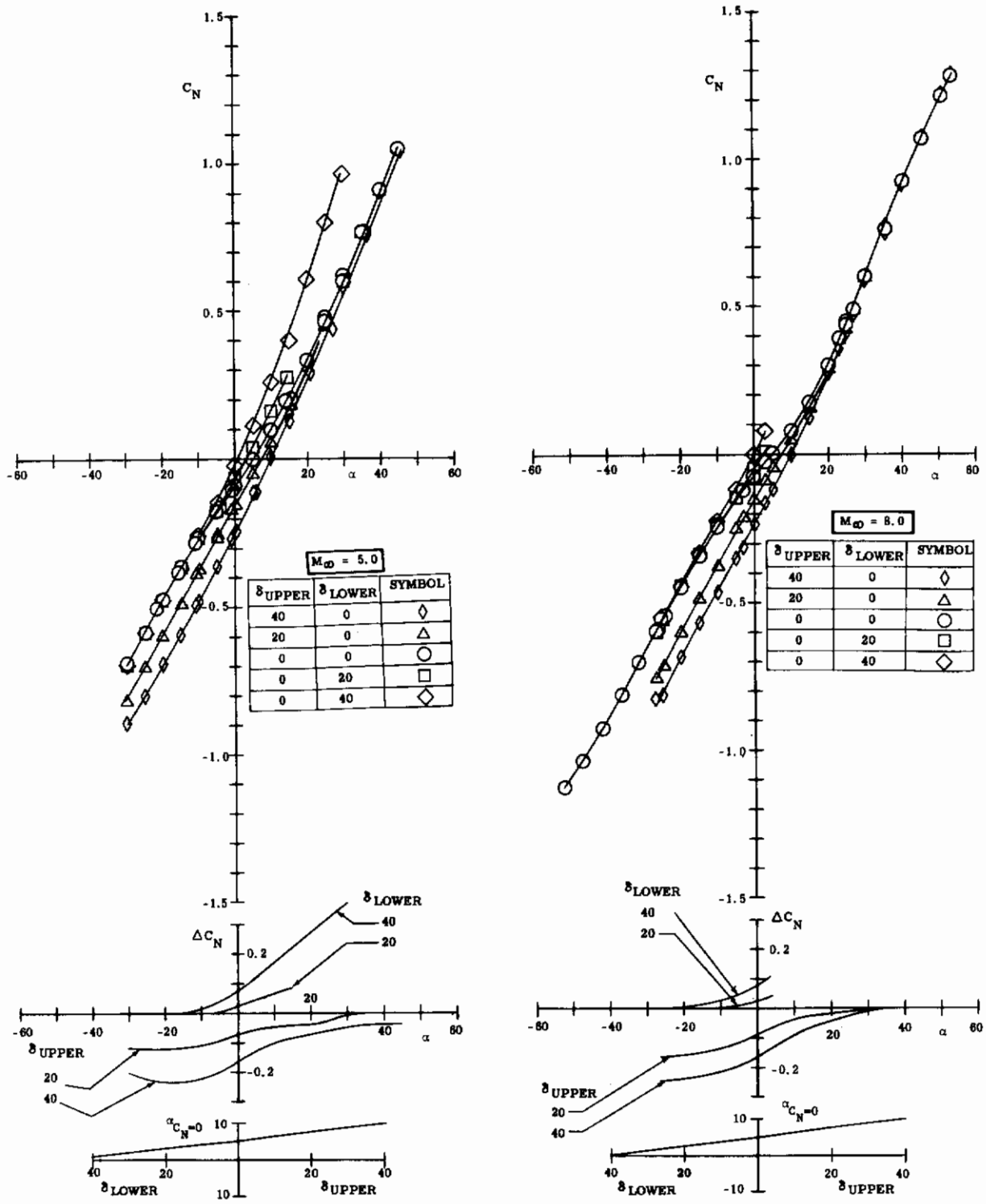

Figure 39 Normal Force Coefficients for Pyramidal Configuration with Symmetric Flap Deflections

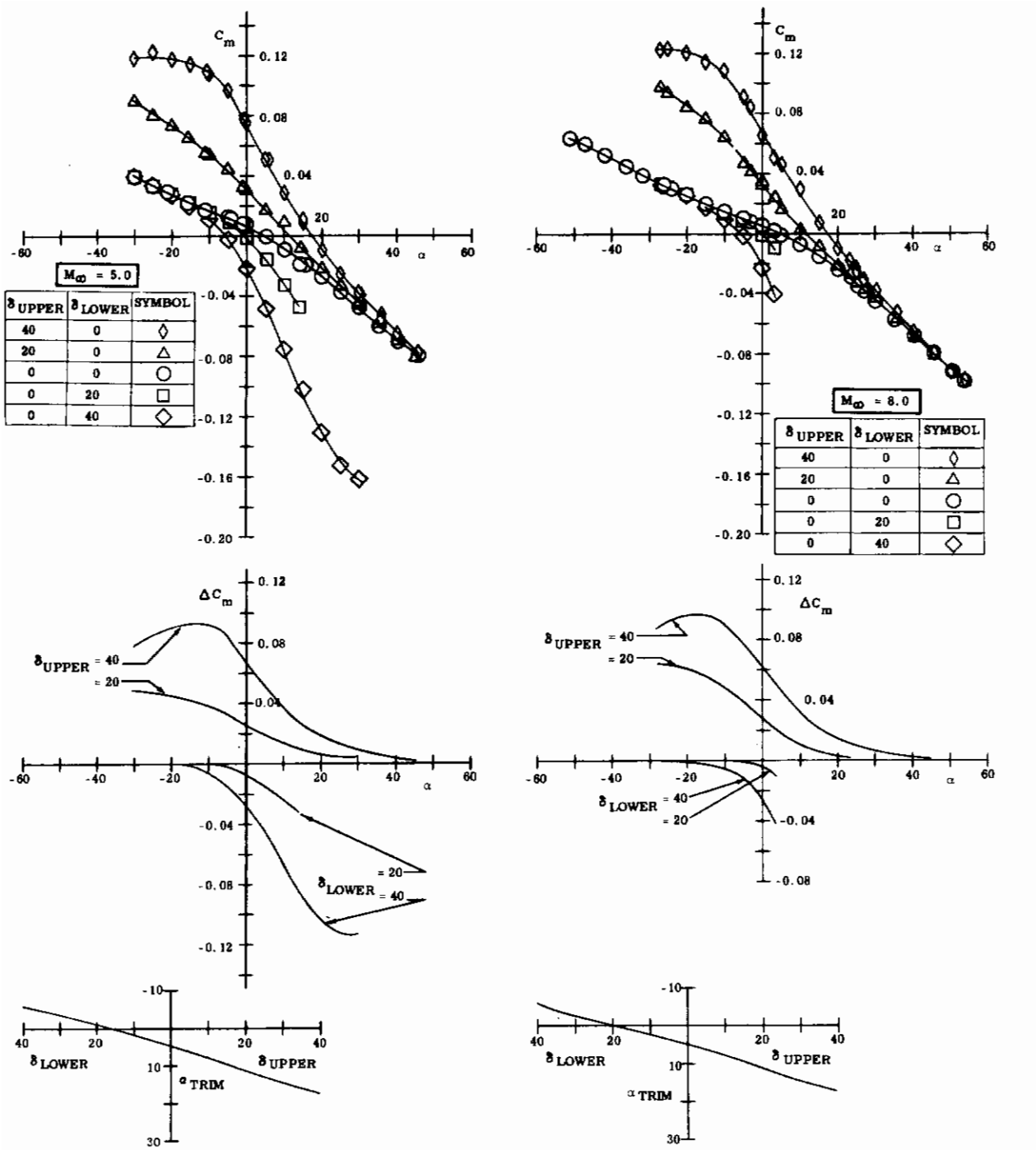

Figure 40. Pitching Moment Coefficients for Pyramidal Configuration with Symmetric Flap Deflections

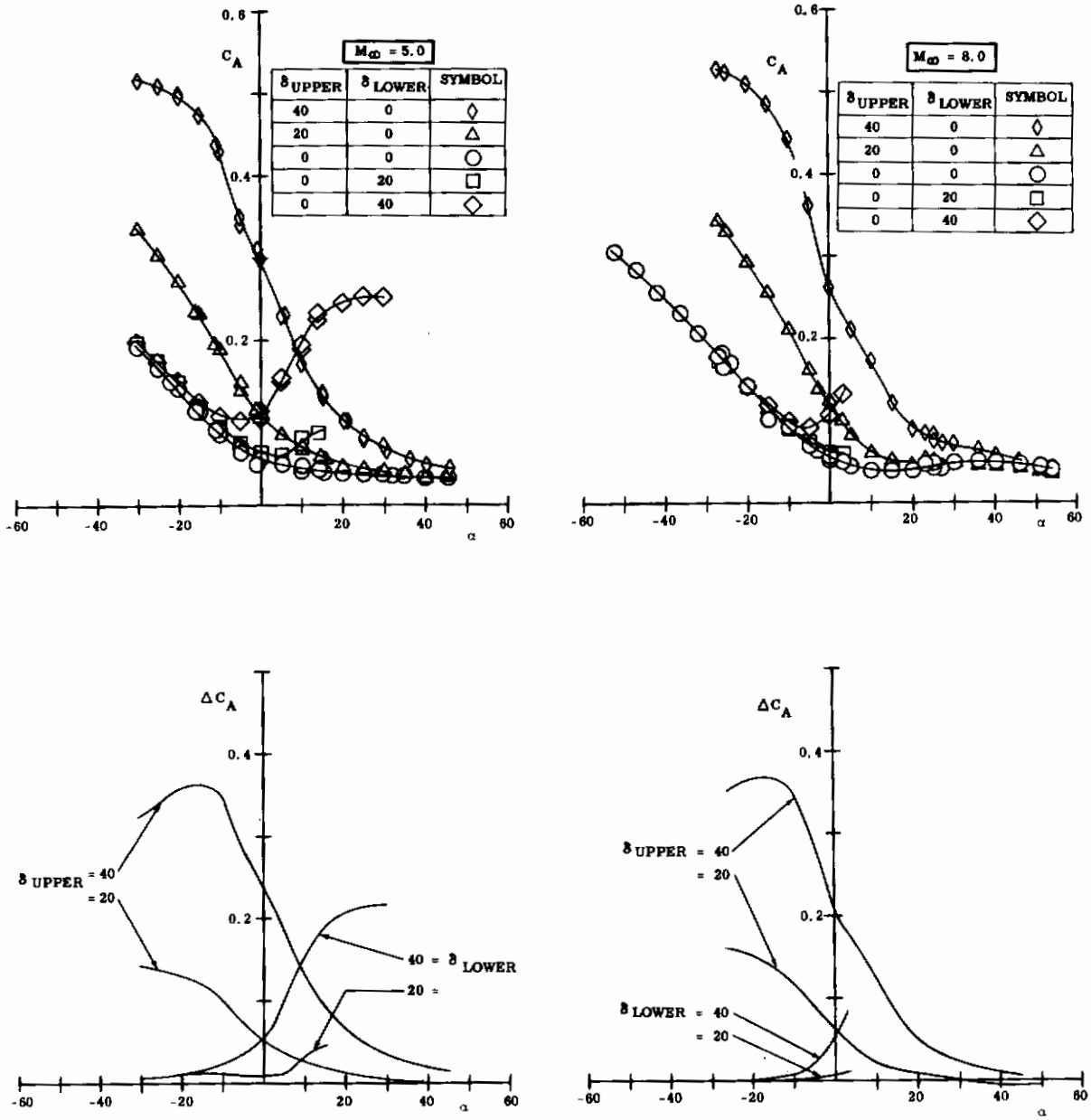

Figure 41. Axial Force Coefficients for Pyramidal Configuration with Symmetric Flap Deflections

The normal force increments increased with flap deflection angle and angle of attack; the increases being in the positive angle of attack range for the lower surface flaps and in the negative angle of attack range for the upper surface flaps. With the moment reference center at 60 percent of the virtual length of the model, this configuration was statically stable for all flap deflection angles at Mach 5 and 8.

Trim points were found for all flap deflection angles. The spread of trim points was small (from $\alpha \sim -10^{\circ}$ to $\alpha \sim +20^{\circ}$) and there were not any regions of neutral or marginal stability. The data available indicate that, if the tests had been extended to higher values of angle of attack, a pitch-up problem would have been encountered. Generally speaking the increments in restoring pitching moment coefficients increased with both flap deflection angle and angle of attack. Deflection of the upper (dihedral) surface flaps produced larger axial force coefficients and larger increments than the lower surface flaps.

The longer chord lower surface flaps (25 percent root chord) produced modest increments in normal force and restoring pitching moment, as indicated in the following sketch.

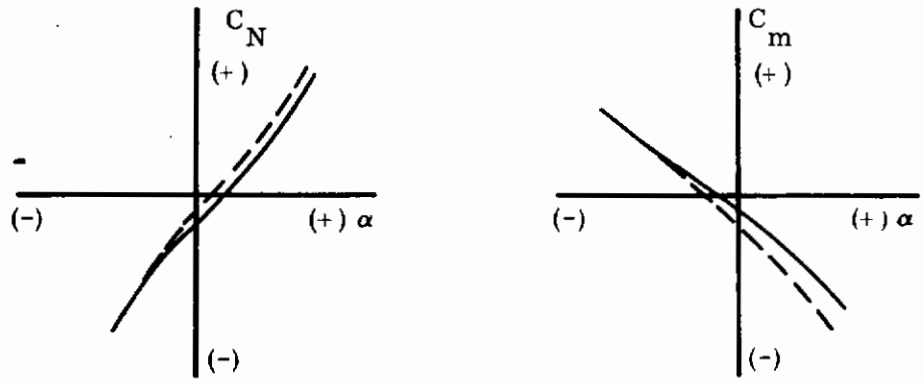

Short Chord Flaps ———

Long Chord Flaps – – – –

Effect of Flap Chord on Pyramidal Body

The lateral and directional aerodynamic characteristics or this configuration due to single flap deflections are shown in Fig. 42. A strong, unstable, yaw-roll coupling exists similar to that for the singly deflected aileron type flap; some form of differential flap deflection would be required to eliminate this problem.

The canards, when mounted on the basic pyramidal configuration, produced positive increments in normal force, axial force, and nose-up (destabilizing) pitching moment. The small ventral fin (see preceding section) had negligible effect on the normal force. It produced

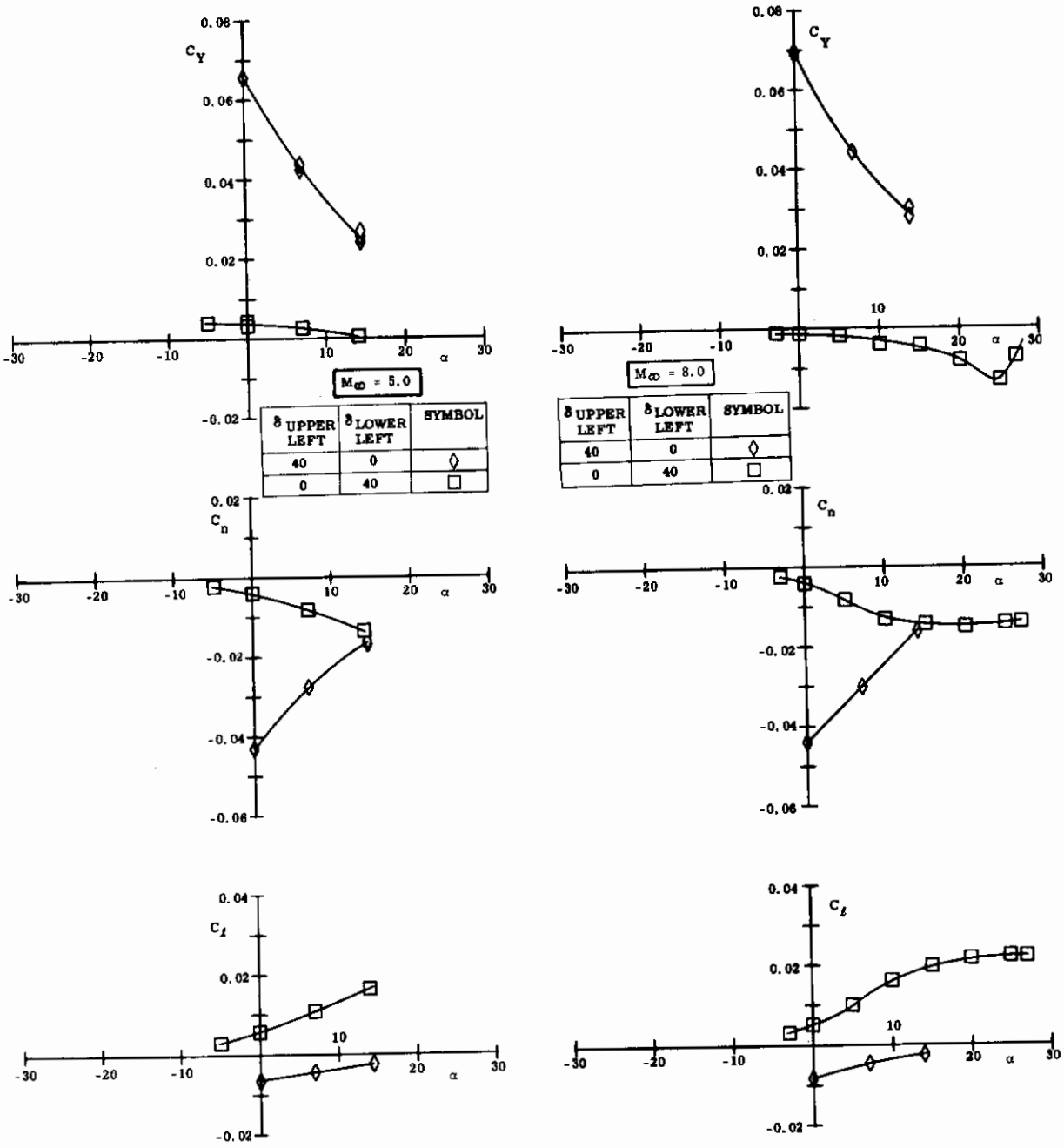

Figure 42. Lateral and Directional Characteristics for Pyramidal Configuration with Asymmetric Flap Deflections

small increases in the axial force and nose-down (stabilizing) pitching moment; in the low side-slip angle range it provided no significant improvement over the basic body. These effects are illustrated in the following sketches.

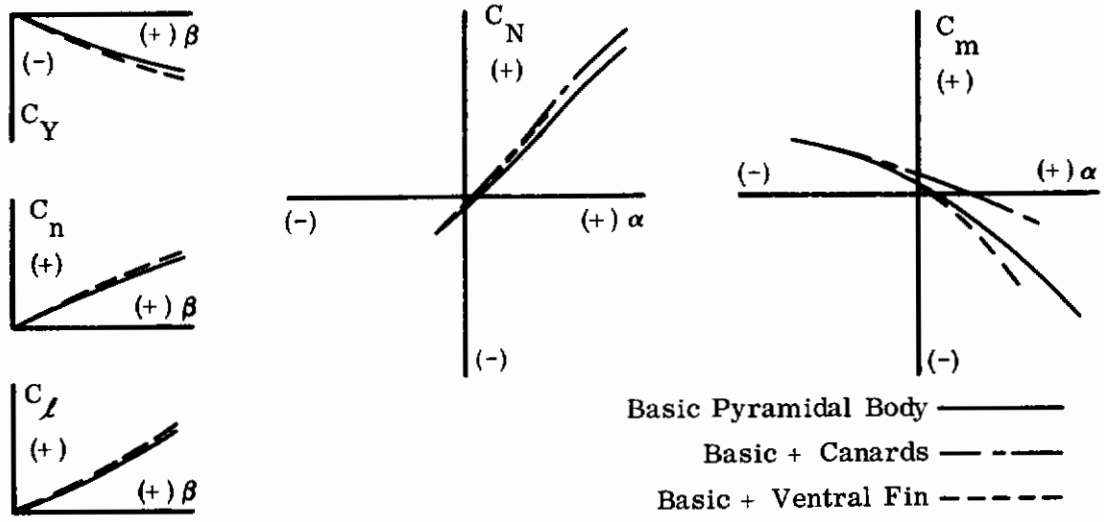

Effect of Fins and Canards on Pyramidal Body

In addition to the six component force and moment data for the configuration, three component flap loads were obtained for all test conditions. Plots of the flap normal force, hinge moment and twisting moment for the particularly wide range of test conditions indicated in Table I, page 43, are presented in Ref. 23.

Typical pressure and heating rate distributions along flap centerlines are shown in Fig. 43. The pressures and aerodynamic heating rates exhibit generally the same effects as previously noted for the flaps on the wing body combination. Again, some representative hypervelocity (Mach 21, Ref. 22) data are included. Plots of all the pressure and heat transfer data are readily available in Refs. 19 through 22.

Some of the results of the investigations described in this section may be summarized as follows:

1) Trailing edge flaps of reasonable proportions are effective pitch and roll controls in the hypersonic regime and are effective trimming devices.

2) Tip fins reduced trim angle changes due to flap settings.

3) Strong, adverse yaw-roll coupling results from the use of a single flap (particularly for $\alpha \approx 0$); differential flap settings reduce this considerably.

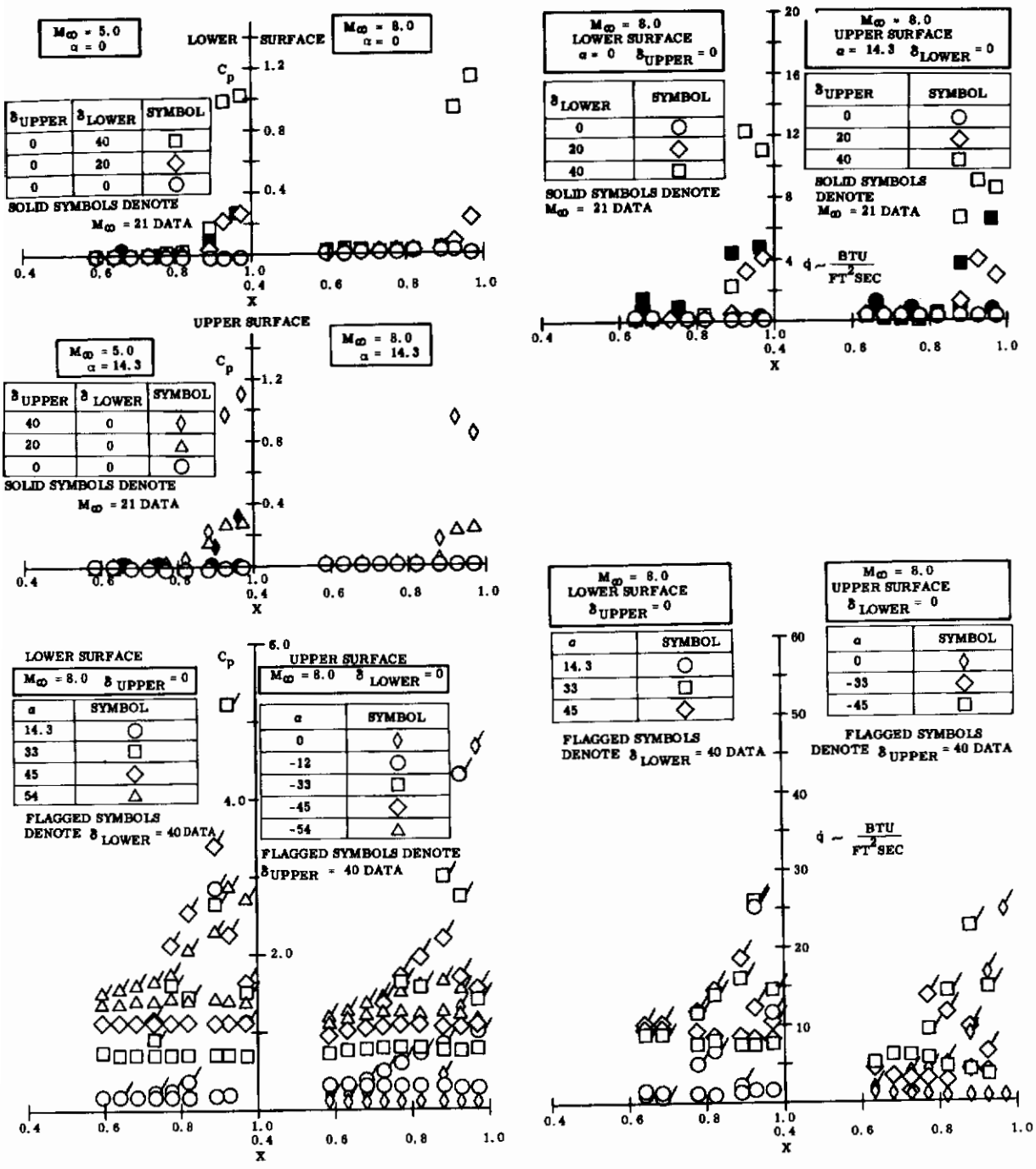

Figure 43 Typical Pressure and Heat Transfer Distributions Along Flap Centerline for Pyramidal Configuration

4) Deflected flaps induce separated flow regions on the vehicle surface forward of the flap and produce very high heating rates and pressures on their own surface and increase the heating rates and pressures on the vehicle surface forward of the flap.

5) Full span flaps, full span spoilers, and canards are also effective pitch control devices.

CONCLUSIONS AND RECOMMENDATIONS

Only the more salient aspects of our research investigation of hypersonic flow separation and control characteristics are presented in this section. The entire report, by its format and intended nature, is a summary of conclusions drawn from the preliminary theoretical and experimental investigations. The experimental results were disseminated widely (Refs. 5 through 21) because of their timeliness and the need for hypersonic flow data, but much work remains to be done in analyzing the data and understanding the observed phenomena.

Aerodynamic heating rates, pressure distributions and loads are severely affected by separation. The extent of separation depends on the nature of the boundary layer, stream conditions, and model geometry. Three-dimensional effects are of first order importance for the highly vortical reverse flow in separation regions. Thus, even for the seemingly two-dimensional models (flat plate with trailing edge flaps), the separated flow is essentially three-dimensional in nature and strongly affected by finite span effects. End plating the model prevented venting of the trapped reverse flow in the separation region and doubled the extent of separation. This greatly changed the chordwise pressure and heating rate distributions, increasing their values on the plate surface while decreasing their values on the flap surface.

Streamwise pressure and heating rate gradients are extremely large just prior to reattachment and lead to exceptionally high pressures and heating rates downstream of reattachment on trailing edge flaps. In many cases the peak pressures and heating rates recorded on the trailing edge flaps were more than twice as large as blunt nose stagnation point values. These high values result from the flow being compressed through many oblique shock waves, thereby avoiding strong normal shock losses. As expected, these effects become more pronounced for the higher Mach number free stream flows.

Leading edge separation and flows over sharp expansion corners were investigated to determine the fluid flow mechanisms responsible for breakaway separation. This type of separation occurs at convex corners where the local pressure gradient, in the inviscid sense, is favorable. It was found that in the complete absence of adverse pressure gradients, even for machined sharp expansion corners, no flow separation occurred. The existence of an adverse pressure gradient is a necessary condition for separation. However, for breakaway separation, the adverse pressure gradient can be far downstream, the pressure rise effects are propagated upstream through the boundary layer. Thus, as for standard boundary layer separation, adverse pressure gradients were found to be the prime cause of breakaway separation.

The interaction due to a fin generated shock wave with the boundary layer on a flat plate is fundamentally different for supersonic and hypersonic flows. In supersonic flows, the region of separation on the plate surface is limited to the vicinity of the shock wave. In hypersonic flows, the separated flow region on the plate extends from the fin root to far outboard of the shock location. The line of separation, far enough downstream of the fin leading edge, more nearly follows a conical ray emanating from the fin leading edge. The large extent of the separated flow region, in part is due to the thickness of the hypersonic boundary layer.

Separated flows ahead of trailing edge flaps on typical hypersonic flight configurations are predominantly three-dimensional. Spanwise gradients of pressure and heating rates are equal in magnitude to their streamwise gradients. When finite span effects are better understood, it is recommended that leading edge bluntness effects also be investigated. These effects should then be included, probably empirically, in establishing engineering methods for predicting the extent of separation ahead of trailing edge flaps. Probably in conjunction with the aerodynamic heating rate estimates, engineering methods should be developed for calculating shear forces.

REFERENCES

1. Kaufman, L. G. II, Oman, R. A., Hartofilis, S.A., Meckler, L. H., Evans, W. J., and Weiss, D., A Review of Hypersonic Flow Separation and Control Characteristics, ASD-TDR-62-168, March 1962.

2. Kaufman, L. G. II, Meckler, L. H., Weiss, D.,and White, R. F., Feasibility of Using Honeycomb Sandwich Construction for Aerodynamic Heat-Transfer Models, Grumman Research Department Memorandum RM-208, July 1962.

3. "Honeycomb Wind Tunnel Models Give Fast Thermal Response," Space/Aeronautics, Vol. 40, No. 5, p. 130, October 1963.

4. Evans, W. J. and Kaufman, L. G. II, Pretest Report on Hypersonic Flow Separation and Control Models for AEDC Tunnels A, B, Hotshot 2 and Grumman Hypersonic Shock Tunnel, Grumman Research Memorandum RM-209, July 1962.

5. Kaufman, L. G. II, Pressure and Heat Transfer Measurements for Hypersonic Flows Over Expansion Corners and Ahead of Ramps, ASD-TDR-63-679, Part I: Mach 5 and 8 Data for Expansion Corner Flows, September 1963, Part II: Mach 5 Pressure Data for Flows Ahead of Ramps, September 1963, Part III: Mach 8 Pressure Data for Flows Ahead of Ramps, December 1963, Part IV: Mach 8 Heat Transfer Data for Flows Ahead of Ramps, July 1964.

6. Kaufman, L. G. II, Pressure Measurements for Mach 8 Flows Over Expansion Corners and Ramps on an Internally Cooled Model, RTD-TDR-63-4044, Part I: Expansion Corner Flows, October 1963, Part II: Flows Over a Flat Plate with and without a Partial Span Ramp, submitted for publication in November 1963, Part III: Flows Over Full Span Ramps Mounted on a Flat Plate, May 1964.

7. Hartofilis, S. A., Pressure and Heat Transfer Measurements at Mach 13 and 19 for Flows Ahead of Ramps, Over Expansion Corners, and Past Fin-Plate Combinations, FDL-TDR-64-144, September 1964.

8. Baer, A. L., An Investigation of Separated Flows on Two-Dimensional Models at Mach Numbers 5 and 8, AEDC-TDR-63-200, October 1963.

9. Burchfield, C. G., Hube, F. K., and Burdette, J. E., An Experimental Heat-Transfer Investigation in Regions of Flow Separation at Mach Number 8, AEDC-TDR 64-30, February 1964.

10. Kaufman, L. G. II and Meckler, L. H., Pressure and Heat Transfer Measurements at Mach 5 and 8 for a Fin - Flat Plate Model, ASD-TDR-63-235, April 1963.

11. Kaufman, L. G. II, Pressure Distributions and Oil Film Photographs for Mach 5 Flows Past Fins Mounted on a Flat Plate, ASD-TDR-63-755, September 1963.

12. Kaufman, L. G. II, Pressure Measurements for Mach 5 Flows Over Winged Re-entry Configurations with Aerodynamic Controls, RTD-TDR-63-4179, Part I: Blunt Cabin Configuration, February 1964, Part II: Conical Cabin Configuration, February 1964.

13. Meckler, L. H., Pressure Measurements at Mach 8 on an Aerodynamically Controllable Winged Re-entry Configuration, FDL-TDR 64-124, submitted for publication in July 1964.

14. Meckler, L. H., Heat Transfer Measurements at Mach 8 on an Aerodynamically Controllable Winged Re-entry Configuration, **FDL-TDR-64-142, submitted for publication in August, 1964.**

15. Donaldson, J. C., Hypersonic Control Effectiveness Tests of a Delta-Winged Re-entry Configuration at Mach 5 and 8, AEDC-TDR-63-268, December 1963.

16. Hartofilis, S. A., Pressure Measurements at Mach 19 for a Winged Re-entry Configuration, ASD-TDR-63-319, May 1963.

17. Lacey, J. J. Jr., Pressure Tests on a Blunt Delta Wing Vehicle at M = 19, AEDC-TDR-63-62, February 1963.

18. Meckler, L. H., Static Aerodynamic Characteristics at Mach 5 and 8 for an Aerodynamically Controllable Winged Re-entry Configuration, FDL-TDR-64-10, **September 1964.**

19. Kaufman, L. G. II, Pressure Measurements for Mach 5 Flows over a Blunt Pyramidal Configuration with Aerodynamic Controls, RTD-TDR-63-4239, January 1964.

20. Kaufman, L. G. II, Pressure and Heat Transfer Measurements for Mach 8 Flows over a Blunt Pyramidal Configuration with Aerodynamic Controls, FDL TDR 64-2, Part I: Pressure Data for Delta Wing Surface, January 1964, Part II: Pressure Data for Dihedral Surfaces, submitted for publication in December 1963, Part III: Heat Transfer Data for Delta Wing Surface, May 1964, Part IV: Heat Transfer Data for Dihedral Surfaces, May 1964.

21. Donaldson, J. C., Hypersonic Control Effectiveness Tests of a Blunted, Triangular-Pyramid Re-entry Configuration at Mach 5 and 8, AEDC TDR 63-250, December 1963.

22. Kaufman, L. G. II, Pressure and Heat Transfer Measurements for Mach 21 Flows Over a Blunt Pyramidal Configuration with Aerodynamic Controls, FDL-TDR 64-120, August 1964.

23. Evans, W. J., and Kaufman, L. G. II, Aerodynamic Characteristics and Flap Loads for a Blunt Pyramidal Configuration at Mach 5 and 8, FDL-TDR 64-128, September 1964.

24. Dorodnitsyn, A. A., "General Method of Integral Relations and Its Application to Boundary-Layer Theory," Advances in Aeronautical Sciences, Pergamon Press, Vol. 3, 1962.

25. Donaldson, C. duP., Note on the Flow in the Near Wake of a Vehicle Traveling at Supersonic Speeds, Aeronautical Research Associates of Princeton Tech. Memo. 61-6, August 1961.

26. Parr, W., Laminar Boundary Layer Calculations by Finite Differences, Naval Ordnance Lab. T. R. 63-261, Math. Dept. Rept. M-42, March 1964.

27. Lees, L. and Reeves, B. L., Supersonic Separated and Reattaching Flows: Part I General Theory and Application to Adiabatic Boundary Layer-Shock Wave Interactions, AIAA Meeting, New York, Preprint No. 64-4, January 20-22, 1964.

28. Tani, I., "On the Approximate Solution of the Laminar Boundary Layer Equations," Journal of the Aerospace Sciences, Vol. 21, No. 7, pp. 487-504, July 1954.

29. Cohen, C. B. and Reshotko, E., Similar Solutions for the Compressible Laminar Boundary Layer with Heat Transfer and Pressure Gradient, NACA Report 1293, 1956.

30. Erdos, J. and Pallone, A., Shock-Boundary Layer Interaction and Flow Separation, Proceedings of the 1962 Heat Transfer and Fluid Mechanics Institute, p. 239, Stanford University Press, Stanford, California.

31. Chapman, D. R., Kuehn, D. M. and Larson, H. K., Investigation of Separated Flows in Supersonic and Subsonic Streams with Emphasis on the Effect of Transition, NACA Report 1356, 1958.

32. Erdos, J. and Pallone, A., Shock-Boundary Layer Interaction and Flow Separation, AVCO/RAD TR-61-23, August 15, 1961.

33. Van Driest, E. R., Investigation of Laminar Boundary Layer in Compressible Fluids Using the Crocco Method, NACA TN 2597, January 1952.

34. Pallone, A., "Non-Similar Solutions of the Compressible-Laminar-Boundary-Layer Equations with Applications to the Upstream-Transpiration Cooling Problem," Journal of the Aerospace Sciences, Vol. 28, No. 6, pp.449-456, June 1961.

35. Libby, P. A., Fox, H., Sanator, R. J., and DeCarlo, J., The Laminar Boundary Layer Near the Plane of Symmetry of a Hypersonic Inlet, AIAA-ASME Hypersonic Ramjet Conference, White Oaks, Md., April 23-25, 1963.

36. Schlichting, Hermann, Boundary Layer Theory, McGraw Hill Book Co. Inc., New York, 1955.

37. Morduchow, Morris, Analysis and Calculation by Integral Methods of Laminar Compressible Boundary Layer with Heat Transfer and with and without Pressure Gradient, NACA Rep. 1245, 1955.

38. Steiger, Martin H., Integral Method Compressible Boundary Layer Calculations for Strong Favorable Streamwise Pressure Gradients, ARL TN 60-149, (also PIBAL Rep. 621), September 1960.

39. Nielsen, Jack N., Change in Boundary-Layer Momentum Thickness Due to Prandtl-Meyer Expansions or Oblique Compression, Appendix 2D of Vidya Rep. 35, 1960.

40. Zakkay, Victor, and Tani, Takashi, Theoretical and Experimental Investigation of the Laminar Heat Transfer Downstream of a Sharp Corner, AFOSR Rep. 1640, (also PIBAL Rep. 708), October 1961.

41. Zakkay, V., Toba, K., and Kuo, T. J., "Laminar, Transitional and Turbulent Heat Transfer after a Sharp Convex Corner," AIAA Journal, Vol. 2, No. 8, August 1964.

42. Sears, W. R. (ed), General Theory of High Speed Aerodynamics, Volume VI, Princeton University Press, Princeton, New Jersey, 1954.

43. Martellucci, A. and Libby, P. A., Supersonic Flow about General Three-Dimensional Blunt Bodies, Vol. II. Heat Transfer Due to the Interaction Between a Swept Planar Shock Wave and a Laminar Boundary Layer, ASD TR 61-727, October 1962.

44. Miller, D. S., Hijman, R. and Childs, M. E., "Mach 8 to 22 Studies of Flow Separation Due to Deflected Control Surfaces," AIAA Journal, Vol. 2, No. 2, February 1964.

45. Test Facilities Handbook, Arnold Engineering Development Center, Arnold Air Force Station, Tenn., July 1962.

46. Wallace, A. R., and Swain, W. N., Pressure Distribution Tests on a 60° and 70° Delta Wing at Mach Numbers 20 to 22, AEDC-TN-61-14, February 1961, CONFIDENTIAL REPORT, title unclassified.

APPENDIX

DATA TABLES AND BIBLIOGRAPHY

This section lists many reports that contain information pertaining to aerodynamic control characteristics with emphasis on hypersonic flows. The types of information contained in many of the reports are outlined in tabular form. The tables provide the reader with a rapid method of determining the general type of information contained in each report or, conversely, just which reports contain the information he desires.

The tables give the type of control investigated, the configuration upon which it was investigated, the test conditions, and the main information presented in each of the referenced reports. An "X" in a row in the data section indicates the data that are presented in a given report. Similarly, in the configuration section, an "X" indicates the configuration upon which the listed control was investigated. In order to maintain the tabular data form and still present a maximum of information, the letter code on the following page was established and used to provide the additional information in compact form.

The tables supersede those in our preliminary survey report (Ref. 1). Many additional references have been added and more information is tabulated for each reference.

LETTER CODE FOR DATA TABLES

a	Tip Control	Control
b	Canard	
c	Spoiler	
d	Nose Cant	
e	Nose Spike	
f	Unswept	Wing Configuration
g	Swept*	
h	Delta*	
i	Trapezoidal Wing	
j	Arrow	
k	Circular	
ℓ	Air Tunnel	Test Facility
m	Helium Tunnel	
n	Free Flight	

* Leading edge sweep indicated in tables.

	Reference Numbers	A 001	A 002	A 003	A 004	A 005	A 006	A 007	A 008
Control	Flap	x	x	x	x	x	x	x	x
	Fin								
	Other					a, c	a, c	a	
Configuration	Wing	x	x	x	x	x	x	x	x
	Wing Planform	f	f	f	f	h 60°	h 60°	g 44.5°	i
	Body								
	Wing-Body Control								
Test Conditions	Range of M_{∞}	1.62	1.62, 2.40	4.04	6.9	1.61, 2.01	1.61, 2.01	1.61	1.61, 2.01
	Range of $Re_{\infty}/Ft \times 10^{-6}$	2.22, 4.28	4.28	1.55	3.96	4.17	4.17	1.74, 3.68	1.74, 5.73
	Range of α	0 to 4	0 to 8	0 to 10	0 to 16	0 to 15	0 to 15	-15 to +15	0 to 15
	Range of δ	-16 to +18	-16 to +16	-12 to +12	-16 to +16	-30 to +30	-30 to +30	-60 to +60	-30 to +30
	Range of β	0	0	0	0	0	0	0	0
	Test Facility	ℓ	ℓ	ℓ	ℓ	ℓ	ℓ	ℓ	ℓ
Data - Configuration	Force	x	x	x	x		x		x
	Pressure	x	x		x	x		x	
	Heat Transfer								
	Theory	x	x		x		x		
	Experiment	x	x	x	x	x	x	x	x
Data - Control Surface	Force								
	Hinge Moment	x	x	x	x		x		x
	Pressure	x	x		x	x		x	
	Heat Transfer								
	Theory	x	x		x		x		
	Experiment	x	x	x	x	x	x	x	x

	Reference Numbers	A 009	A 010	A 011	A 012	A 013	A 014	A 015	A 016
Control	Flap	x	x	x		x	x	x	x
	Fin								
	Other	a, c	c	c	a			a, c	a, c
Configuration	Wing	x	x	x	x	x	x	x	x
	Wing Planform	g 44.5°	i	h 60°	h 60°	i	i	h 60°	h 60°
	Body								
	Wing-Body Control								
Test Conditions	Range of M_∞	1.61, 2.01	1.61, 2.01	1.61	1.61	1.61, 2.01	1.61, 2.01	1.61, 2.01	1.61, 2.01
	Range of $Re_\infty/Ft \times 10^{-6}$	1.74, 3.68	3.68	4.17	4.17	1.74, 5.6	1.7, 5.6		4.2
	Range of α	-15 to +15	-15 to +15	0 to 12	0 to 12	-15 to +15	-15 to +15	0 to 15	0 to 12
	Range of δ	-60 to +60	-20 to +20	-30 to +30	-30 to +30	-30 to +30	-30 to +30	-30 to +30	-30 to +30
	Range of β	0	0	0	0	0	0	0	0
	Test Facility	ℓ	ℓ	ℓ	ℓ	ℓ	ℓ	ℓ	ℓ
Data - Configuration	Force		x	x					
	Pressure	x	x	x		x	x	x	
	Heat Transfer								
	Theory				x				
	Experiment	x	x	x	x	x	x	x	
Data - Control Surface	Force								
	Hinge Moment			x	x				x
	Pressure	x	x	x		x	x	x	
	Heat Transfer								
	Theory				x				
	Experiment	x	x	x	x	x	x	x	x

	Reference Numbers	A 017	A 018	A 019	A 020	A 021	A 022	A 023	A 024
Control	Flap	x	x	x	x	x	x	x	x
	Fin				x		x		
	Other			a	a		b	b	d
Configuration	Wing	x			x	x			
	Wing Planform	f	h 75°	h 73°	h, j 78°	h 60°	h 72.9	h 63° 26'	h 75°
	Body						x		
	Wing-Body Control		x	x	x		x	x	x
Test Conditions	Range of M_∞	2.4	2.91	2.01	1.41, 2.01	.72 to 1.96	2.01	0.7 to 2.22	2.91
	Range of $Re_\infty/Ft \times 10^{-6}$	3.12	2.45	1.0	2.41, 2.9	6.11, 8.64	2.48		2.5
	Range of α	0 to 10	- 4 to +90	0 to 90	- 1 to +27	-10 to +10	0 to 29	- 6 to +18	- 3 to +90
	Range of δ	-16 to +16	-90 to +90	0 to 90	0 to -28	-90 to +90	0 to -31	+ 4 to -20	-70 to +70
	Range of β	0	- 4 to +15	0	0 to 27	0	0 to 29	0	-14 to + 4
	Test Facility	ℓ	ℓ	ℓ	ℓ	ℓ	ℓ	ℓ	ℓ
Data - Configuration	Force	x	x	x	x	x	x	x	x
	Pressure	x							
	Heat Transfer								
	Theory	x							
	Experiment	x	x	x	x	x	x	x	x
Data - Control Surface	Force								
	Hinge Moment	x				x			
	Pressure	x							
	Heat Transfer								
	Theory	x							
	Experiment	x				x			

	Reference Numbers	A 025	A 026	A 027	A 028	A 029	A 030	A 031	A 032
Control	Flap	x	x	x	x	x	x	x	x
	Fin			x	x	x			
	Other		c		d		a, d		d
Configuration	Wing		x						x
	Wing Planform	h 73°	f	g- 65.9° j- 77.4	g 70°	g inboard 76° outboard 60°	h 78.2	h 73°	h 70°
	Body								
	Wing-Body Control	x		x	x	x	x	x	
Test Conditions	Range of M_∞	1.66 to 4.65	3.0 to 5.05	0.6 to 18	1.62 to 9.6	1.62 to 9.6	6.7 to 18.4	8.08	6.7
	Range of $Re_\infty/Ft \times 10^{-6}$	3.02, 5.54	4.24 to 9.51	4 to 9	1.2 to 4	1.2 to 4.0	1.2 to 8.6	2	1.25
	Range of α	- 3 to +16	- 2 to +12	0 to 12	- 5 to +25	- 5 to +25	- 3 to +12	-25 to +50	27 to 56
	Range of δ	0 to -20	-30 to +30	0, ±20	+15 to -30	+10 to -20	Nose 0-20 Others: 0- -20	0 to -45	Flap 0 to -30, Nose 0 to +20
	Range of β	0, -4.1	0		+ 2 to -15	- 3 to +20	0, + 4	0	0
	Test Facility	ℓ	ℓ	ℓ, π_ℓ	ℓ	ℓ	ℓ, π_ℓ	ℓ	ℓ
Data - Configuration	Force	x	x	x	x	x	x	x	x
	Pressure								
	Heat Transfer								
	Theory		x	x			x		
	Experiment	x	x	x	x	x	x	x	x
Data - Control Surface	Force								
	Hinge Moment		x						
	Pressure								
	Heat Transfer								
	Theory		x						
	Experiment		x						

	Reference Numbers	A 033	A 034	A 035	A 036	A 037	A 038	A 039	A 040
Control	Flap	x	x	x	x	x	x		
	Fin						x		
	Other	a	d					b	b
Configuration	Wing		x	x	x	x	x		
	Wing Planform	h 78°	h 70°	h 75°, 79.3°	h 60°	h 60°	h 73°	h 63° 26' 1	h 63° 26' 1
	Body		x	x				x	x
	Wing-Body Control	x					x	x	x
Test Conditions	Range of M_∞	6.9	6.9	3.05	1.7 to 2.6	1.5 to 2.6	8	0.7 to 2.22	0.7 to 2.22
	Range of $Re_\infty/Ft \times 10^{-6}$		.2 to .5	8	9	7 to 11.5	1	1.25, 2.5	1.74, 3.48
	Range of α	0 to +12	0 to 30	- 4 to +24	0 to + 6	1	-20 to +30	- 6 to +18	- 6 to +18
	Range of δ	0, 20	Flap -20 to +20 Nose 0 to 20	0, ±20	0 to 20	0 to 20	0 to 45	0 to 20	0 to +20
	Range of β	0	0	0	0	0	0	0	0
	Test Facility	*l*	*l*	*l*	*n*	*n*	*l*	*l*	*l*
Data - Configuration	Force	x	x	x				x	x
	Pressure						x		
	Heat Transfer				x	x	x		
	Theory	x	x		x	x			
	Experiment	x	x	x	x	x	x	x	x
Data - Control Surface	Force							x	x
	Hinge Moment							x	x
	Pressure						x		
	Heat Transfer				x	x	x		
	Theory				x	x			
	Experiment				x	x	x	x	x

	Reference Numbers	A 041	A 042	A 043	A 044	A 045	A 046	A 047	A 048
Control	Flap							x	x
	Fin				x	x	x	x	x
	Other	b	b	b		d			
Configuration	Wing								
	Wing Planform	h 63^{o} 26' i	h 63^{o} 26' i	h 70^{o}		h 60^{o} 74.25^{o}	f	i	i
	Body	x	x		x		x	x	x
	Wing-Body Control	x	x	x		x	x	x	x
Test Conditions	Range of M_{∞}	0.7 to 2.22	0.7 to 2.22	2.01	3.0 to 6.25	0.06, 0.92 1.62 to 9.6	4.08	6.86	6.83
	Range of $Re_{\infty}/Ft \times 10^{-6}$	1.25, 2.5	1.25, 2.5		1.84 to 9.6	1 to 6	19.2	2.4, 3.96	3.12
	Range of α	- 6 to +18	- 6 to +18	0 to 20	- 2 to 22.5	0 to 20	0 to 6	0 to 25	- 4 to +24
	Range of δ	- 6 to +30	0 to +20	0 to 15	-30 to +30	0	0	0	Fins: +10 to -20 Flaps: 0 to +45
	Range of β	0	0, 5	0	0	-12 to +12	0 to 5	0	0, - 5
	Test Facility	ℓ	ℓ	ℓ	ℓ	ℓ	ℓ	ℓ	ℓ
Data - Configuration	Force	x	x	x	x	x	x	x	x
	Pressure								
	Heat Transfer								
	Theory				x				
	Experiment	x	x	x	x	x	x	x	x
Data - Control Surface	Force	x	x		x				
	Hinge Moment	x	x						
	Pressure				x				
	Heat Transfer								
	Theory				x				
	Experiment	x	x		x				

	Reference Numbers	A 049	A 050	A 051	A 052	A 053	A 054	A 055	A 056
Control	Flap		x	x					x
	Fin	x	x	x					
	Other	a			a	a			
Configuration	Wing				x	x	x	x	
	Wing Planform	k	i	i	h 60°	h 60°	h 75°	h $70^{\circ}, 75^{\circ}$	
	Body		x	x					x
	Wing-Body Control	x	x	x					
Test Conditions	Range of M_{∞}	3.11	6.86	6.86	4.04	6.9	6.9, 9.6	6.8, 9.6, 18.4	5, 9
	Range of $Re_{\infty}/Ft \times 10^{-6}$	12.05, 13.06	2.4	2.4	17.45	4.56			
	Range of α	- 5 to +13	0 to 25	- 5 to +25	0 to 12	-12 to +12	60 to 90	0 to 60	-17 to + 7
	Range of δ	0, -20	0	0 to -20	-16 to +14	-14 to +14			0 to 90
	Range of β	0, 6	- 5 to +10	- 5 to +10	0	0	0	0	0
	Test Facility	ℓ	ℓ	ℓ	ℓ	ℓ	ℓ	ℓ, m	
Data - Configuration	Force	x	x	x	x		x		
	Pressure						x	x	
	Heat Transfer							x	x
	Theory				x		x	x	
	Experiment	x	x	x	x		x	x	x
Data - Control Surface	Force								
	Hinge Moment				x	x			
	Pressure								x
	Heat Transfer								x
	Theory				x	x			
	Experiment				x	x			x

	Reference Numbers	A 057	A 058	A 059	A 060	A 061	A 062	A 063	A 064
Control	Flap	x	x	x	x		x	x	x
	Fin					x			
	Other	e		a		a, b			
Configuration	Wing				x	x		x	x
	Wing Planform			h 75°	f, g 40°	h 65°		f	f
	Body	x	x				x		
	Wing-Body Control			x		x			
Test Conditions	Range of M_{∞}	9.6	3 to 18	2.94 to 4.78	2.0 to 4.5	3.0 3.5 4.0	.6 to 6.0	3, 5	8 to 22
	Range of $Re_{\infty}/Ft \times 10^{-6}$	.936		2.2	0.216 to 1.88	8.8 to 10.7		.4 to 10	.04 to 3.0
	Range of α	-15 to +25	20 to 60	- 5 to 90	0 to 60	- 4 to +12	0 to 8	0	0
	Range of δ	0 to +40	-40 to +54	-20 to +20	0 to 55.6	- 9 to + 9		0 to 30	0 to 30
	Range of β	0	0	0	0	0, +4	0	0	0
	Test Facility	ℓ	ℓ, m	ℓ	ℓ	ℓ	ℓ	ℓ	ℓ
Data - Configuration	Force	x	x	x	x	x	x		
	Pressure							x	x
	Heat Transfer								x
	Theory				x	x	x		
	Experiment	x	x	x	x	x	x	x	x
Data - Control Surface	Force								
	Hinge Moment								
	Pressure							x	x
	Heat Transfer								x
	Theory								
	Experiment							x	x

	Reference Numbers	A 065	A 066	A 067	A 068	A 069	A 070	A 071	A 072
Control	Flap	x	x	x	x	x	x	x	x
	Fin			x					
	Other				d, e	e	e	e	
Configuration	Wing	x	x	x					x
	Wing Planform	f	f	f	h 60°	h 60°	h 60°	h 60°	h 60°
	Body								
	Wing-Body Control				x	x	x	x	x
Test Conditions	Range of M_∞	5, 8	8	13, 19	5, 8	5	8	8	19
	Range of $Re_\infty/Ft \times 10^{-6}$	1.1, 3.3	1.1, 3.3	.08, .15	1.1, 3.3	1.1, 3.3	1.1, 3.3	1.1, 3.3	0.15
	Range of α	+15 to -45	+10 to -43	+30 to -15	+54 to -54	+45 to -30	+50 to -50	+20 to -20	0 to +30
	Range of δ	0 to 45	0 to 30	0 to +45	+40 to -40	+40 to -40	+39 to -39	+39 to -39	0 to +40
	Range of β								
	Test Facility	ℓ	ℓ	ℓ	ℓ	ℓ	ℓ	ℓ	
Data - Configuration	Force				x				
	Pressure	x	x	x		x	x		x
	Heat Transfer	x		x				x	
	Theory								
	Experiment	x	x	x	x	x	x	x	x
Data - Control Surface	Force								
	Hinge Moment								
	Pressure	x	x	x		x	x		x
	Heat Transfer	x		x				x	
	Theory								
	Experiment	x	x	x		x	x	x	x

	Reference Numbers	A 073	A 074	A 075	A 076	A 077	A 078	A 079	
Control	Flap	x	x	x	x			x	
	Fin	x	x	x	x	x	x		
	Other	b		b				d	
Configuration	Wing					x	x	x	
	Wing Planform					f	f	h 70°	
	Body	x	x	x	x				
	Wing-Body Control								
Test Conditions	Range of M_∞	5, 8	5	8	21	5, 8	5	6.83	
	Range of $Re_\infty/Ft \times 10^{-6}$	1.1, to 3.3	3.3	1.1, to 3.3	.07	1.1 to 6.6	1.1 to 6.6	2.4	
	Range of α	+54 to -54	+45 to -30	+54 to -54	+45 to -30	+10 to -14	+10 to - 5	30° to 90°	
	Range of δ	0 to +40	0 to +40	0 to +40	0 to 40	0	0	Flap: +10 to -90 Apex: 0 to 20	
	Range of β	0 to 14	0 to 14	0 to 12				0	
	Test Facility	ℓ	ℓ	ℓ	ℓ	ℓ	ℓ	ℓ	
Data - Configuration	Force	x						x	
	Pressure		x	x	x	x	x		
	Heat Transfer			x	x	x			
	Theory							x	
	Experiment	x	x	x	x	x	x	x	
Data - Control Surface	Force	x						x	
	Hinge Moment	x						x	
	Pressure		x	x	x	x	x		
	Heat Transfer			x	x	x			
	Theory							x	
	Experiment	x	x	x	x	x	x	x	

BIBLIOGRAPHY

A001 Czarnecki, K.R., and Mueller, J.N., Investigation at Mach Number 1.62 of the Pressure Distribution Over a Rectangular Wing with Symmetrical Circular-Arc Section and 30-Percent-Chord Trailing-Edge Flap, NASA RM L9J05, January 1950.

A002 Czarnecki, K.R., and Mueller, J.N., Investigation at Supersonic Speeds of Some of the Factors Affecting the Flow Over a Rectangular Wing with Symmetrical Circular-Arc Section and 30-Percent-Chord Trailing-Edge Flap, NACA RM L50J18, January 1951 (Confidential - Unclassified Title).

A003 Dunning, R.W., and Ulmann, E.F., Aerodynamic Characteristics at Mach Number 4.04 of a Rectangular Wing of Aspect Ratio 1.33 Having a 6-Percent-Thick Circular-Arc Profile and a 30-Percent-Chord Full-Span Trailing-Edge Flap, NACA RM L53D03, May 1953 (Confidential - Unclassified Title).

A004 Ridyard, H.W., and Fetterman, D.E., Aerodynamic Characteristics of a 6-Percent-Thick Symmetrical Circular-Arc Airfoil Having a 30-Percent-Chord Trailing-Edge Flap at a Mach Number of 6.9, NACA RM L56B24, June 1956.

A005 Lord, D.R., and Czarnecki, K.R., Analysis of Pressure Distributions for a Series of Tip and Trailing-Edge Controls on a 60° Delta Wing at Mach Numbers of 1.61 and 2.01, NACA RM L58C07, May 1958.

A006 Czarnecki, K.R., and Lord, D.R., Span Loadings and Aerodynamic Characteristics for a Series of Tip and Trailing-Edge Controls on a 60° Delta Wing at Mach Numbers of 1.61 and 2.01, NASA TM X-51, September 1959 (Confidential - Unclassified Title).

A007 Lord, D.R., Analysis of Pressure Distributions for a Series of Controls on a 40° Sweptback Wing at a Mach Number of 1.61, NASA TM X-139, November 1959 (Confidential - Unclassified Title).

A008 Lord, D.R., and Czarnecki, K.R., Aerodynamic Characteristics of Several Flap-Type Trailing-Edge Controls on a Trapezoidal Wing at Mach Numbers of 1.61 and 2.01, NACA RM L54D19, June 1954.

A009 Lord, D.R., Tabulated Pressure Data for a Series of Controls on a 40° Sweptback Wing at Mach Numbers of 1.61 and 2.01, NACA RM L57H30, November 1957 (Confidential - Unclassified Title).

A010 Lord, D.R., and Czarnecki, K.R., Pressure Distributions and Aerodynamic Characteristics of Several Spoiler-Type Controls on a Trapezoidal Wing at Mach Numbers of 1.61 and 2.01, NACA RM L56E22, July 1956.

A011 Lord, D.R., and Czarnecki, K.R., Aerodynamic Characteristics of a Full-Span Trailing-Edge Control on a 60° Delta Wing with and without a Spoiler at Mach Number 1.61, NACA RM L53L17, March 1954 (Confidential - Unclassified Title).

A012 Czarnecki, K.R., and Lord, D.R., Preliminary Investigation of the Effect of Fences and Balancing Tabs on the Hinge-Moment Characteristics of a Tip Control on a 60° Delta Wing at Mach Number 1.61, NACA RM L53D14, May 1953 (Confidential - Unclassified Title).

A013 Lord, D.R., and Czarnecki, K.R., Tabulated Pressure Data for General Flap-Type Trailing-Edge Controls on a Trapezoidal Wing at Mach Numbers of 1.61 and 2.01, NACA RM L55J04, February 1956.

A014 Lord, D.R., and Czarnecki, K.R., Pressure Distribution and Aerodynamic Loadings for Several Flap-Type Trailing-Edge Controls on a Trapezoidal Wing at Mach Numbers of 1.61 and 2.01, NACA TM L55J03, March 1956.

A015 Lord, D.R., and Czarnecki, K.R., Tabulated Pressure Data for a Series of Controls on a 60° Delta Wing at Mach Numbers of 1.61 and 2.01, NACA RM L55L05, March 1956 (Confidential - Unclassified Title).

A016 Lord, D.R., and Czarnecki, K.R., Hinge-Moment Characteristics for a Series of Controls and Balancing Devices on a 60° Delta Wing at Mach Numbers of 1.61 and 2.01, NACA RM L57B01, April 1957.

A017 Mueller, J.N., An Investigation at Mach Number 2.40 of Flap-Type Controls Equipped with Overhang Nose Balances, NACA RM L53I21, November 1953 (Confidential - Unclassified Title).

A018 Clark, F., and Evans, J., Some Aerodynamic and Control Studies of Lifting Reentry Configurations at Angles of Attack Up to 90° at a Mach Number of 2.91, NASA Technical Memorandum X-338, November 1960.

A019 Foster, G.V., Exploratory Investigation at Mach Number of 2.01 of the Longitudinal Stability and Control Characteristics of a Winged Reentry Configuration, NASA TM X-178, December 1959.

A020 Foster, G.V., Static Stability Characteristics of a Series of Hypersonic Boost-Glide Configurations at Mach Numbers of 1.41 and 2.01, NASA TM X-167, November 1959.

A021 Guy, L. D., Hinge-Moment and Effectiveness Characteristics of an Aspect-Ratio-8.2 Flap-Type Control on a 60° Delta Wing at Mach Numbers from 0.72 to 1.96, NACA RM L56J17, January 1957.

A022 Robinson, R. B., and Spearman, M. L., Aerodynamic Characteristics for Combined Angles of Attack and Sideslip of a Low-Aspect-Ratio Cruciform-Wing Missile Configuration Employing Various Canard and Trailing-Edge Flap Controls at a Mach Number of 2.01, NASA Memo 10-2-58L, October 1958.

A023 Boyd, J. W., and Menees, G. P., Longitudinal Stability and Control Characteristics at Mach Numbers from 0.70 to 2.22 of a Triangular Wing Configuration Equipped with a Canard Control, a Trailing-Edge-Flap Control, or a Cambered Forebody, NASA Memo 4-21-59A, April 1959 (Confidential - Unclassified Title).

A024 Grimaud, J. E., Wind-Tunnel Investigation at a Mach Number of 2.91 of Stability and Control Characteristics of Three Lifting Reentry Configurations at Angles of Attack up to 90 Degrees, NASA TM X-455, March 1961 (Confidential - Unclassified Title).

A025 Presnell, J. G., Investigation of the Aerodynamic and Control Characteristics of a Hypersonic Glider at Mach Numbers from 1.66 to 4.65, NASA TM X-520, June 1961.

A026 Gloria, H. R., and Wong, T. J., Effects of Two Trailing-Edge Controls on the Aerodynamic Characteristics of a Rectangular Wing and Body at Mach Numbers from 3.00 to 5.05, NACA RM A55K07, February 1956 (Confidential - Unclassified Title).

A027 Syvertson, C. A., Gloria, H. R., and Sarabia, M. F., Aerodynamic Perfromance and Static Stability and Control of Flat-Top Hypersonic Gliders at Mach Numbers from 0.60 to 18, NACA RM A58G17, September 1958 (Confidential - Unclassified Title).

A028 Ladson, C. L., and Johnston, P. J., Aerodynamic Characteristics of a Blunt-Nosed Winged Re-entry Vehicle at Supersonic and Hypersonic Speeds, NASA TM X-357, February 1961 (Confidential - Unclassified Title).

A029 Ladson, C. L., and Johnston, P. J., Aerodynamic Characteristics of Two Winged Re-entry Vehicles at Supersonic and Hypersonic Speeds, NASA TM X-346, February 1961 (Confidential - Unclassified Title).

A030 Rainey, R. W., Fetterman, D. E., and Smith, R., Summary of the Static Stability and Control Results of a Hypersonic Glider Investigation, NASA TM X-277, May 1960.

A031 Clark, E. L., Kayser, L. D., Mallard, S. R., and Morris, S., Force Tests of the AD-490I-1 Dyna-Soar Models at Mach Number 8, AEDC TN 60-213, November 1960.

A032 Close, W. H., Hypersonic Longitudinal Trim, Stability, and Control Characteristices of a Delta Wing Configuration at High Angles of Attack, NASA TM X-240, April 1960.

A033 Rainey, R. W., Static Stability and Control of Hypersonic Gliders, NACA RM L58E12a, July 1958 (Confidential - Unclassified Title).

A034 Penland, J. A., and Armstrong, W. O., Preliminary Aerodynamic Data Pertinent to Manned Satellite Re-entry Configurations, NACA RM L58E13a, July 1958.

A035 Whitcomb, C. F., and Foss, W. E., Static Stability and Control Characteristics of Two Large Dihedral Right Triangular Pyramid Lifting Re-entry Configurations at a Mach Number of 3.05, NASA TM X-295, July 1960.

A036 Chauvin, L. T., Aeordynamic Heating of Aircraft Components, NACA RM L55L19b, February 1956.

A037 Chauvin, L. T., and Buglia, J. J., Measurement of Aerodynamic Heat Transfer to a Deflected Trailing-Edge Flap on a Delta Fin in Free Flight at Mach Numbers from 1.5 to 2.6, NASA TN D-250, June 1960.

A038 Hiers, R. S., and Hillsamer, M. E., Heat Transfer and Pressure Distribution Test of a Blunted Delta Wing and Several Body, Elevon and Fin Attachments, AEDC TN 60-238, January 1961 (Confidential - Unclassified Title).

A039 Peterson, V. L., and Menees, G. P., Static Stability and Control of Canard Configurations at Mach Numbers from 0.70 to 2.22 - Longitudinal Characteristics of a Triangular Wing and Unswept Canard, NACA RM A57K26, February 1958 (Confidential - Unclassified Title).

A040 Peterson, V. L., and Boyd, J. W., Static Stability and Control of Canard Configurations at Mach Numbers from 0.70 to 2.22 - Longitudinal Characteristics of an Unswept Wing and Canard, NACA RM A57K27, February 1958.

A041 Boyd, J. W., and Peterson, V. L., Static Stability and Control of Canard Configurations at Mach Numbers from 0.70 to 2.22 - Longitudinal Characteristics of a Triangular Wing and Canard, NACA RM A57J15, January 1958.

A042 Boyd, J. W., and Peterson, V. L., Static Stability and Control of Canard Configurations at Mach Numbers from 0.70 to 2.22 - Triangular Wing and Canard on an Extended Body, NACA RM A57K14, February 1958.

A043 Spearman, M. L., and Drener, C., Effects of Forebody Length and Canard-Surface Size on the Stability and Control Characteristics of a 70° Delta Wing Canard Airplane Configurations at a Mach Number of 2.01, NASA Memo 4-10-59L, March 1959 (Confidential - Unclassified Title).

A044 Wong, T. J., and Gloria, H. R., Aerodynamic Characteristics of Two Rectangular-Plan-Form, All-Moveable Controls in Combination with a Slender Body of Revolution at Mach Numbers from 3.00 to 6.25, NACA RM A55J07, December 1955.

A045 Ladson, C. L., Johnston, P. J., and Trescot, C. D., Effects of Wing Plan-form Geometry on the Aerodynamic Characteristics of a Hypersonic Glider at Mach Numbers up to 9.6, NASA TM X-286, May 1960 (Confidential - Unclassified Title).

A046 Smith, F. M., Ulmann, E. F., and Dunning, R. W., Longitudinal and Lateral Aerodynamic Characteristics at Combined Angles of Attack and Sideslip of a Generalized Missile Model having a Rectangular Wing at a Mach Number of 4.08, NACA RM L58E26, August 1958 (Confidential - Unclassified Title).

A047 Penland, J. A., Ridyard, H. W., and Fetterman, D. E., Lift, Drag and Static Longitudinal Stability Data from an Exploratory Investigation at a Mach Number of 6.86 of an Airplane Configuration having a Wing of Trapezoidal Plan-Form, NACA RM L54L03b, January 1955 (Confidential - Unclassified Title).

A048 Fetterman, D. E., and Penland, J. A., Static Longitudinal Directional and Lateral Stability and Control Data from an Investigation at a Mach Number of 6.83 of Two Developmental X-15 Airplane Configurations, NASA TM X-209, March 1960 (Confidential - Unclassified Title).

A049 Jaquet, B. M., Static Longitudinal and Lateral Stability Characteristics at a Mach Number of 3.11 of Square and Circular Plan-Form Re-entry Vehicles, with Some Effects of Controls and Leading-Edge Extensions, NASA TM X-272, May 1960 (Confidential - Unclassified Title).

A050 Ridyard, H. W., Fetterman, D. E., and Penland, J. A., Static Lateral Stability Data from an Exploratory Investigation at a Mach Number of 6.86 of an Airplane Configuration having a Wing of Trapezoidal Plan Form, NACA RM L55A21a, February 1955 (Confidential - Unclassified Title).

A051 Penland, J. A., Fetterman, D. E., and Ridyard, H. W., Static Longitudinal and Lateral Stability and Control Characteristics of an Airplane Configuration having a Wing of Trapezoidal Plan Form with Various Tail Airfoil Sections and Tail Arrangements at a Mach Number of 6.86, NACA RM L55F17, August 1955 (Confidential - Unclassified Title).

A052 Ulmann, E. F., and Smith, F. M., Aerodynamic Characteristics of a 60° Delta Wing having a Half-Delta Tip Control at a Mach Number of 4.04, NACA RM L55A19, April 1955.

A053 Fetterman, D. E., and Ridyard, H. W., The Effect of a Change of Airfoil Section on the Hinge-Moment Characteristics of a Half-Delta Tip Control with a 60° Sweep Angle at a Mach Number of 6.9, NACA RM L54H16a, October 1954.

A054 Phillips, W.H., Research on Blunt-Faced Entry Configurations at Angles of Attack Between 60° and 90°, USAF-NASA Joint Conference, April 1960.

A055 Bertram, M.H., Feller, W.V., and Dunavant, J.C., Flow Fields, Pressure Distributions, and Heat Transfer for Delta Wings at Hypersonic Speeds, USAF-NASA Joint Conference, April 1960.

A056 Reller, J.O., and Seegmiller, H.L., Convective Heat Transfer to a Blunt Lifting Body, USAF-NASA Joint Conference, April 1960.

A057 Armstrong, W.O., Effect of Various Forebody Modifications on the Static Longitudinal Stability and Control Characteristics of a Re-entry Capsule at a Mach Number of 9.6, NASA TM X-469, April 1961 (Confidential-Unclassified Title).

A058 Armstrong, W.O., Stainback, C.P., and McLellan, C.H., The Aerodynamic Force and Heat Transfer Characteristics of Lifting Re-entry Bodies USAF-NASA Joint Conference, April 1960.

A059 Wiggins, L.F., and Kaattari, G.F., Supersonic Aerodynamic Characteristics of Triangular Plan-Form Models at Angles of Attack to 90°, NASA TM X-568, July 1961.

A060 Amick, J.L., and Carvalho, G.F., Low Reynolds Number Aerodynamics of Flapped Airfoils at Supersonic Speeds, WADC TR 58-466, ASTIA AD 155854, September 1958.

A061 Petersen, R., The Effects of Wing-Tip Droop on the Aerodynamic Characteristics of a Delta-Wing Aircraft at Supersonic Speeds, NASA Technical Memorandum X-363, May 1960.

A062 Dennis, D.H., and Edwards, G.G., The Aerodynamic Characteristics of Some Lifting Bodies, USAF-NASA Joint Conference, April 1960.

A063 Pate, S.R., Investigation of Flow Separation on a Two-Dimensional Flat-Plate Having A Variable-Span Trailing Edge Flap at M = 3 and 5, AEDC TDR 64-14, March 1964.

A064 Miller, D.S., Hijman, R., Childs, M.E., Mach 8 to 22 Studies of Flow Separation Due to Deflected Control Surfaces, AIAA Journal, February 1964, also AIAA Preprint 63-173.

A065 Kaufman, L.G. II, Pressure and Heat Transfer Measurements for Hypersonic Flows Over Expansion Corners and Ahead of Ramps, Aeronautical Systems Division Technical Documentary Report ASD-TDR-63-679, Part I: Mach 5 and 8 Data for Expansion Corner Flows, October 1963, Part II: Mach 5 Pressure Data for Flows Ahead of Ramps, September 1963, Part III: Mach 8 Pressure Data for Flows Ahead of Ramps, November 1963, Part IV: Mach 8 Heat Transfer Data for Flows Ahead of Ramps, to be published.

A066 Kaufman, L.G. II, Pressure Distributions for Mach 8 Flows Over Expansion Corners and Ramps on an Internally Cooled Model, RTD-TDR-63-4044, Part I: Expansion Corner Flows, November 1963, Part II: Flows Over A Flat Plate with and without a Partial Span Ramp, December 1963, Part III: Flows Over Full Span Ramps Mounted on a Flat Plate, to be published.

A067 Hartofilis, S.A., Pressure and Heat Transfer Measurements at Mach 13 and 19 for Flows Ahead of Ramps, over Expansion Corners and Fin-Flat Plate Combinations, to be published as an FDL Technical Documentary Report.

A068 Meckler, L., Static Aerodynamic Characteristics at Mach 5 and 8 for an Aerodynamically Controllable Winged Re-entry Configuration, FDL-TDR-64-10.

A069 Kaufman, L.G. II, Pressure Measurements for Mach 5 Flows Over Winged Re-entry Configurations with Aerodynamic Controls, RDT-TDR-63-4179. Part I: Blunt Cabin Configuration, Part II: Conical Cabin Configuration.

A070 Meckler, L., Pressure Measurements at Mach 8 on Aerodynamically Controllable Winged Re-entry Configuration, to be published as an FDL Technical Documentary Report.

A071 Meckler, L., Heat Transfer Measurements at Mach 8 on an Aerodynamically Controllabe Winged Re-entry Configuration, to be published as an FDL Technical Documentary Report.

A072 Hartofilis, S.A., Pressure Measurements at Mach 19 for a Winged Re-entry Configuration, Aeronautical Systems Division Technical Documentary Report ASD-TDR-63-319, May 1963.

A073 Evans, W.J. and Kaufman, L.G.II, Aerodynamic Characteristics and Flap Loads for a Blunt Pyramidal Configuration at Mach 5 and 8, to be published as an FDL Technical Documentary Report.

A074 Kaufman, L.G. II, Pressure Measurements for Mach 5 Flows over a Blunt Pyramidal Configuration with Aerodynamic Controls, RTD-TDR-63-4239.

A075 Kaufman, L.G. II, Pressure and Heat Transfer Measurements for Mach 8 Flows over a Blunt Pyramidal Configuration with Aerodynamic Controls, FDL-TDR-64-2, Part I: Pressure Data for Delta Wing Surface, January 1964, Part II: Pressure Data for Dihedral Surfaces, to be published, Part III: Heat Transfer Data for Delta Wing Surface, to be published, Part IV: Heat Transfer Data for Dihedral Surfaces, to be published.

A076 Kaufman, L.G. II, Pressure and Heat Transfer Measurements for Mach 21 Flows over a Blunt Pyramidal Configuration with Aerodynamic Controls, to be published as an FDL Technical Documentary Report.

A077 Kaufman, L.G. II, and Meckler, L.H., Pressure and Heat Transfer Measurements at Mach 5 and 8 for a Fin-Flat Plate Model, ASD TDR 63-235, April 1963.

A078 Kaufman, L.G. II, Pressure Distributions and Oil Film Photographs for Mach 5 Flows Past Fins Mounted on a Flat Plate, ASD-TDR-63-755.

A079 Fetterman, D.E., and Neal, L., Jr., An Analysis of the Delta-Wing Hypersonic Stability and Control Behavior at Angles of Attack Between 30° and 90°, NASA TN D-1602, March 1963.

OTHER REPORTS OF INTEREST

A080 Rockhold, V.G., et al., Study to Determine Aerodynamic Characteristics on Hypersonic Re-Entry Configurations. Part I - Experimental Phase. Volume 1 - Experimental Report - Mach Number 2, WADD TR 61-56, Part I, Volume 1, March 1961 (Confidential - Unclassified Title).

A081 Rockhold, V.G., et al., Study to Determine Aerodynamic Characteristics on Hypersonic Re-Entry Configurations. Part I - Experimental Phase. Volume 2 - Experimental Report - Mach Number 5, WADD TR 61-56, Volume 2, March 1961 (Confidential - Unclassified Title).

A082 Onspaugh, C.M., and Sullivan, P.J., Study to Determine Aerodynamic Characteristics on Hypersonic Re-Entry Configurations. Part I - Experimental Phase. Volume 3 - Experimental Report - Mach Number 8, WADD TR 61-56, Part I, Volume 3, March 1961 (Confidential - Unclassified Title).

A083 Onspaugh, C.M., and Sullivan, P.J., Study to Determine Aerodynamic Characteristics on Hypersonic Re-Entry Configurations. Part I - Experimental Phase, Volume 4. High Angle of Attack Force Studies on Two Hypersonic Configurations Mach Number 8, WADD TR 61-56, Part I, Volume 4, August 1962 (Confidential - Unclassified Title).

A084 Malvestuto, F.S., et al., Study to Determine Aerodynamic Characteristics on Hypersonic Re-Entry Configurations. Analytical Phase. Volume I - Analysis, WADD TR 61-56, Part II, Volume 1, March 1962 (Confidential), Part II - Analytical Phase, Volume 2 - Design Charts, WADD TR 61-56, Part II, Volume 2, August 1962 (Confidential - Unclassified Title).

A085 Onspaugh, C.M., and March, W.L., Study to Determine Aerodynamic Characteristics on Hypersonic Re-Entry Configurations. Part III. Pressure Distribution Studies on Three Hypersonic Configurations, Volume I. Experimental Report, WADD TR 61-56, Part III, Volume 1, August 1962 (Confidential - Unclassified Title).

A086 Malvestuto, F. S., et al., Study to Determine Aerodynamic Characteristics on Hypersonic Re-Entry Configurations. Part III. Pressure Distribution Studies on Three Hypersonic Re-Entry Configurations. Volume 2. Analysis, WADD TR 61-56, Part III, Volume 2, August 1962 (Confidential - Unclassified Title).

A087 Mazelsky, B., and Amey, H.B., Jr., Lift, Pitching Moment and Rolling Moment Coefficients on Planar, Twisted and Cambered Wings and Flaps for 70° Delta Wing. Pt. I - Supersonic Flow, ASD-TDR-62-155, Pt. I, June 1962.

A088 Mazelsky, B., and Amey, H.B., Jr., Lift, Pitching Moment and Rolling Moment Coefficients on Planar, Twisted and Cambered Wings and Flaps for 70° Delta Wing. Pt. II - Transonic Flow, ASD-TDR-62-155, Pt. II, November 1962.

A089 Mazelsky, B., and Amey, H.B., Jr., Lift, Pitching Moment and Rolling Moment Coefficients on Planar, Twisted and Cambered Wings and Flaps for 70° Delta Wing. Pt. III - Hypersonic Flow, ASD-TDR-62-155 Pt. III, April 1963.

A090 Sanlorenzo, E. A., Centerline Pressure Distributions of Blunted Delta Wings at Hypersonic Speeds, GASL Technical Report Number 186 (AD 323147) (Confidential - Unclassified Title).

A091 Sanlorenzo, E. A., Pressure Distribution on Blunt Delta Wings at Angle of Attack, GASL Technical Report Number 192 (AD 323144) (Confidential - Unclassified Title).

A092 Seidman, M., Pressure Distribution for Blunted Delta Wings at Mach 21, GASL TR-205, January 1961 (Confidential - Unclassified Title).

A093 Sanlorenzo, E. A., Heat Transfer Distributions on Several Blunt Delta Wing Configurations at Angle of Attack, GASL TR-206, December 1960 (Confidential - Unclassified Title).

A094 Galowin, L., Heat Transfer Correlations for 90° Corner Interference Effects on Fin-Plate Model at a Mach Number of 8, GASL TR-207, February 1961 (Confidential - Unclassified Title).

A095 Daskin, W., and Seidman, M. H., Investigation of Hypersonic Viscous and Inviscid Effects (Pressure and Heat Transfer Distributions) on Lifting Configurations, GASL TR-214 (WADD TR 61-74), May 1961 (Confidential - Unclassified Title).

A096 Analysis of Wind Tunnel Aerodynamic Heating and Pressure Tests at M=9.6 on a Series of Generalized Glider Configurations, Boeing Airplane Co. Document N. D5-4384, March 1959 (Confidential - Unclassified Title).

A097 Clark, E. L., Payne, R. G., and Burchfield, C. G., Heat Transfer and Pressure Distribution Tests of Boeing Dyna-Soar Models at Mach Number 8, Arnold Engineering Development Center Report Number TN-59-151, December 1959 (Confidential - Unclassified Title).

A098 Force Tests of the Boeing S-3661-1 Dyna-Soar Model at Mach Number 8, AEDC-TN-59-166, January 1960 (Secret - Unclassified Title).

A099 Force Tests of the Boeing S-3661-1 Dyna-Soar Model at Mach Number 8, AEDC-TN-60-86, May 1960 (Secret - Unclassified Title).

A100 Edenfield, E. E., Wolny, W., and Shelton, P. C., Pressure Distributions Tests to Determine Trailing Edge Control Effectiveness on a Boeing Dyna-Soar Model at Mach Numbers from 16 to 20, Arnold Engineering Development Center Report Number TN-60-146 (Secret - Unclassified Title).

A101 Griffith, B. J., Drag Tests of Two Hypersonic Glide Configurations at Mach Numbers 16 to 20, Arnold Engineering Development Center Report Number TN-61-37, March 1961 (Confidential - Unclassified Title).

A102 Hiers, R. S., and Hillsamer, M. E., and Morris, S. D., Heat Transfer and Pressure Distribution Tests on a Version of the Dynasoar Glider at Mach 8, Arnold Engineering Development Center Report Number TN-61-70, July 1961 (Confidential - Unclassified Title).

A103 Clark, E. L., and Spurlin, C. J., Force Test of the AD-5991-1 Dyna-Soar Model at Mach Number 8, Arnold Engineering Development Center Report Number TN-61-145, November 1961 (Confidential - Unclassified Title).

A104 Kayser, L. D., and Merz, G. H., Force Tests on the Boeing AD-5991-1 Dyna-Soar Model at Mach 5, 8, and 10, AEDC TDR-62-105, May 1962.

A105 Wallace, A. R., and Knox, E. C., Pressure Distribution on Two Hypersonic Glide Vehicle Configurations at Mach Number 19, Arnold Engineering Development Center Report Number TDR-62-138, July 1962 (Confidential - Unclassified Title).

A106 Mauersberg, J. D., and Thomas, R. E., A Study of Some Aerodynamic Characteristics of the Dyna-Soar Glider at M=12.89", Ohio State University Research Foundation TN-ALOSU-163-8, February 1963 (Confidential - Unclassified Title).

A107 Rhudy, R. W., Burt, R. H., and Burdette, J. E., Pressure Distribution and Heat-Transfer Tests on the Dyna-Soar X-20 Configuration with Various Control Settings at Mach 10, Arnold Engineering Development Center Report Number TDR-63-40, March 1963 (Confidential - Unclassified Title).

A108 Rhudy, R. W., Burdette, J. E., Pressure Distributions and Heat Transfer Tests of the Dyna-Soar X-20 Configuration with Modified Control Surfaces at Mach 10, AEDC-TDR-63-151, August 1963 (Confidential - Unclassified Title).

A109 Rhudy, R.W., and Burdette, J.E., Pressure Distribution Tests of the Dyna-Soar X-20A Configuration with Redesigned Control Surfaces at Mach 10, AEDC TDR 64-8, January 1964 (Confidential - Unclassified Title).

A110 Rhudy, J.P., Hiers, R.S., and Rippey, J.O., Investigation of Hypersonic Flow over Blunted Plates and Cone, Arnold Engineering Development Center Report Number TN-60-93, May 1960 (Confidential - Unclassified Title).

A111 Rhudy, J.P., Hiers, R.S., and Rippey, J.O., Pressure Distribution and Heat Transfer Tests on Two Fin-Flat Plate Interference Models and Several Blunt Leading Edge Delta Wing Models, Arnold Engineering Development Center Report Number TN-60-168, September 1960 (Confidential - Unclassified Title).

A112 Wallace, A.R., and Swain, W.N., Pressure Distribution Tests on a 60° and 70° Delta Wing at Mach Numbers 20 to 22, AEDC-TN-61-14, February 1961 (Confidential - Unclassified Title).

A113 Palko, R.L., Rhudy, R.W., and Trimmer, L.L., Pressure Distribution and Heat-Transfer Test of a Nike-Zeus Model at Mach 6 and 8, Arnold Engineering Development Center Report Number TN-61-17, March 1961 (Confidential - Unclassified Title).

A114 Hiers, R.S., and Hillsamer, M.E., Heat Transfer and Pressure Distribution Tests of the Leading Edge Region of a Nike-Zeus Canard at Mach 4, 6, and 8, Arnold Engineering Development Center Report No. TN-61-135, October 1961 (Confidential - Unclassified Title).

A115 Rhudy, R.W., and Burt, R.H., Pressure Distribution and Heat Transfer Test on FSL-ASD Delta Wing Configurations at Mach Number 8, Phase II, Arnold Engineering Development Center Report Number TN-61-132, October 1961 (Confidential - Unclassified Title).

A116 Myers, J.R., Roberts, B.W., and Dunkin, O.L., Static Stability, Pressure Distribution, and Heat Transfer Tests on the McDonnell Asset Model at Mach Number 10, Arnold Engineering Development Center Report Number TDR-62-44, March 1962 (Confidential - Unclassified Title).

A117 Jones, J.H., and Mallard, S.R., Pressure Tests on Blunt-Leading-Edge Wing and Wing-Body Configurations at Mach Number 5 and 8, Arnold Engineering Development Center Report Number TDR-62-140, July 1962.

A118 Burt, R.H., and Rhudy, R.W., Pressure Distribution Tests on a 70° Swept Delta Wing at Angles of Attack from 0 to 90 Deg. and Mach Numbers of 8 and 10, AEDC-TDR-64-5, January 1964 (Confidential - Unclassified Title).

A119 Edenfield, E.E., Eaves, R.H., Jr., Longitudinal Stability and Control Tests of an ASD-Norair Blunt-Lifting-Body Re-Entry Configuration at Mach Number 20, AEDC-TDR-64-15, January 1964 (Confidential - Unclassified Title).

A120 Hobbs, R.B., Experimental Wind Tunnel Results for the Static Stability and Control Effectiveness of a 9 Degree Cone with Trailing Flaps at M=8.0, General Electric Co. Document Number 63SD761, 6 September 1963 (Secret - Unclassified Title).

A121 Bogdonoff, S.M., and Vas, J.E., A Study of Hypersonic Wings and Controls, IAS, Paper No. 59-112, June 1959.

A122 Metcalfe, H., Some Considerations of Shape and Control for Hypersonic Vehicles, IAS Paper No. 59-144, 1959.

A123 Kaufman, L.G. II, Oman, R.A., Hartofolis, S.A., Meckler, L.H., Evans, W.J., Weiss, D., A Review of Hypersonic Flow Separation and Control Characteristics, ASD-TDR-62-168, March 1962.

A124 Isenberg, J.S., Gasdynamic and Aerodynamic Problems Associated with Hypersonic and Re-Entry Vehicles, ARL 62-347, Pt. 1, May 1962 (Confidential - Unclassified Title).

A125 Samet, S., and Isenberg, J.S., An Experimental Investigation of Hypersonic Aerodynamic Heating on Highly Swept Delta Wing Configurations, Aeronautical Systems Division Report Number ASD-TDR-62-798, March 1963 (Confidentail - Unclassified Title).

A126 Burke, A.F., Ellison, R.K., and Carlson, D.R., The Aerodynamic Force Characteristics of Simple, Unyawed Wing Configurations at High Mach Number and low Reynolds Number, Aeronautical Systems Division Report Number ASD-TDR-62-255, October 1962 (Confidential - Unclassified Title).

A127 Wallace, J.E., and Burke, A.F., Skin Friction, Heat Transfer, and Pressure Distributions Over a Flat Plate and Highly Swept Delta Wings with Sharp and Blunt Leading Edges at Angles at Attack in Hypersonic Flow, ASD-TDR-63-772, September 1963 (Confidential - Unclassified Title).

A128 Nielsen, J.N., and Goodwin, F.K., Investigation of Hypersonic Flow Separation and its Effect on Aerodynamic Control Characteristics, Vidya Report 63, January 1962.

A129 Buck, M.L., and McLaughlin, E.J., A Technique for Predicting Pressure Distributions and Aerodynamic Force Coefficients for Hypersonic Winged Re-Entry Vehicles, Aeronautical Systems Division Report Number TDR-63-522 (Confidential - Unclassified Title).

A130 Hankey, W.L., Prediction of Hypersonic Aerodynamic Characteristics for Lifting Vehicles, ASD-TDR-63-668, September 1963 (Confidential - Unclassified Title).

A131 Kahn, S.F., A Modified Analytical Method for Estimating Flap Characteristics, GE-63SD588, June 1963 (Confidential - Unclassified Title).

A132 Dugan, D. W., Estimation of Static Longitudinal Stability of Aircraft Configurations at High Mach Numbers and at Angles of Attack Between 0° and ±180°, NASA Memo 1-17-59A, March 1959.

A133 Fetterman, D. E., A Method for Predicting the Normal Force Characteristics of Delta Wings at Angles of Attack from 0° to 90°, NASA TM X-757, 1963.

A134 Bertram, M. H., and Henderson, A., Effects of Boundary-Layer Displacement and Leading-Edge Bluntness on Pressure Distribution, Skin Friction, and Heat Transfer of Bodies at Hypersonic Speeds, NACA TN 4301, July 1958.

A135 Bertram, M. H., Boundary-Layer Displacement Effects In Air at Mach Numbers of 6.8 and 9.6, NASA Tech. Rep. R-22, 1959.

A136 Creager, M. O., The Effect of Leading-Edge Sweep and Surface Inclination on the Hypersonic Flow Field Over a Blunt Flat Plate, NASA Memo 12-26-58A, January 1959.

A137 Creager, M. O., Surface Pressure Distribution at Hypersonic Speeds for Blunt Delta Wings at Angle of Attack, NASA Memo 5-12-59A, May 1959.

A138 Rainey, R. W., and Close, W. H., Studies of Stability and Control of Winged Reentry Configurations, National Aeronautics and Space Administration Report Number TM X-327, September 1960.

A139 Bertram, M. H., Feller, W. V., and Dunavant, J. C., Flow Fields, Pressure Distributions and Heat Transfer for Delta Wings at Hypersonic Speeds, National Aeronautics and Space Administration Report Number TM X-316, September 1960 (Confidential - Unclassified Title).

A140 Bertram, M. H., and Everhart, P. E., An Experimental Study of the Pressure and Heat Transfer Distribution on a 70° Sweep Slab Delta Wing in Hypersonic Flow, NASA TR R-153, December 1963.

A141 Hodge, L. B., and Burbank, P. B., Pressure Distribution of a 0.0667-Scale Model of the X-15 Airplane for an Angle-of-Attack Range of 0° to 28° at Mach Numbers of 2.30, 2.88, and 4.65, National Aeronautics and Space Administration Report Number TM X-275, May 1960.

A142 Penland, J. A., and Fetterman, D. E., Jr., Static Longitudinal, Directional and Lateral Stability and Control Data at a Mach Number of 6.83 of the Final Configuration of the X-15 Research Airplane, National Aeronautics and Space Administration Report Number TM X-236, April 1960 (Confidential - Unclassified Title).

A143 Wornom, D. E., and Olstad, W. B., Static Longitudinal Aerodynamic Characteristics of a Right Triangular Pyramidal Lifting Reentry Configuration at Mach Numbers of 3.00, 4.50, and 6.00 for Angles of Attack up to 56°, National Aeronautics and Space Administration Report Number TM X-675, March 1962 (Confidential - Unclassified Title).

A144 Ladson, Charles L., Directional and Lateral Stability Characteristics of a Winged Reentry Vehicle at Hypersonic Speeds, National Aeronautics and Space Administration Report Number TM X-550, August 1961 (Confidential - Unclassified Title).

A145 Jones, R. A., and Gallagher, J. J., Heat Transfer and Pressure Distributions of a 60° Swept Delta Wing with Dihedral at a Mach Number of 6 and Angles of Attack from 0° to 52°, National Aeronautics and Space Administration Report Number TM X-544, May 1961 (Confidential - Unclassified Title).

A146 Mayo, E. E., Static Control Characteristics of a Glider Reentry Configuration Having 79.5° Sweepback and 45° Dihedral at a Mach Number of 6.01, National Aeronautics and Space Administration Report Number TM X-538, April 1961.

A147 Cooper, M., and Gunn, C. R., Pressure Measurements on a Hypersonic Glide Configuration Having 79.5° Sweepback and 45° Dihedral at a Mach Number of 4.95, National Aeronautics and Space Administration Report Number TM X-223, November 1959 (Confidential - Unclassified Title).

A148 Hondros, J. G., and Goldberg, T. J., Aerodynamic Characteristics of a Group of Winged Reentry Vehicles at Mach Number 6.01 at Angles of Attack from 60° to 120° and -10° to 30° Roll at 90° Angle of Attack, National Aeronautics and Space Administration Report Number TM X-511 (Confidential - Unclassified Title).

A149 Goldberg, T. J., and Hondros, J. G., Pressure Distributions on a Flat Plate Delta Wing Swept 65° at a Mach Number of 5.97 at Angles of Attack from 65° to 115° and Roll Angles from 0° to 25° at a 90° Angle of Attack, National Aeronautics and Space Administration TM X-702, August 1962 (Confidential - Unclassified Title).

A150 Hall, C. F., and Boyd, J. W., Effects of Canards on Airplane Performance and Stability, National Advisory Committee for Aeronautics Report Number RM A58D24, July 1958.

A151 Love, E. S., The Use of Cones as Stabilizing and Control Surfaces at Hypersonic Speeds, National Advisory Committee for Aeronautics Report Number RM L57F14, August 1957 (Confidential - Unclassified Title).

A152 Smith, F. M., Experimental and Theoretical Aerodynamic Characteristics of Two Low-Aspect-Ratio Delta Wings at Angles of Attack to 50° at a Mach Number of 4.07, National Advisory Committee for Aeronautics Report Number RM L57E02, July 1957.

A153 Jacobson, C. R., Control Characteristics of Trailing-Edge Spoilers on Untapered Blunt Trailing-Edge Wings of Aspect Ratio 2.7 with 0° and 45° Sweepback at Mach Numbers of 1.41 and 1.96, NACA RM L52J28, December 1952.

A154 Czarnecki, K.R., and Lord, D.R., Hinge-Moment Characteristics for Several Tip Controls on a 60° Sweptback Delta Wing at Mach Number 1.61, NACA RM L52K28, January 1953.

A155 Guy, L.D., Control Hinge-Moment and Effectiveness Characteristics of a 60° Half-Delta Tip Control on a 60° Delta Wing at Mach Numbers of 1.41 and 1.96, NACA RM L52H13, October 1952.

A156 Morris, O.A., Control Hinge-Moment and Effectiveness Characteristics of Several Interchangeable Tip Controls on a 60° Delta Wing at Mach Numbers of 1.41, 1.62, and 1.96, NACA RM L53J08a, November 1953.

A157 Lord, D.R., and Czarnecki, K.R., Aerodynamic Characteristics of Several Tip Controls on a 60° Delta Wing at a Mach Number of 1.61, NACA RM L54E25, August 1954.

A158 Mueller, J.N., Investigation of Spoilers at a Mach Number of 1.93 to Determine the Effects of Height and Chordwise Location on the Section Aerodynamic Characteristics of a Two-Dimensional Wing, NACA RM L52L31, March 1953.

A159 Conner, W.D., and Mitchell, M.H., Effects of Spoiler on Airfoil Pressure Distribution and Effects of Size and Location of Spoilers on the Aerodynamic Characteristics of a Tapered Unswept Wing of Aspect Ratio 2.5 at a Mach Number of 1.90, NACA RM L50L20, January 1951.

Contrails

Unclassified
Security Classification

DOCUMENT CONTROL DATA - R&D
(Security classification of title, body of abstract and indexing annotation must be entered when the overall report is classified)

1. ORIGINATING ACTIVITY (Corporate author) Grumman Aircraft Engineering Corp. Bethpage, Long Island, N. Y.	2a. REPORT SECURITY CLASSIFICATION Unclassified 2b. GROUP

3. REPORT TITLE
An Investigation of Hypersonic Flow Separation and Control Characteristics

4. DESCRIPTIVE NOTES (Type of report and inclusive dates)

5. AUTHOR(S) (Last name, first name, initial)
Kaufman, Louis G. II Hartofilis, Stavros A.
Meckler, Lawrence Weiss, Daniel

6. REPORT DATE	7a. TOTAL NO. OF PAGES	7b. NO. OF REFS
December 1964	121	159

8a. CONTRACT OR GRANT NO.	9a. ORIGINATOR'S REPORT NUMBER(S)
AF33(616)-8130 b. PROJECT NO. 8219 c. d.	AFFDL TR 64-174 9b. OTHER REPORT NO(S) (Any other numbers that may be assigned this report) None

10. AVAILABILITY/LIMITATION NOTICES
None

11. SUPPLEMENTARY NOTES	12. SPONSORING MILITARY ACTIVITY
None	AFFDL (FDCC) Wright-Patterson AFB, Ohio 45433

13. ABSTRACT Hypersonic flow separation and its effects on control characteristics were investigated analytically and experimentally. Included are conclusions drawn from extensive test data for hypersonic flows over "basic" geometries and over "typical" flight configurations with aerodynamic controls.

The basic flow geometries discussed include: separation on flat plates ahead of ramps (flaps); flows over sharp expansion corners; "breakaway" separation; and fin plate interactions. Force data and limited pressure and heating rate distributions are presented for the flight configurations for various trailing edge flap settings. As a supplement to this work, available sources of pertinent hypersonic controls data are tabulated in the Appendix.

DD FORM 1 JAN 64 1473

Security Classification

14. KEY WORDS	LINK A		LINK B		LINK C	
	ROLE	WT	ROLE	WT	ROLE	WT
Hypersonic control effectiveness						

INSTRUCTIONS

1. ORIGINATING ACTIVITY: Enter the name and address of the contractor, subcontractor, grantee, Department of Defense activity or other organization *(corporate author)* issuing the report.

2a. REPORT SECURITY CLASSIFICATION: Enter the overall security classification of the report. Indicate whether "Restricted Data" is included. Marking is to be in accordance with appropriate security regulations.

2b. GROUP: Automatic downgrading is specified in DoD Directive 5200.10 and Armed Forces Industrial Manual. Enter the group number. Also, when applicable, show that optional markings have been used for Group 3 and Group 4 as authorized.

3. REPORT TITLE: Enter the complete report title in all capital letters. Titles in all cases should be unclassified. If a meaningful title cannot be selected without classification, show title classification in all capitals in parenthesis immediately following the title.

4. DESCRIPTIVE NOTES: If appropriate, enter the type of report, e.g., interim, progress, summary, annual, or final. Give the inclusive dates when a specific reporting period is covered.

5. AUTHOR(S): Enter the name(s) of author(s) as shown on or in the report. Enter last name, first name, middle initial. If military, show rank and branch of service. The name of th ncipal author is an absolute minimum requirement.

6. REPORT DATE: Enter the date of the report as day, month, year; or month, year. If more than one date appears on the report, use date of publication.

7a. TOTAL NUMBER OF PAGES: The total page count should follow normal pagination procedures, i.e., enter the number of pages containing information.

7b. NUMBER OF REFERENCES: Enter the total number of references cited in the report.

8a. CONTRACT OR GRANT NUMBER: If appropriate, enter the applicable number of the contract or grant under which the report was written.

8b, 8c, & 8d. PROJECT NUMBER: Enter the appropriate military department identification, such as project number, subproject number, system numbers, task number, etc.

9a. ORIGINATOR'S REPORT NUMBER(S): Enter the official report number by which the document will be identified and controlled by the originating activity. This number must be unique to this report.

9b. OTHER REPORT NUMBER(S): If the report has been assigned any other report numbers *(either by the originator or by the sponsor)*, also enter this number(s).

10. AVAILABILITY/LIMITATION NOTICES: Enter any limitations on further dissemination of the report, other than those imposed by security classification, using standard statements such as:

(1) "Qualified requesters may obtain copies of this report from DDC."

(2) "Foreign announcement and dissemination of this report by DDC is not authorized."

(3) "U. S. Government agencies may obtain copies of this report directly from DDC. Other qualified DDC users shall request through _____."

(4) "U. S. military agencies may obtain copies of this report directly from DDC. Other qualified users shall request through _____."

(5) "All distribution of this report is controlled. Qualified DDC users shall request through _____."

If the report has been furnished to the Office of Technical Services, Department of Commerce, for sale to the public, indicate this fact and enter the price, if known.

11. SUPPLEMENTARY NOTES: Use for additional explanatory notes.

12. SPONSORING MILITARY ACTIVITY: Enter the name of the departmental project office or laboratory sponsoring *(paying for)* the research and development. Include address.

13. ABSTRACT: Enter an abstract giving a brief and factual summary of the document indicative of the report, even though it may also appear elsewhere in the body of the technical report. If additional space is required, a continuation sheet shall be attached.

It is highly desirable that the abstract of classified reports be unclassified. Each paragraph of the abstract shall end with an indication of the military security classification of the information in the paragraph, represented as *(TS), (S), (C), or (U)*.

There is no limitation on the length of the abstract. However, the suggested length is from 150 to 225 words.

14. KEY WORDS: Key words are technically meaningful terms or short phrases that characterize a report and may be used as index entries for cataloging the report. Key words must be selected so that no security classification is required. Identifiers, such as equipment model designation, trade name, military project code name, geographic location, may be used as key words but will be followed by an indication of technical context. The assignment of links, rules, and weights is optional.